

Technische Universität München  
TUM School of Engineering and Design

# **Qualification of water-based anode dispersions for the inkjet printing process**

**Cara Greta Kolb**

Vollständiger Abdruck der von der TUM School of Engineering and Design der Technischen Universität München zur Erlangung einer

**Doktorin der Ingenieurwissenschaften (Dr.-Ing.)**

genehmigten Dissertation.

**Vorsitz:** Prof. Dr. techn. Jan Torgersen

**Prüfende der Dissertation:**

1. Prof. Dr.-Ing. Michael F. Zäh
2. Assoc. Prof. Mihaela Vlasea, Ph.D.
3. Prof. Dr.-Ing. habil. Gerd Witt

Die Dissertation wurde am 24.06.2024 bei der Technischen Universität München eingereicht und durch die TUM School of Engineering and Design am 16.01.2025 angenommen.



## Editors' Preface

Production engineering is crucial for the advancement of our industrial society because the performance of manufacturing companies depends heavily on the equipment and resources employed, the production processes applied, and the established manufacturing organization. A company's full potential for corporate success can only be taken advantage of by optimizing the interaction between humans, operational structures, and technologies. Being able to remain competitive while balancing the varying and often conflicting priorities of complexity, cost, time, and quality requires constant thought, adaptation, and the development of new manufacturing structures. Thus, there is an essential need to reduce the complexity of products, manufacturing processes, and systems. Yet, at the same time, it is also vital to gain a better understanding and command of these aspects.

The objective of the research activities at the Institute for Machine Tools and Industrial Management (*iwb*) is to continuously improve product development and manufacturing planning systems, manufacturing processes, and production facilities. A company's organizational, manufacturing, and work structures, as well as the underlying systems for order processing, are developed under strict consideration of employee-related requirements and sustainability issues. Although an increasing degree of automation is unavoidable, labor will remain an important component in production processes. Thus, questions concerning the optimization of human involvement in all planning and development processes are of utmost importance.

The volumes published in this book series reflect and report the results from the research conducted at the *iwb*. Research areas covered span from the design and development of manufacturing systems to the application of technologies in manufacturing and assembly. The management and operation of manufacturing systems, quality assurance, availability, and autonomy are overarching topics, which affect all areas of our research. In this series, the latest results and insights from our application-oriented research are published. This will foster an improvement in the transfer of knowledge between universities and towards a wide industrial sector.



## Preface

This doctoral thesis was elaborated during my work as a research associate at the *iwb* of the Technical University of Munich.

First and foremost, I would like to thank my highly appreciated supervisor Prof. Dr.-Ing. Michael F. Zaeh, Head of the Chair of Machine Tools and Manufacturing Technology, for giving me the opportunity of pursuing a doctorate. He has offered me to deepen my knowledge in the field of additive manufacturing and scientific working already during my master's program as a trainee at his institute. I would like to sincerely thank him for giving me the chance to develop myself both personally and professionally.

I would also like to greatly thank Assoc. Prof. Mihaela Vlasea, Ph.D., and Prof. Dr.-Ing. habil. Gerd Witt for assuming the position of the external examiners and Prof. Dr. techn. Jan Torgersen for taking over the chair of the doctoral examination.

Additionally, I thank Prof. Saeed Maleksaeedi, Ph.D., for his great scientific contribution and for giving me the opportunity to support with initiating related activities in the field of all-solid-state-batteries.

Lastly, I thank Assoc. Prof. Michael Pope, Ph.D., and Prof. Dr.-Ing. Rüdiger Daub for challenging my work and for giving me further scientific advice.

Furthermore, I thank my colleagues at the *iwb*, in particular the research groups for additive manufacturing and battery production, and at the Multi-Scale Additive Manufacturing Lab (MSAM) of the University of Waterloo. Particular credit goes to my colleague and friend Maja Lehmann. We have gone through so many ups and downs together. I would not have achieved this without her. Moreover, I appreciate the mental support of my colleague and friend Sophie Grabmann.

In addition, I would like to thank all of the colleagues and students who contributed to my publications and doctoral thesis. I highly appreciate the valuable discussions and the ideas that have been developed during the common research. In particular, I want to thank Florian Guenter, Andreas Bachmann, Jan Bernd Habedank, Alessandro Sommer, and Kshiti Patel.

Additionally, my sincere gratitude goes to the *iwb e.V.* for giving faith in my

research topic already during my trainee program and the financial support for further investigations in this field.

Finally, my greatest thanks go to my parents. They gave me the support and confidence as well as particularly encouraged me from a very early age onwards. Thank you that I could always rely on you and that you visited me even in the most remote places during my studies and doctorate!

Munich, March 2025

*Cara Greta Kolb*

# Contents

<b>List of Abbreviations</b>	<b>xi</b>
<b>List of Symbols</b>	<b>xiii</b>
<b>1 Introduction</b>	<b>1</b>
1.1 Inkjet printing — a disruptive technology for the fabrication of customized lithium-ion batteries . . . . .	1
1.2 Conceptual outline . . . . .	3
1.3 Structure . . . . .	3
<b>2 Fundamentals</b>	<b>5</b>
2.1 Chapter overview . . . . .	5
2.2 Lithium-ion batteries . . . . .	5
2.2.1 Principle and characteristics . . . . .	5
2.2.2 Electrode and dispersion composition . . . . .	7
2.2.3 Battery performance characteristics . . . . .	9
2.2.4 Conventional electrode production . . . . .	11
2.2.5 Electrode structuring . . . . .	12
2.3 Dispersion systems . . . . .	13
2.3.1 Terminology and characteristics . . . . .	13
2.3.2 Physics of the phase boundaries . . . . .	18
2.3.3 Mechanisms affecting the stability . . . . .	20
2.3.4 DLVO theory . . . . .	23
2.3.5 Wetting of substrates . . . . .	24
2.3.6 Preparation of a stable dispersion . . . . .	25
2.4 Piezoelectric inkjet printing . . . . .	27
2.4.1 Principle of the process . . . . .	27
2.4.2 Principle of the print head . . . . .	28
2.4.3 Potentials and restrictions . . . . .	30
<b>3 State of the art in science and technology</b>	<b>33</b>
3.1 Chapter overview . . . . .	33
3.2 Inkjet printing of water-based electrode dispersions . . . . .	33

3.2.1	Composition of the dispersions . . . . .	33
3.2.2	Preparation of the dispersions . . . . .	35
3.2.3	Reliable processability . . . . .	37
3.2.4	Characteristics of the printed electrode layers . . . . .	38
3.3	Modeling of the dispersion stability using the DLVO theory . . .	39
3.3.1	Modeling approaches . . . . .	39
3.3.2	Applications of the DLVO theory . . . . .	45
3.4	Qualification of non-Newtonian fluids for the inkjet printing process . . . . .	46
3.4.1	Drop formation . . . . .	46
3.4.2	Drop deposition . . . . .	51
<b>4</b>	<b>Problem statement and approach</b>	<b>55</b>
4.1	Chapter overview . . . . .	55
4.2	Problem statement and sub-objectives . . . . .	55
4.3	Approach . . . . .	56
4.4	Scientific contributions of the author . . . . .	58
<b>5</b>	<b>Materials and methods</b>	<b>61</b>
5.1	Chapter overview . . . . .	61
5.2	Dispersions . . . . .	61
5.2.1	Materials . . . . .	61
5.2.2	Characterization . . . . .	62
5.2.3	Test setups for the drop monitoring . . . . .	63
5.3	Electrodes and cells . . . . .	64
5.3.1	Materials . . . . .	64
5.3.2	Electrode fabrication and cell assembly . . . . .	65
5.3.3	Characterization . . . . .	65
<b>6</b>	<b>Publication I: Analysis of the product- and process-specific requirements according to KOLB ET AL. (2022a)</b>	<b>67</b>
6.1	Summary . . . . .	67
6.2	Summary of the key findings and contributions of the lead author	69
<b>7</b>	<b>Publication II: Stabilization of the dispersions according to KOLB ET AL. (2021)</b>	<b>71</b>
7.1	Summary . . . . .	71
7.2	Summary of the key findings and contributions of the lead author	72
<b>8</b>	<b>Publication III: Modeling of the dispersion stability according to KOLB ET AL. (2022b)</b>	<b>73</b>
8.1	Summary . . . . .	73
8.2	Summary of the key findings and contributions of the lead author	74

---

<b>9 Publication IV: A-priori evaluation of the dispersion printability according to KOLB ET AL. (2023a)</b>	<b>75</b>
9.1 Summary . . . . .	75
9.2 Summary of the key findings and contributions of the lead author	76
<b>10 Publication V: Analysis of the role of binder derivatives on product and process conditions according to KOLB ET AL. (2023b)</b>	<b>79</b>
10.1 Summary . . . . .	79
10.2 Summary of the key findings and contributions of the lead author	80
<b>11 Discussion</b>	<b>83</b>
<b>12 Summary and outlook</b>	<b>87</b>
<b>Bibliography</b>	<b>91</b>
<b>A List of the supervised research projects</b>	<b>107</b>
<b>B Publications of the author</b>	<b>109</b>



---

## List of Abbreviations

---

Acronym	Description
A	Advancement
AM	Active material
BDM	Bockris-Devanathan-Mueller
BET	Brunauer-Emmett-Teller
Bi	Binder
Bu	Buffer
CA	Conductive additives
CMC	Carboxymethyl cellulose
D	Dispersant
DLVO	Derjaguin, Landau, Verwey, and Overbeek
DoD	Drop-on-Demand
dpi	Dots per inch
<i>iwb</i>	Institute for Machine Tools and Industrial Management of TUM
e.g.	For example (lat.: <i>exempli gratia</i> )
EC	Ethylene carbonate
EMC	Ethyl methyl carbonate
FA	Further additive
KF	Key finding
LCO	Lithium cobalt oxide
LFP	Lithium iron phosphate

LMO	Lithium nickel manganese cobalt oxide
LTO	Lithium titanate oxide
LVE	Linear viscoelastic
M	Mixture
$\mu\text{L}$	Micro liter (also $\mu\text{l}$ )
NCA	Lithium nickel cobalt aluminum oxide
NMC	Lithium nickel manganese cobalt oxide
NMP	<i>N</i> -Methyl-2-pyrrolidone
N/A	Data not available
PAA	Polyacrylic acid
PAMA	Poly-acrylic-co-maleic acid
PD	Printable dispersion
pL	Pico liter (also pl)
S	Solvent
SBR	Styrene-butadiene rubber
SEI	Solid electrolyte interface
SO	Sub-objective
SMCS	Sodium carboxymethyl cellulose
TUM	Technical University of Munich
WP	Work package

---

## List of Symbols

### Greek symbols

Variable	Unit	Description
$\gamma$	%	Shear strain
$\dot{\gamma}$	$s^{-1}$	Shear rate
$\Delta$	m	Range of the depletion effect
$\Delta E_0$	V	Difference of the equilibrium potentials
$\Delta\rho$	$kg\ m^{-3}$	Density difference between the dispersed and the continuous phase
$\Delta x$	$\mu m$	Particle span
$\delta$	$^\circ$	Loss factor
$\epsilon_1, \epsilon_2$	-	Dielectric constant of the particle 1, 2
$\epsilon_3$	-	Dielectric constant of the medium
$\epsilon_0$	$C^2\ N^{-1}m^{-1}$	Permittivity of the vacuum
$\eta$	Pa s	Dynamic viscosity
$\eta_{eject}$	Pa s	Dynamic viscosity at drop ejection
$\theta$	$^\circ$	Contact angle
$\kappa$	$m^{-1}$	Debye constant
$\lambda$	s	Relaxation time
$\lambda_i$	m	Characteristic wavelengths of the retardation effects
$\lambda_1$	m	Decay length
$\mu_1, \mu_1^0$	$J\ mol^{-1}$	Chemical potentials of the solvent molecules at bulk volume fraction

$\xi$	m	Thickness of a polymer shell
$\rho$	$\text{kg m}^{-3}$	Density
$\sigma_{\text{lg}}$	$\text{N m}^{-1}$	Liquid-gas interfacial energy
$\sigma_{\text{sg}}$	$\text{N m}^{-1}$	Solid-gas interfacial energy
$\sigma_{\text{sl}}$	$\text{N m}^{-1}$	Solid-liquid interfacial energy
$\tau$	Pa	Shear stress
$\tau_f$	Pa	Flow point
$\tau_y$	Pa	Yield point
$\psi$	V	Surface potential of a particle
$\Phi$	-	Volume fraction
$\phi$	-	Shape factor
$\omega$	$\text{s}^{-1}$	Characteristic relaxation frequency of the ultraviolet region

---

## Latin symbols

Variable	Unit	Description
$A$	$\text{m}^2$	Surface area of a plate in the two-plate model
$A_1, A_2$	J	Hamaker constant of the particle 1, 2
$A_3$	J	Hamaker constant of the medium
$A_{ij}$	J	Hamaker constant of mixtures of the phase $i$ and $j$
$A_{132}$	J	Hamaker constant of the dispersion
$A_{132}^0$	J	Zero-frequency Hamaker constant of the dispersion
$A_{132}^\zeta$	J	Non-zero-frequency Hamaker constant of the dispersion
$a$	m	Particle radius
$B_1, B_2, B_3$	-	Parameters of the oscillator model
$B_i$	-	Parameter of the oscillator model
$C$	-	Standardized capacity
C-rate	$\text{h}^{-1}$	-
$Ca$	-	Capillary number
$CE$	%	Coulombic efficiency
$c$	$\text{m s}^{-1}$	Speed of light
$De_0$	-	Deborah number
$d_{\text{drop}}$	$\mu\text{m}$	Drop diameter
$d_{\text{nozzle}}$	$\mu\text{m}$	Nozzle diameter
$d_{\text{particle}}$	$\mu\text{m}$	Particle diameter
$d_{\text{ph}}$	mm	Distance between the print head and the substrate
$Ec$	-	Elasto-capillary number
$E_{0,\text{anode}}$	V	Anode potential at equilibrium
$E_{0,\text{cathode}}$	V	Cathode potential at equilibrium
$F$	N	Force

$f$	$s^{-1}$	Frequency
$f_c$	-	Geometric conversion factor of the Derjaguin approximation
$ G^* $	Pa	Complex shear modulus
$G'$	Pa	Storage modulus
$G''$	Pa	Loss modulus
$g$	$m\ s^{-2}$	Gravitational constant
$h$	m	Particle separation distance
$h_{eb}$	m	Particle separation distance at the energy barrier
$h_p$	m	Distance between two plates in the two-plate model
$h_{pri}$	m	Particle separation distance at the primary minimum
$h_{sec}$	m	Particle separation distance at the secondary minimum
$\hbar$	$m^2kg\ s^{-1}$	Planck's constant divided by $2\pi$
$I$	A	Electrical current
$I_s$	$mol\ L^{-1}$	Ionic strength
$i$	-	Imaginary number
$j$	-	Index number of the size class
$k$	-	Hydrophobic modification coefficient
$k_B$	$J\ K^{-1}$	Boltzmann constant
$L$	m	Characteristic length of the print head nozzle
$L_c$	m	Length of a nozzle cavity
$L_p$	m	Thickness of a polymer layer
$m$	-	Best fit parameter
$m_{PVP}$	m%	Polyvinylpyrrolidone content
$n_i$	$m^{-3}$	Electrolyte concentration of the type $i$
$Pe$	-	Péclet number

---

$p$	m	Extent of the overlap of polymer shells
$Q_0$	Ah	Nominal capacity
$Q_{\text{ch}}$	Ah	Charge capacity
$Q_{\text{dis}}$	Ah	Discharge capacity
$q$	m	Compression of a polymer shell
$q_r(\ln d_{\text{particle}})$	-	Normalized density distribution in a plot with logarithmic abscissa
$q_r(\ln d_{\text{particle}})$	%	Share of particles in a plot with logarithmic abscissa
$Re$	-	Reynolds number
$r$	m	Inter-center particle separation distance
$r_{\text{nozzle}}$	m	Nozzle radius
$r_{\text{particle}}$	m	Particle radius
$r_{\text{particle},i}$	m	Particle radius of the particle $i$
$s$	m	Mean distance between polymer chain attachment points
$T$	K	Temperature
$t$	s	Time
$t_{\text{wet}}$	s	Wetting time
$U$	V	Voltage applied to the piezoelectric actuator
$U_0$	V	Equilibrium voltage
$\bar{U}$	V	Average discharge voltage
$Oh$	-	Ohnesorge number
$V$	J	Interaction energy
$V_{\text{dep}}$	J	Depletion interaction energy
$V_{\text{el}}$	J	Electrostatic double layer interaction energy
$V_{\text{hyd}}$	J	Hydrophobic interaction energy
$V_s$	J	Steric interaction energy
$V_T$	J	Total interaction energy (DLVO theory in its

---

		original form)
$V_{T,ex}$	J	Total interaction energy (extended DLVO theory)
$V_{vdw}$	J	Van-der-Waals interaction energy
$v$	$m\ s^{-1}$	Relative motion of the plates in the two-plate model
$v_{eject}$	$m\ s^{-1}$	Velocity of the drop upon ejection
$v_{impact}$	$m\ s^{-1}$	Velocity of the drop upon impact
$v_1^0$	$m^3\ mol^{-1}$	Molar volume of the pure solvent
$We$	-	Weber number
$Wi$	-	Weissenberg number
$z_i$	-	Ion charge

---

---

## Chapter 1

# Introduction

## 1.1 Inkjet printing — a disruptive technology for the fabrication of customized lithium-ion batteries

Lithium-ion batteries have emerged as the prevalent energy storage systems for portable devices and electric vehicles (SCROSATI and GARCHE 2010). This is attributed to the larger amount of energy stored and the higher power delivery compared to other systems (ANDRE et al. 2015).

The core components of a lithium-ion battery are the electrodes, which are designated as anode and cathode. They allow for an almost reversible lithium-ion exchange through an ion-conducting medium during charging and discharging (see Figure 1.1 a).

The key performance characteristics of a lithium-ion battery are the energy density and the power density, where a conflict of objectives is prevalent. While a high energy density increases the run time at constant loads, a high power density facilitates fast charging and discharging. These parameters are largely governed by the electrode thicknesses. A high energy density is commonly promoted by thick and low-porosity electrodes, whereas the power density is enhanced by thin and high-porosity electrodes. This is attributed to the elongated lithium-ion distances that are associated with an increasing electrode thickness (CHOI et al. 2013; ZHENG et al. 2012). However, achieving high energy and power densities is crucial for the majority for applications.

This trade-off can be alleviated through maintaining short lithium-ion transport pathways by customizing the electrode microstructure. Miscellaneous approaches aim to reduce the pathways by introducing a two-dimensional structuring of the electrodes using various techniques, such as laser ablation processes (HABEDANK et al. 2018, 2019), co-extrusion (BAE et al. 2013), or mechanical milling (REALE and SMITH 2018). A greater potential is ascribed to three-dimensional battery concepts (CHANG et al. 2019; ZHU et al. 2017), in which tailored electrodes interlock on a micrometer scale (see Figure 1.1 b). The positive impact of the interlocking electrode design even increases with a rising area mass loading of the electrodes.

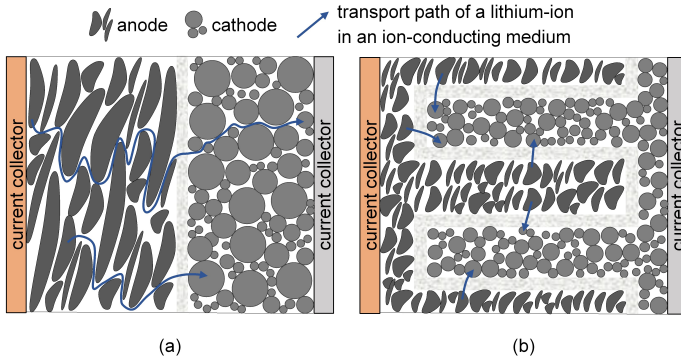


**Figure 1.1:** Schematic depiction of the transport pathways of the lithium ions during discharging with (a) conventional planar electrodes and (b) interlocked electrodes (extended on the basis of HABEDANK (2021))

Novel approaches targeting interlocked electrode structures pursue the exploitation of additive manufacturing technologies due to their high achievable freedom of design (YANG et al. 2020; ZHANG et al. 2017). Particular relevance was attributed to the liquid-based process piezoelectric inkjet printing (ZHANG et al. 2017). Due to the superior printing resolution, this process has already proven to be a suitable technology for customized electronics and microelectronics as well as for printed functionalities, such as for optical and photonical applications (ALAMÁN et al. 2016). Accordingly, the piezoelectric inkjet printing process promises to generate interlocking electrode structures through processing electrode dispersions that are comparable to the slurries employed in conventional electrode coating processes (DELANNOY et al. 2015; ZHANG et al. 2017). The trend towards new manufacturing routes is accompanied by an increased aqueous processing of electrodes resulting in an improved environmental impact combined with reduced costs (ZACKRISSON et al. 2010).

Despite the enormous potentials of the piezoelectric inkjet printing for lithium-ion batteries, there are process-inherent restrictions that impede the leveraging of the technology in this field. The process sets high requirements for the electrode dispersions to be printed, which themselves exhibit a complex material behavior. At the same time, no standardized methods exist to systematically formulate electrode dispersions at minimal empirical effort. These constraints presently lead to the situation that electrode dispersions cannot be processed in a reliable and reproducible fashion.

Consequently, this dissertation is intended to contribute to gaining profound understanding in this area and to provide fundamental evidence. The overall goal is thus to elaborate a methodology to qualify electrode dispersions for the piezoelectric inkjet printing process.

## 1.2 Conceptual outline

In order to achieve the overall objective of this dissertation, fundamental proof is required that demonstrates the feasibility of processing electrode dispersions in piezoelectric inkjet printing. Based on an in-depth requirements analysis, the physical interactions between the dispersion formulation and the process conditions need to be thoroughly investigated. Particular attention is paid to the respective dispersion components and their impact on the process. Standard recommendations must be defined that specify stability ranges both for the dispersion characteristics and the process conditions. In this regard, formula-based approaches are additionally pursued that are able to reduce the empirical effort along the entire qualification process.

## 1.3 Structure

This work represents a publication-based doctoral thesis. The core contents have been summarized in five publications. Chapter 2 provides the fundamentals required for understanding this work. Chapter 3 presents the current state of the art in science and technology, leading to the problem statement and the approach in Chapter 4. Following the description of the materials and methods in Chapter 5, the content of the publications are summarized in a concise form in Chapter 6 through Chapter 10. The results are discussed in Chapter 11, reflecting the objectives defined in Chapter 4. The doctoral thesis concludes in Chapter 12 with a summary and an outlook on future research activities.



## Chapter 2

# Fundamentals

## 2.1 Chapter overview

This chapter provides the fundamentals required to understand this doctoral thesis and the terminology employed throughout this work. Section 2.1 is concerned with the relevant background knowledge on lithium-ion batteries. This is followed by an overview of the relevant physics of dispersion systems in Section 2.2. The chapter concludes with the fundamentals of the piezoelectric inkjet printing process in Section 2.3.

## 2.2 Lithium-ion batteries

### 2.2.1 Principle and characteristics

A lithium-ion battery is an interconnection of a multitude of galvanic elements, in which chemical energy is reversibly converted into electrical energy (CHO et al. 2015). The compound consists of multiple layers of porous anodes, cathodes, and separators. The electrodes are composed of active materials as well as binders, and if required, conductive additives and further additives, which are deposited onto metallic substrates (HAWLEY and LI 2019; KRAYTSBERG and EIN-ELI 2016). The active materials represent the electrochemically active components of a cell, capable of reversibly storing and releasing lithium-ions at a given time. This mechanism of inserting a lithium-ion into a layered host structure is denoted as intercalation, while the reverse process is referred to as deintercalation (MASSÉ et al. 2017). Copper and aluminum foils, which serve as current collectors, are employed on the anode and the cathode sides, respectively (KIM and CHO 2015). The separators act as electrical insulators between the electrodes (DEIMEDE and ELMASIDES 2015). A liquid electrolyte is introduced to fill the pores within the electrodes and the separators to allow for an ionic conductivity (BLOMGREN 2003). The smallest unit consisting of a single anode, a cathode, and a separator in between is referred to as a galvanic cell (ANDREA 2010) (see Figure 2.1). During discharge, the lithium-ions deintercalate from the active material particles within the anode into the liquid electrolyte and

migrate through the separator to the cathode, where they intercalate into the active material of the cathode (MASSÉ et al. 2017). Simultaneously, electrons move externally from the anode to the cathode for charge equalization while generating an electrical current, which can be drawn at the current collectors (MASSÉ et al. 2017). These processes are reversed during charging by applying an external voltage (MASSÉ et al. 2017).

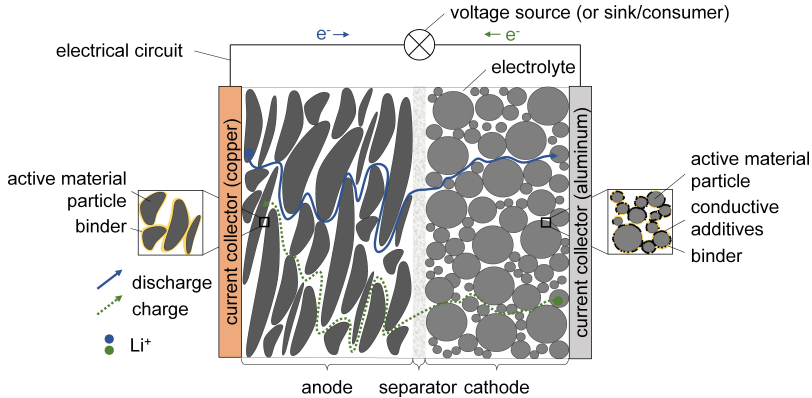
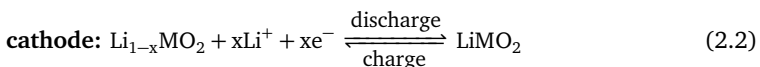
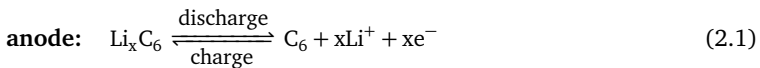


**Figure 2.1:** Schematic illustration of the main constituents and the principle of a lithium-ion battery cell; exemplary transport pathways of the lithium-ions are depicted for the discharge and charge modes; for the discharge mode, the voltage source is replaced by an electrical consumer (modified from HABEDANK (2021) and LIU et al. (2011)).

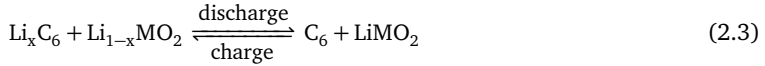
According to the electrochemical terminology, the terms anode (place of oxidation) and cathode (place of reduction) for the negative and the positive electrode apply only for the discharge mode, since reduction and oxidation are reversed during charging. However, a component-specific nomenclature has been established that also uses the terms for the charge mode (LI et al. 2018).

The reversible processes at the anode and the cathode during charging and discharging are demonstrated for the exemplary active material combination of an anode based on graphite (C) and a lithium metal oxide ( $\text{LiMO}_2$ ) as cathode. Here, the placeholder M can be adapted to the active material used, taking into account the stoichiometry. The partial reactions at the anode and the cathode occur as follows (KURZWEIL and DIETLMEIER 2018, p. 166):



$e^-$  signifies an electron and  $x$  represents the stoichiometric factor of the lithium in the reaction.

From the partial reactions, the total reversible redox reaction proceeds as follows:



### 2.2.2 Electrode and dispersion composition

The prevalent electrode components and their characteristics are briefly described below.

**Active materials** primarily define the performance characteristics of the lithium-ion battery cell (KRAYTSBERG and EIN-ELI 2016).

Carbon compounds, such as graphite in the form of natural and synthetic graphite, represent the state-of-the-art anode active materials (ASENBAUER et al. 2020). Both types have advantages and disadvantages so that an application-related selection is necessary to be pursued. Spherical graphite has a higher purity, is subject to a lower thermal expansion, and shows an improved thermal stability (MAGAMPA et al. 2013). Furthermore, it allows for paramount intercalation and deintercalation kinetics, although the initial cycles are subject to a larger incidence of irreversible processes (ALLART et al. 2018; GLAZIER et al. 2017). Due to the synthesis process, spherical graphite is more expensive than natural graphite (SCHMUCH et al. 2018). Driven by the energy transition, the demand for both types is expected to increase as lithium-ion batteries gain importance for a widespread adoption in various industries (MUNDSZINGER et al. 2017; OLIVETTI et al. 2017). Aiming at further enhancing the energy density, graphite compounds are also emerging, such as with silicon or understoichiometric silicon oxide as drop-in materials (CHAE et al. 2020).

Cathode active materials are composed of lithium transition metal compounds (WHITTINGHAM 2004). A variety of materials have already been commercialized, which can be classified on the basis of their crystal structure into oxides with a layered structure  $\text{LiMO}_2$  (with  $M = \text{Co, Mn, Ni, Al}$ ), spinels, such as lithium nickel manganese cobalt oxides  $\text{LiMn}_2\text{O}_4$  (LMO), and phosphates, such as lithium iron phosphate  $\text{LiFePO}_4$  (LFP) (ANDRE et al. 2015). For vehicle applications, the most promising active materials are lithium nickel manganese cobalt oxides  $\text{LiNi}_{1-y-z}\text{Mn}_y\text{Co}_z\text{O}_2$  (NMC) and lithium nickel cobalt aluminum oxides  $\text{LiNi}_{1-y-z}\text{Co}_y\text{Al}_z\text{O}_2$  (NCA) in different stoichiometric composition, respectively (ANDRE et al. 2015). Current developments in the field of NMC are aiming at increasing the nickel content (Ni-rich NMC) at the expense of the cobalt content. This is associated with an enhanced capacity (WU et al. 2020), coupled with reduced costs (WU et al. 2020) and an improved sustainability (YANG et

al. 2021). LFP represents one of the most mature active materials (WU et al. 2020). Despite its lower energy density compared to layered oxides, it still has a high relevance with regard to market demands (WU et al. 2020). Due to the long battery service life, the non-toxicity, and the low price, it is nowadays primarily used in the stationary sector, for portable devices, and non-fully-electric mobile applications, such as electric bicycles and hybrid electric vehicles (ELWERT et al. 2019; LIU et al. 2021). In consumer electronics, including cellular phones, notebooks, tablets, and digital cameras,  $\text{LiCoO}_2$  still has the highest market share (ELWERT et al. 2019).

**Conductive additives** are used to increase and maintain the electronic conductance of the electrodes over the lifetime (ZHANG et al. 2010). This is particularly relevant for cathode active materials, as they commonly exhibit a low electronic conductivity in the range of  $1 \cdot 10^{-3}$  and  $1 \cdot 10^{-9} \text{ S cm}^{-1}$  (WHITTINGHAM 2004). Therefore, conductive additives are routinely added to cathode dispersions, as the conductive network mitigates the low immanent electronic conductivity of the active materials (ZHANG et al. 2010). In contrast, anode active materials have a comparably high electric conductivity (ZHANG et al. 2010). However, with increasing charge and discharge cycles, the active material particles separate from each other, leaving behind inactive zones. When adding conductive additives, the electronic conductance is kept by the percolating conductive network (ZHANG et al. 2010). Furthermore, conductive additives adsorb the electrolyte, allowing a close contact between migrating ions and active material particles through the insulating binder zones (ZHANG et al. 2010). The most commonly used conductive additives are carbon nanomaterials, including carbon black, acetylene black, carbon nanofibers, and carbon nanotubes (ZHANG et al. 2010).

**Binders** ensure a good cohesion between the particulate electrode components and a strong adhesion to the respective current collectors (LINGAPPAN et al. 2021). The state-of-the-art water-compatible binder system consists of carboxymethyl cellulose (CMC) and its derivatives as well as styrene-butadiene rubber (SBR) (BRESSER et al. 2018). The combined use aims to complement the intrinsic properties of the two binders (SHIN et al. 2017). Further relevant binders for aqueous processing include polyacrylic acid (PAA) and xanthan gum (BRESSER et al. 2018).

The dispersion represents the precursor of the electrode. In addition to the electrode components, it contains solvents and volatile additives, which are briefly explained in the following.

**Solvents** represent the media, in which the electrode components are dispersed or dissolved (WOOD III et al. 2015). In the case of water-based electrode dispersions, the solvent is purified water (BRESSER et al. 2018).

**Further additives** are not routinely added to electrode dispersions. Commonly, they are employed to improve the dispersion behavior of the particulate active materials (LEE et al. 2006) or conductive additives (GONZALEZ-GARCIA et al. 2000; PORCHER et al. 2010), or to adjust the rheological properties (BITSCH et al. 2016, 2014) or the surface tension (KRAYTSBERG and EIN-ELI 2016).

### 2.2.3 Battery performance characteristics

The electrochemical behavior of lithium-ion batteries is described by the performance characteristics. The predominant parameters required for a thorough characterization are introduced below according to KURZWEIL and DIETLMEIER (2018), JULIEN et al. (2016), and BRODD (2012).

The **equilibrium voltage**  $U_0$  of a cell is determined by its cell chemistry, corresponding to the difference of the two electrode equilibrium potentials  $\Delta E_0$  (KURZWEIL and DIETLMEIER 2018, pp. 43, 170):

$$U_0 = \Delta E_0 = E_{0,\text{cathode}} - E_{0,\text{anode}}. \quad (2.4)$$

Here,  $E_{0,\text{cathode}}$  and  $E_{0,\text{anode}}$  represent the cathode and the anode potentials at equilibrium, respectively.

The **average discharge voltage**  $\bar{U}$  indicates the average voltage value over the entire discharge of a cell.

The **nominal capacity**  $Q_0$  describes the quantity of electrical charge that can theoretically be stored by the cell.  $Q_0$  is a material-specific characteristic, which is defined by the atomic structure of the active materials used and their amount employed in the cell. The **capacity**  $Q$  is the amount of electrical charge delivered by the cell under specific operation conditions.

The **charge rate** and the **discharge rate** are commonly described by the C-rate, which relates the electric current  $I$  to the nominal capacity of the cell  $Q_0$  (KURZWEIL and DIETLMEIER 2018, p. 195):

$$\text{C-rate} = \frac{I}{Q_0}. \quad (2.5)$$

The **energy** is calculated from the product of the average discharge voltage  $\bar{U}$  and the capacity  $Q$  (JULIEN et al. 2016, p. 13):

$$E = \bar{U} \cdot Q. \quad (2.6)$$

$E$  can be related either to the volume (energy density) or the mass (specific energy) of a system. At the electrode level, these characteristics predominantly depend on the type and the quantity of the active materials as well as the areal

mass loading. The energy density is further impacted by the electrode porosities and the cell design. The higher the amount of the respective active material is, the higher is the energy density. Accordingly, the energy density is negatively affected when the quantity of passive components within the electrodes is increased (GULBINSKA 2014).

The **power density** indicates the amount of electrical power, which can be charged or discharged per mass unit. The power density is primarily affected by the length of the transport pathways of the ions. Shorter ion pathways result in a faster ion exchange between the electrodes and thus in a higher power density (GULBINSKA 2014). The **rate capability** is often used to express the power density, indicating the extent to which high charge and discharge rates limit the available capacity.

The **cycle stability** describes the behavior of a cell to lose capacity with an increasing cycle number due to cyclic aging or at rest due to calendrical aging (MEISSNER and RICHTER 2005). In this context, the **coulombic efficiency**  $CE$  is a vital characteristic, which is defined as the ratio between the discharge capacity  $Q_{\text{dis}}$  and the charge capacity  $Q_{\text{ch}}$  for each cycle (JULIEN et al. 2016, p. 18):

$$CE = \frac{Q_{\text{dis}}}{Q_{\text{ch}}}. \quad (2.7)$$

The irreversible loss of capacity can occur for various reasons. In addition to mechanically-induced deterioration leading to a partial loss of cohesion or adhesion (ZHU et al. 2020), and structural evolution of the active materials over the cycles (SARRE et al. 2004), the surface reactions between the active material particles and the consumption of electrolyte lead to a considerable loss of capacity. On the anode side, a small portion of the ions reacts with components of the electrolyte, irreversibly forming a passivation layer on the surface-active materials (AN et al. 2016). The formation of this solid electrolyte interface (SEI) leads to capacity losses during the initial charge phases. Accordingly, it impedes further electrolyte decomposition upon the SEI formation and ensures cycling without further major capacity losses. Cathode materials are also subject to irreversible parasitic reactions, such as surface layer formation (BIRKL et al. 2017). Furthermore, capacity losses can be attributed to a lattice distortion of the cathode active material (JULIEN et al. 2016, p. 585). This effect can occur during the first charge cycles when lithium ions are intercalated and deintercalated. As a result, some of the ions can no longer leave the active material.

### 2.2.4 Conventional electrode production

In the literature, minor differences exist in the assignment of the process steps belonging to the electrode production. The following categorization is derived from REINHART et al. (2013) (see Figure 2.2).

The electrode production begins with the blending of the respective components to obtain a homogeneous dispersion, also referred to as slurry (KRAYTSBERG and EIN-ELI 2016). Depending on the type of electrode, a sequence of dry and wet mixing processes is applied. The dry mixing processes are needed when using active materials with a low electrical conductivity that require the addition of conductive additives. The pre-mixing of the active material particles and the conductive additive particles is essential for the formation of the conductive matrix in the final electrode (KIM et al. 1999). The average particle size of common conductive additives is about two orders of magnitude (by  $1 \cdot 10^2$ ) smaller than that of relevant active materials. Driven by the desire to reduce the surface energy, the conductive additive particles adsorb at the surface of the active material particles (KIM et al. 1999).

The as-prepared dispersions are coated on both sides of the metallic current collector foils (KWADE et al. 2018). Commonly, the top and the bottom sides of the foils are coated sequentially, followed by a respective drying step (KWADE et al. 2018). The solvents and volatile additives contained in the dispersion evaporate, leaving behind the porous electrode (BRYNTESEN et al. 2021).

Subsequently, the electrode coating undergoes a rolling process, also referred to as calendaring (BRYNTESEN et al. 2021). The electrode is intentionally compressed to achieve the desired target specific thickness and density (BRYNTESEN et al. 2021). This increases the energy density and strengthens the interparticular contact, leading to an enhanced electrical conductivity (HASELRIEDER et al. 2013).

On an industrial scale, the coating, the drying, and the calendaring step are usually implemented as continuous roll-to-roll processes, resulting in electrode coils as end products (KWADE et al. 2018).

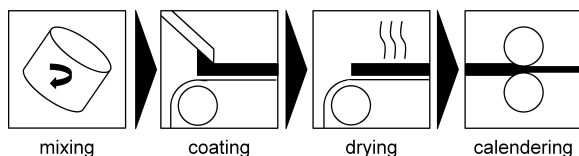


**Figure 2.2:** Process steps of a conventional electrode production process (modified from REINHART et al. (2013))

The electrode production represents the first sub-process in the production of lithium-ion batteries, followed by the cell assembly, and the cell conditioning.

### 2.2.5 Electrode structuring

The conventional electrode production without downstream processes shows stringent restrictions in achieving a customized electrode geometry and, as a result, the electrodes are typically planar (CHANG et al. 2019). The planarity causes a limited electrolyte infiltration and associated with that a sluggish lithium-ion diffusion as well as a slow lithium-ion transport through the electrolyte due to the tortuous ion paths (CHEN and XUE 2016). These drawbacks affect the cell performance, particularly at high charging and discharging rates (NING et al. 2003; SINGH et al. 2015). Furthermore, conventional cell setups necessitate a large footprint area to achieve a sufficient application-dependent capacity (CAI et al. 2018). However, the constantly growing need for small-scale functionalized products has driven the demand for cell setups with decreasing footprints (CHANG et al. 2019). Aiming at further enhancing the areal capacity, thicker electrodes are targeted to increase the material loading without compromising the rapid lithium-ion diffusion (CHANG et al. 2019). This increases the lithium-ion transport distances and simultaneously the effective ionic resistance (CHOI et al. 2013; ZHENG et al. 2012), leading to a reduced rate capability and thus an inhibited power density (BEIDAGHI and WANG 2012). Structured electrodes that are non-planar and exhibit a targeted geometry allow to alleviate this trade-off due to an extreme increase in the surface area (CHANG et al. 2019). In recent years, numerous processes have emerged to realize the fabrication of these microstructurally optimized geometries. The disruptive technologies can be either subtractive, forming, additive, or caused by a conversion of materials and are at an early stage of development. The most prevalent technologies are as follows:

- **Mechanical treatment:** This technique uses a mechanical tool, such as a pre-structured roller, to insert a surface pattern into an as-prepared electrode (SAUTER 2014).
- **Co-extrusion:** This technology allows for the generation of hole structures through a combined process of co-extrusion, assembly, and sintering (BAE et al. 2013).
- **Capillary dispersion:** This term refers to a novel type of dispersion in which a secondary fluid acts as a pore-forming agent that is evaporated during the process (BITSCH et al. 2016, 2014).
- **Laser technology:** This technology uses a laser for the targeted removal of material to create a surface pattern onto an as-prepared electrode (PFLEGING 2018).
- **Additive manufacturing:** This term summarizes the additive manufacturing technologies that allow for the thorough build-up of electrode structures (ZHANG et al. 2017; ZHU et al. 2017). The highest potential was attributed to the liquid-based processes, such as inkjet printing, direct ink writing, and aerosol jet printing.

The diversity of the technologies demonstrates the potential pertinence of electrode structuring for the competitiveness of future cell systems. Particular appeal is attributed to the additive manufacturing technologies, as these processes promise a unique design flexibility within a three-dimensional cell setup (COSTA et al. 2020), coupled with no loss of active material (ZHANG et al. 2017). In addition, these technologies allow for utilizing the space allocated for the electrochemical energy storage in the device more efficiently, which promotes the energy density (WEI et al. 2017). Despite the currently low process speeds compared to conventional lead times, additive manufacturing technologies additionally offer the potential to shorten the process chain (COBB and HO 2016).

## 2.3 Dispersion systems

### 2.3.1 Terminology and characteristics

Dispersion systems consist of at least two different phases, in particular a continuous, liquid phase and a dispersed, particulate phase (GENOVESE 2012). Precisely, if the particulate constituents are approximately between 1 nm and 1  $\mu\text{m}$  in one dimension, the dispersion is referred to as a colloidal dispersion (SLOMKOWSKI et al. 2011). Commonly, the particle size distribution of printable electrode dispersions can be found below this upper threshold. However, for reasons of simplicity, the general term dispersion is employed throughout this thesis independent of the precise particle size distribution.

The dispersion composition governs the rheological behavior, according to which these fluids are classified. Commonly, the well-established two-plate model is introduced to describe the rheological interactions (see Figure 2.3).

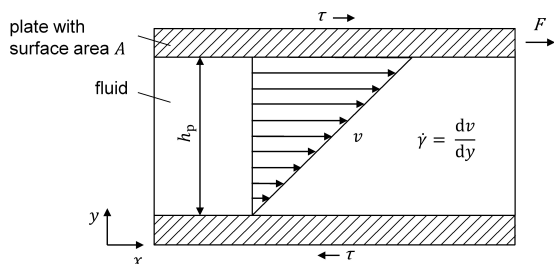


**Figure 2.3:** Two-plate model consisting of two plates with the surface area  $A$  and the distance  $h_p$  with a fluid in between; the relative motion of the plates with the velocity  $v$  in x-direction provokes a shear stress  $\tau$  and a shear rate  $\dot{\gamma}$  in y-direction (modified from LAUTH and KOWALCZYK (2016, p. 350) and HOATH (2016, p. 16))

Between the plates with the surface area  $A$  and the distance  $h_p$ , a fluid is introduced which adheres to the plates. If the plates are set in relative motion

to each other, it can be observed that the required force depends on the fluid properties. Furthermore, the force  $F$  is proportional to the surface area  $A$  and the velocity of the relative motion  $v$  and inversely proportional to the distance  $h_p$ , leading to the following definition (LAUTH and KOWALCZYK 2016, p. 349):

$$F \propto \frac{A \cdot v}{h_p} \rightarrow F = \eta \cdot \frac{A \cdot v}{h_p}. \quad (2.8)$$

Here,  $\eta$  represents the proportionality constant, also referred to as dynamic viscosity.

In motion, the adhesion of the fluid to the plates forms a shear stress and a velocity profile. The simplest case is a linear profile (see Figure 2.3), corresponding to a Newtonian fluid. No real fluid perfectly meets the definition of a Newtonian fluid. However, a multitude of common liquids and gases can be approximated as Newtonian fluids for practical applications under normal conditions. Examples of Newtonian fluids range from water and air to certain dispersions with a low particle content (BARNES 2000; TADROS 2011).

The resulting shear stress  $\tau$  is therefore defined as (LAUTH and KOWALCZYK 2016, p. 350)

$$\tau = \eta \cdot \frac{\partial v}{\partial y}. \quad (2.9)$$

In addition, the shear rate  $\dot{\gamma}$  is given by LAUTH and KOWALCZYK (2016, p. 351) as

$$\dot{\gamma} = \frac{dv}{dy}. \quad (2.10)$$

If the velocity profile does not form a linear curve, the fluids are called non-Newtonian (CHHABRA and RICHARDSON 2008, p. 5). The non-linear behavior can be classified according to the shear rate dependence and the time dependence (MEZGER 2020).

The shear-rate-dependent fluids can be further subdivided into dilatant, pseudoplastic, and Bingham plastic fluids (see Figure 2.4). The respective characteristics are discussed in more detail in the following according to TADROS (2011, pp. 40 ff.):

- **Pseudoplastic fluids (shear-thinning fluids):** The shear stress decreases inversely proportional with the shear rate. Although the underlying mechanisms are not yet fully understood, this behavior is expected to result from the microscale structural rearrangement in the fluid that facilitates the shearing. In dispersions, the behavior is caused by the phase

separation during shearing (BROWN and RENNIE 2001). In polymer solutions, the shear-thinning behavior is driven by the disentanglement of the particular polymer chains during flow (BARNES 2000, pp. 141 ff.).

- **Dilatant fluids (shear-thickening fluids):** The shear stress increases inversely proportional with the shear rate. This increase results from fluid particles, which interact more strongly with each other during the reorientation within a motion, leading to a limited movement.
- **Bingham plastic fluids:** The flow behavior is linear, as it is typical for Newtonian fluids, but the fluid is still considered as a non-Newtonian fluid due to the elastic behavior under a certain shear stress. This fluid type behaves like a liquid only above this stress.
- **Pseudoplastic fluids with a yield stress:** The flow behavior is linear as for a plastic Bingham fluid, but shows non-linear behavior below a certain shear stress.

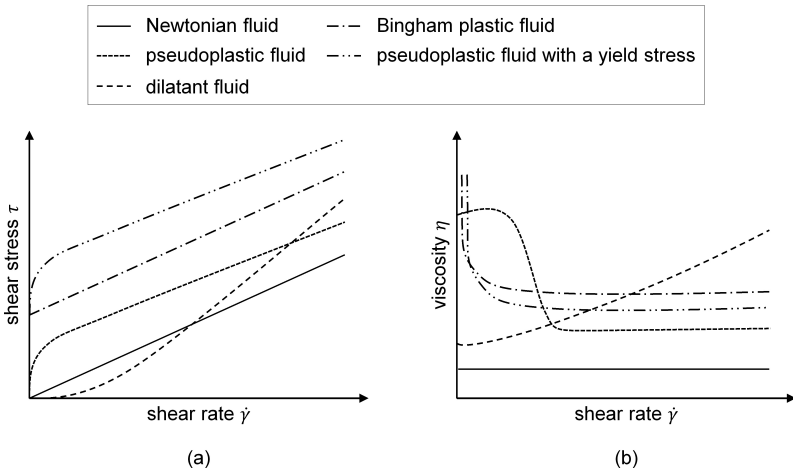


**Figure 2.4:** Shear-dependent behavior of the different types of fluids for (a) flow curves and (b) viscosity-shear-rate relationship (modified from TADROS (2011, p. 41))

The time-dependent fluid behavior can be subdivided into thixotropic and rheopectic fluids (see Figure 2.5). According to CHHABBRA and RICHARDSON (2008, pp. 18–20), they are defined as follows:

- **Thixotropic fluids:** The fluid exhibits a reduction of the structural strength during the shearing phase and a more or less rapid but complete reconstruction during the subsequent recovery phase.
- **Rheopectic fluids:** The fluid behaves in the opposite way to a thixotropic fluid. Hence, it shows an increase in the structural strength during shearing and completely reverses during the recovery phase.

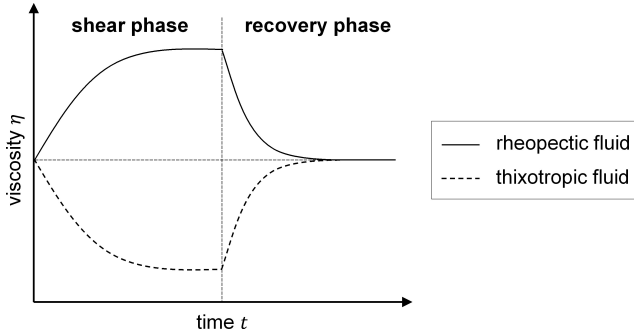


**Figure 2.5:** Time-dependent behavior of the different types of fluids (modified from RÜTTEN (2018, p. 135) and RUBIO-HERNÁNDEZ et al. (2020))

Furthermore, fluids can be classified by their material behavior (MEZGER 2020, pp. 153 ff.). Accordingly, real fluids exhibit the properties of both a viscous fluid and an elastic solid, although the strength and the interactions between the contributions vary. This behavior is referred to as viscoelasticity (MEZGER 2020, pp. 108 ff.). Thereby, the extremes are defined as follows (MEZGER 2020, pp. 108 ff.):

- **Viscous fluids:** A purely viscous material behavior causes a time-dependent, unlimited, irreversible deformation.
- **Elastic solids:** A purely elastic material is subject to a spontaneous, limited, reversible deformation.

The nature and the expression of the material behavior can be quantitatively determined using the complex shear modulus  $|G^*|$ . This key characteristic represents the ratio of the shear stress  $\tau$  to the shear strain  $\gamma$  under vibratory conditions and is defined as follows (TADROS 2011, p. 76):

$$|G^*| = G' + i \cdot G'' \quad (2.11)$$

Here,  $G'$  represents the measure for the elastic fraction of the deformation energy stored in the material during shearing (MEZGER 2020, pp. 159 ff.).  $G''$  is the loss modulus, which is defined as the deformation energy consumed during shearing and thus represents the viscous behavior (MEZGER 2020, pp. 159 ff.). The loss factor  $\delta$  represents the ratio between the loss modulus  $G''$  and the storage modulus  $G'$ , which is defined as follows (TADROS 2011, p. 76):

$$\delta = \arctan\left(\frac{G''}{G'}\right) \quad (2.12)$$

These numbers allow a finer subdivision of the substances according to their material behavior (see Table 2.1). The range of viscoelasticity includes viscoelastic liquids, viscoelastic gels or solids, and the threshold area of the sol-gel transition in between. At the sol-gel transition, the viscoelastic fluid exhibits equal shares of the viscous and the elastic behavior (MEZGER 2020, p. 214).

**Table 2.1:** Categorization of substances by their material behavior according to MEZGER (2020, p. 164)

Ideal viscous liquid	Viscoelastic liquid	Sol-gel transition	Viscoelastic gel or solid	Ideal elastic solid
$\tan \delta \rightarrow \infty$	$\tan \delta > 1$	$\tan \delta = 1$	$\tan \delta < 1$	$\tan \delta \rightarrow 0$
$G' \rightarrow 0$	$G'' > G'$	$G' = G''$	$G' > G''$	$G'' \rightarrow 0$

The practical determination of the rheological parameters is complex and follows defined measuring procedures, which are outlined below. Unless otherwise indicated, the technical explanations were derived from MEZGER (2020, pp. 33 ff., 153 ff.).

**Controlled shear rate tests** serve to determine the shear-dependent behavior of a sample. For that purpose, a defined shear rate is applied, from which the shear stress can be determined and then the viscosity derived. This measurement sequence can be used to either obtain a flow curve or the viscosity at a single shear rate, where the shear rate is either increased incrementally or kept constant at a specific value.

**Amplitude sweeps** are characterized by a gradual increase of the deflection, while the frequency is kept at a constant value. The results obtained are usually presented as a plot of the storage modulus  $G'$  and the loss modulus  $G''$  over the strain  $\gamma$  or the shear stress  $\tau$  (see Figure 2.6 a).

Amplitude sweeps allow for a determination of both the linear viscoelastic (LVE) region and the yield point as well as the flow point. The LVE region represents the range in which the test can be performed without irreversibly degrading the structure of the sample. It is characterized by the range in which both the storage modulus  $G'$  and the loss modulus  $G''$  show a constant value, also referred to as a plateau value. The yield point  $\tau_y$  marks the value of the shear stress at the limit of the LVE region. It represents the transition between the elastic and the plastic behavior. The flow point  $\tau_f$  is defined as the value of the shear stress at the intercept of the storage modulus  $G'$  and the loss modulus  $G''$ . It indicates the transition between the solid and the viscous behavior.

**Frequency sweeps** are used to analyze the time-dependent deformation behavior of a sample in the range of non-destructive deformation at a constant amplitude (see Figure 2.6 b). The short-term behavior is simulated by applying

high frequencies, whereas the long-term behavior is imitated by low frequencies. To ensure a non-destructive deformation, the shear-strain or shear-stress amplitude employed has to be within the LVE region identified in the amplitude sweep. The results obtained are usually provided as a plot of the storage modulus  $G'$  and the loss modulus  $G''$  over the frequency  $f$ .

Therefore, frequency sweeps allow for a determination of the material behavior of the investigated dispersion and thus its long-term stability (see Section 2.3.1). In addition, the relaxation time  $\lambda$  can be derived (YAN et al. 2017). This characteristic represents the duration required for dispersions to return to a more viscous state after stress (BARNES 2000; TADROS 2011). It is defined as the inverse of the frequency  $f$  at the intersection of the storage modulus  $G'$  and the loss modulus  $G''$ .

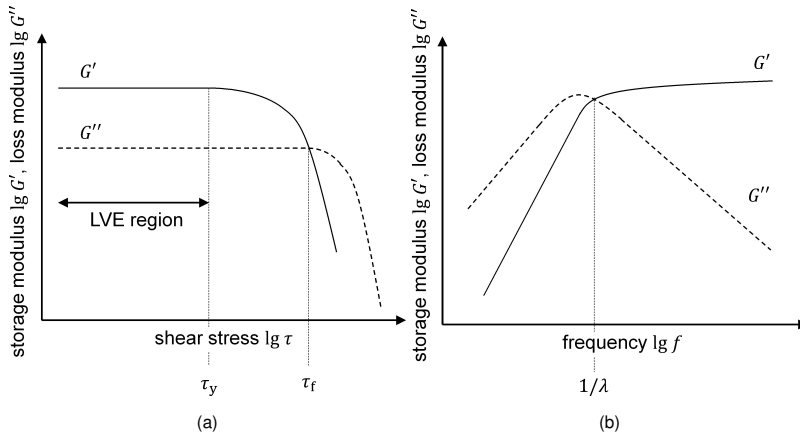


**Figure 2.6:** Schematic illustration of an arbitrary progression of the results of (a) an amplitude sweep showing the course of the storage modulus  $G'$  and the loss modulus  $G''$  over the shear stress  $\tau$  with the LVE region, the yield point  $\tau_y$ , and the flow point  $\tau_f$  and (b) a frequency sweep depicting the course of the storage modulus  $G'$  and the loss modulus  $G''$  over the frequency  $f$  with the inverse of the relaxation time  $1/\lambda$  (modified from MEZGER (2020, pp. 175, 194))

### 2.3.2 Physics of the phase boundaries

A boundary layer of charge carriers, also known as electrical double layer, forms around the particles dispersed in a solvent. This leads to a potential difference between the respective solid and liquid phases. The state-of-the-art model to describe this electrical double layer is the Bockris-Devanathan-Mueller (BMD) model, which was jointly published in 1963 by John O' Mara Bockris, Klaus Mueller, and Michael Angelo Vincent Devanathan (BOCKRIS et al. 1963). A schematic illustration of the model is given in Figure 2.7.

Compared to previously published models, the BDM model also takes into account the interactions between the solid and the solvent (LAUTH and KOWALCZYK 2016, pp. 258–260). The first solvate shell is formed by the solvent. This is followed by a solvate layer with the gravity plane, also referred to as the inner Helmholtz layer. The solvated ions in the outer Helmholtz layer, which attach directly to the inner Helmholtz layer, represent its counter-ions. The inner Helmholtz layer with the outer Helmholtz layer forms the so-called Stern layer, which is also referred to as the rigid electrical double layer. This is followed by the shear layer and then the diffuse layer, in which the charge carriers are more loosely arranged. Finally, the diffuse layer merges into the free volume.

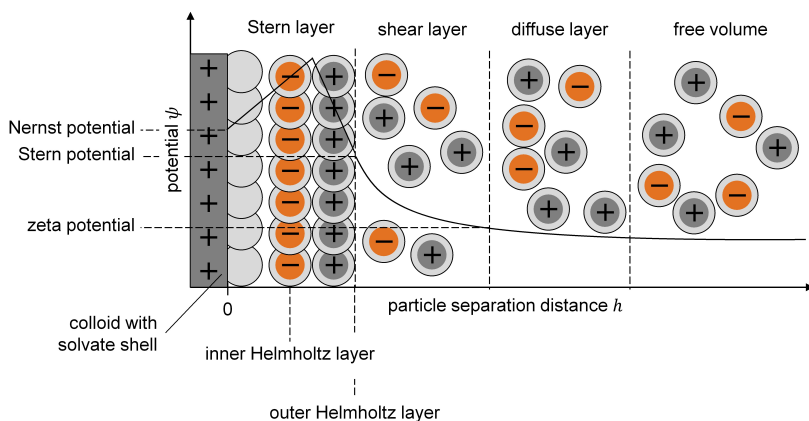


**Figure 2.7:** Schematic illustration of the BMD model (modified from LAUTH and KOWALCZYK (2016, p. 259))

The course of the potential  $\Psi$  can be described as a function of the distance to the particle surface  $h$  according to BOCKRIS et al. (1963) and LAUTH and KOWALCZYK (2016, pp. 258–260).

The surface potential, also referred to as Nernst potential, appears at the surface plane of the particle. In the area of the inner and the outer Helmholtz layer, a linear potential curve applies, as these layers are always fully occupied with charge carriers. The potential of the outer Helmholtz layer is designated as Stern potential. In the region of the shear layer and the diffuse layer, an exponential course of the potential occurs due to the exponential decrease of the solvent concentration and thus the present charge carriers. The potential prevailing at the interface between the shear layer and the diffuse layer is referred to as zeta potential. Accordingly, it represents the potential at the interface between the mobile solvent and the stationary layer of solvent remaining on the solid. As equally charged ion layers repel each other, the zeta potential also in-

icates the magnitude of the so-called electrostatic forces between the colloidal particles contained in a dispersion. The particles are thus prevented from sticking to each other and spontaneously forming irregular particle clusters. The higher the solvent concentration is, the more ions are contained in the shear layer. This results in a stronger potential drop, so that a lower zeta potential is present at the transition to the diffuse layer. The lower the zeta potential is, the less significant are the electrostatic forces (ZHU et al. 2007). As the free volume is reached, the potential decreases to its minimum.

### 2.3.3 Mechanisms affecting the stability

The term stability in the context of dispersions refers to the characteristics of a dispersion not to change or fluctuate in its properties over a period of time. Accordingly, the precise definition of the stability, in particular regarding the time duration, depends on the application of a dispersion and its specific requirements (LERCHE 2002; MCCLEMENTS 2015). In terms of the interparticle interactions, stability can be defined as the ratio of attractive and repulsive forces (LAUTH and KOWALCZYK 2016, p. 285).

Instability phenomena are related to the mechanisms that cause a migration of the particles (LERCHE 2002). The predominant instability phenomena occurring in dispersions are the following (see Figure 2.8):

- **Sedimentation:** This process describes the settling or the deposition of particles due to gravity or other forces (LAUTH and KOWALCZYK 2016, p. 169).
- **Flotation:** This phenomenon, also referred to as negative sedimentation, describes the buoyancy of particles, which is driven by density differences between the phases (LERCHE 2002).
- **Aggregation:** This mechanism comprises the effects of coagulation and agglomeration (NGUYEN and SCHULZE 2003, p. 4). While coagulation describes an irreversible process, agglomeration is assigned to a reversible process (LAUTH and KOWALCZYK 2016, p. 286). However, these terms are not used consistently throughout the literature and many different definitions exist. LAGALY et al. (1997, p. 49) even stated that the term *irreversible* should be avoided, as coagulates can also be separated under certain conditions. Furthermore, the terms agglomeration and aggregation are used synonymously without their respective meaning being discernible (NICHOLS et al. 2002). To avoid misconceptions, this thesis follows the definitions explained above.

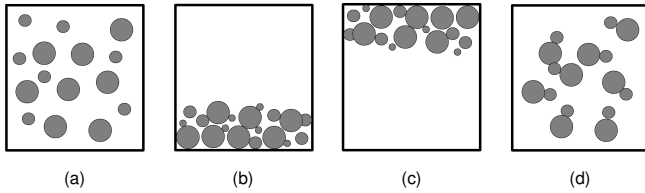


**Figure 2.8:** Instability phenomena occurring in dispersions with (a) a stable dispersion as a reference: (b) sedimentation, (c) flotation, and (d) aggregation (illustration style derived from LAGALY et al. (1997, p. 235))

There is no universal procedure to achieve a stable dispersion. The dominant effects of destabilization must be determined and counteracted. These mechanisms can be of kinetic or thermodynamic origin. Kinetic influences are predominantly driven by gravity, whereas thermodynamic ones are caused by Brownian motion (LARSSON et al. 2012). A measure of the driving factor is the Péclet number  $Pe$ , which is defined as the ratio of both effects. LARSSON et al. (2012) formulated  $Pe$  based on the derivations of LARSON (1998) as follows:

$$Pe = \frac{\Delta\rho \cdot g \cdot r_{\text{particle}}^4}{k_B \cdot T}. \quad (2.13)$$

Here,  $\Delta\rho$  represents the density difference between the dispersed and the continuous phase,  $g$  the gravitational constant,  $r_{\text{particle}}$  the particle radius,  $T$  the temperature, and  $k_B$  the Boltzmann constant.

For Péclet numbers  $> 100$ , the dispersions are referred to as non-Brownian and are dominated by gravity (RAMAYWAMY 2001). For Péclet numbers  $\ll 1$ , the particle movements are dominated by Brownian motion (MEWIS 1996; RAMAYWAMY 2001).

These dispersion types can be further characterized as follows:

- **Gravity-dominated dispersions:** This type dominates for dispersions with particles in the micrometer range or when there is a significant difference between the density of the dispersed and the continuous phases (LARSSON et al. 2012).
- **Brownian-dominated dispersions:** This type usually applies for submicron dispersions, in which the Brownian motion counteracts the gravitational sedimentation to keep the particles dispersed (LARSSON et al. 2012). The Brownian motion is a thermodynamically driven stochastic process of randomly acting movements of particles (MOERTERS and PERES 1912).

Since the particle size distribution of the raw materials used for printable electrode dispersions is in the submicron range, these dispersions are dominated by

the Brownian motion. Therefore, solely the mechanisms related to this dispersion type are discussed in more detail below.

According to LAGALY et al. (1997, p. 15), the following stabilization mechanisms are present in Brownian-dominated dispersions that counteract the occurring instabilization phenomena (see Figure 2.9):

- **Electrostatic stabilization:** This mechanism is driven by the diffusive ion layers. Equally charged ion layers repel each other, thus preventing the formation of agglomerates.
- **Steric stabilization:** This phenomenon occurs when macromolecules are attached to the particle surface by adsorption or by covalent bonds. These form shells, which cannot be moved significantly into each other and therefore keep the dispersion stable.
- **Electrosteric stabilization:** This mechanism combines both electrostatic and steric effects.

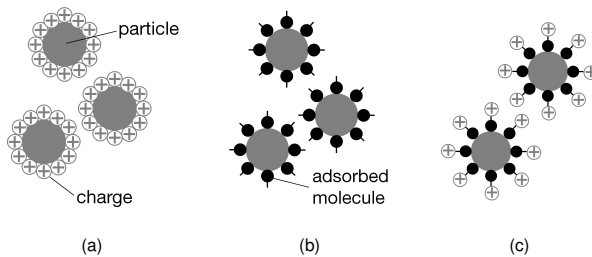


**Figure 2.9:** Stabilization mechanisms of dispersions: (a) electrostatic stabilization, (b) steric stabilization, and (c) electrosteric stabilization (modified from LAGALY et al. (1997, p. 15) and LAUTH and KOWALCZYK (2016, p. 287))

The effect of these stabilization mechanisms can be enhanced by the use of dispersants, whereby the strength strongly depends on the content (DOBIAS et al. 1999). These additives are surfactants or polymers that can stabilize the dispersion either electrostatically, sterically, or both (UEKI et al. 2018).

In case of electrostatic stabilization, the dispersant adsorbs on the particle surface and affects the electrochemical double layer. Therefore, also naturally uncharged particles can form a charge or polarization through a reaction with a dispersant (LAUTH and KOWALCZYK 2016, p. 285). In case of steric stabilization, the dispersant molecules adsorb on the particle surface, whereby parts of the dispersant reach into the solvent, leading to the spatial separation of the particles.

Furthermore, there are mechanisms that have either a stabilizing or destabilizing effect, which are briefly introduced below.

**Depletion** is caused by dissolved, non-absorbing polymer molecules that restrict the movement of the particles (LAGALY et al. 1997, pp. 147–148). However, this diffusion inhibition only comes into effect at higher polymer concentrations (LAUTH and KOWALCZYK 2016, pp. 133, 302). At low polymer concentrations, shells form around the particles, also known as depletion zones. This process is driven by the potential loss of entropy. As particles approach each other, the depletion zones overlap. This leads to an imbalance of the osmotic pressure and consequently to an aggregation of the particles (CHHABBRA and BASAVARAJ 2019, pp. 718–720).

**Structural forces** comprise both the attractive hydrophobic forces for hydrophobic surfaces and the repulsive hydration forces for hydrophilic surfaces (NGUYEN and SCHULZE 2003, p. 359). Hydrophobic means that the particle surface cannot interact or bind with water, while the opposite applies for hydrophilic (NGUYEN and SCHULZE 2003, p. 359). Generally, the resulting forces increase with the degree of hydrophobicity or hydrophilicity.

#### 2.3.4 DLVO theory

The DLVO theory represents the most established approach to mathematically describe the dispersion stability (RUSSEL et al. 1991). It was independently developed in the 1940s by DERJAGUIN and LANDAU (1941) and VERWEY and OVERBEEK (1947).

This theory explains the effects of particle interactions in dispersions by determining the potential energy between the particles. The total interaction energy  $V_T$  is a result of the entirety of the repulsive and the attractive interactions as a function of the inter-surface particle separation distance  $h$ . A schematic illustration of a typical course is given in Figure 2.10.

If the curve remains above the baseline, the repulsive forces dominate. A curve below the baseline indicates the prevalence of the attractive forces. At the particle separation distance  $h_{eb}$ , the interaction energy  $V_T$  shows a maximum, which is designated as the energy barrier. At this point, the dispersion shows the highest stability and the aggregation of particles is successfully inhibited. For particle separation distances smaller and higher than  $h_{eb}$ , two characteristic minima occur. The minimum at the particle separation distance  $h_{pri}$  is referred to as the primary minimum and the one at the particle separation distance  $h_{sec}$  is termed the secondary minimum. While the primary minimum is deep, the secondary minimum is comparatively shallow. Therefore, reaching the secondary minimum indicates a reversible aggregation process and thus agglomeration. Particles which are able to overcome the energy barrier are trapped in the primary minimum. This process is understood to be irreversible under normal conditions, therefore leading to coagulation. Hence, the height of the energy barrier indicates the degree of the stability of a dispersion.

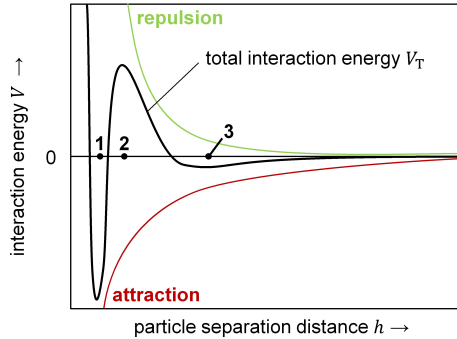


**Figure 2.10:** Schematic illustration of the DLVO theory with a typical progression of the total interaction energy  $V_T$  with 1: the particle separation distance  $h_{pri}$  at the primary minimum, 2: the particle separation distance  $h_{cb}$  at the energy barrier, and 3: the particle separation distance  $h_{sec}$  at the secondary minimum (modified from KULSHRESHTHA et al. (2010, p. 49))

According to the theory in its original form, two major forces are acting on the particles, in particular the repulsive electrostatic forces (see Subsection 2.3.2) induced by the electrochemical double layers and the attractive van-der-Waals forces. However, various studies have shown that the sole consideration of the forces postulated in the original DLVO theory is not sufficient to obtain a well-founded statement about the stability of all dispersion types (MITCHELL et al. 2005; YANGSHUAI et al. 2017). Accordingly, extensions of the DLVO theory have been elaborated over the years. The state-of-the-art extended DLVO theory also takes into account the depletion forces, the steric forces, and the structural forces, which are summarized under the term non-DLVO forces (NGUYEN and SCHULZE 2003, p. 359).

### 2.3.5 Wetting of substrates

The wettability describes the property of a liquid to spread on a solid substrate (VIANCO and FREAR 1993). It can be characterized by the degree of wetting over time until an equilibrium is maintained (HUHTAMAELKI et al. 2018). The extent can be quantitatively described by the contact angle formed at the three-phase interface between the liquid, the solid, and the gas atmosphere. This mechanism depends on a multitude of parameters, such as the type of liquid, the solid material, and the nature of the solid surface.

The fundamental law to mathematically describe the wetting of a solid substrate by a liquid is given by the Young equation (YOUNG 1805). It represents the relationship between the interfacial energies and the contact angle  $\theta$  formed at the three-phase contact point under equilibrium conditions (YOUNG 1805):

$$\cos \theta = \frac{\sigma_{sg} - \sigma_{sl}}{\sigma_{lg}}. \quad (2.14)$$

Here,  $\sigma_{sg}$  is the solid-gas interfacial energy,  $\sigma_{sl}$  the solid-liquid interfacial energy, and  $\sigma_{lg}$  the liquid-gas interfacial energy, also referred to as the surface tension of the liquid (see Figure 2.11) (YOUNG 1805).

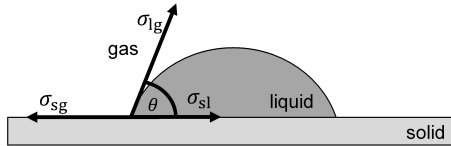


**Figure 2.11:** Schematic depiction of a liquid drop wetting a solid substrate with the contact angle  $\theta$  resulting from the interfacial energies, in particular between the solid and the gas ( $\sigma_{sg}$ ), the solid and the liquid ( $\sigma_{sl}$ ), and the liquid and the gas ( $\sigma_{lg}$ ) (modified from HUHTAMAELI et al. (2018))

Depending on the wetting angle  $\theta$ , the following wetting modes can be distinguished in theory (SIKARWAR et al. 2012):

- non-wetting:  $\theta = 180^\circ$
- partial wetting:  $0^\circ < \theta < 180^\circ$
- complete wetting:  $\theta = 0^\circ$

According to PRABHU et al. (2009) and DUVIVIER et al. (2013), for practical purposes, non-wetting is referred to the condition when  $\theta > 90^\circ$ .

The Young equation is valid only for ideal conditions, assuming that the surface of the solid is perfectly smooth and has a homogeneous texture. However, real surfaces are typically rough and thus not ideally homogeneously wettable (DUVIVIER et al. 2013; PRABHU et al. 2009).

### 2.3.6 Preparation of a stable dispersion

The preparation of dispersions is governed by the emerging solid-liquid interactions. For stable dispersions, the following mechanisms are targeted for successfully according to CONLEY (1996, pp. 31–32) and WENZEL et al. (2015):

- **Wetting:** displacement of the prevailing gas on the particle surfaces by the liquid phase
- **Layer formation:** formation of a protective layer on the particle surfaces to prevent a direct particle-particle contact
- **Deagglomeration:** spatial separation of the particles to allow for a complete encapsulation in the liquid phase

- **Homogenization:** homogeneous spatial redistribution of the particulate materials throughout the liquid phase

Furthermore, the material-specific characteristics also determine the selection of suitable mixing equipment. In particular, the following properties are paramount (CONLEY 1996, p. 214):

- **Viscosity** of both the raw materials and the target dispersion
- **Particle size and shape** of both the raw and the target particulate materials
- **Agglomeration energy** of the particulate materials

Different dispersion-specific input and target characteristics require a varying energy input and thus breakage energy. Accordingly, mixing devices differ in the amount of energy that is imparted to the system. General mixing types can be distinguished, which are explained below (see Figure 2.12) (CONLEY 1996, pp. 214–255).

**Impeller mixers** are characterized by a propeller-shaped shaft that is rotated closely below the dispersion surface. The design of the shaft can vary greatly and has to be selected with regard to the viscosity (DICKEY and FASANO 2004).

**Ball mills** are suitable dispersers for high-viscosity systems with medium energy consumption. The dispersion is filled into a hollow cylinder along with the grinding media and rotated around its axis. The grinding media are the balls, which can comprise of various abrasion-resistant materials. The energy imparted to the dispersion can be precisely regulated by adjusting the ball size as well as the ball density, the rotational speed, and the mill diameter.

**Stirred-media mills** were designed for dispersing superfine pigments in systems with low or medium viscosity. They consist of a vertically or horizontally arranged, usually cylindrical vessel, which is filled with grinding media and the dispersion (TAYLOR et al. 2020). The momentum is achieved by an impeller.

**Vibratory mills** were developed to disperse superfine pigments in high-viscosity systems with non-thixotropic behavior. For comminution, a vertically or horizontally orientated vessel filled with the grinding media and the dispersion is vibrated.

**Ultrasonic treatment** represents the most energy-intensive procedure for deagglomeration. Sound waves from an ultrasonic transducer cause pressure differences in the dispersion that cause the generation of air bubbles. This phenomenon is also called cavitation. At the cavitation interface, a high pressure and temperature arise locally. This causes an immediate separation of adjacent particles.

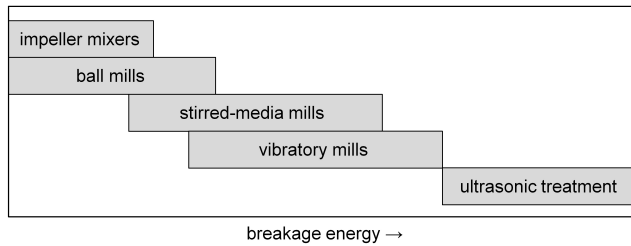


**Figure 2.12:** Schematic illustration of the mixing device classes and their typical breakage energy range (modified from CONLEY (1996, p. 214))

## 2.4 Piezoelectric inkjet printing

### 2.4.1 Principle of the process

According to DIN EN ISO/ASTM 52900, the piezoelectric inkjet printing process (abbreviated form used in this dissertation: inkjet printing) is assigned to the material jetting category, in which individual drops of a liquid feedstock material are selectively deposited to form a desired part geometry. It represents the most widely used process of the discontinuous drop-on-demand (DoD) technologies (SOUSA et al. 2015). Accordingly, drops are only generated when they are required (LANCEROS-MÉNDEZ and COSTA 2018, pp. 38–41).

The piezoelectric inkjet printing process follows the typical layer-by-layer principle of the additive manufacturing technologies. The particular process steps are described by DERBY (2010).

First, the dispersion is deposited drop by drop onto a substrate by the print head (see Figure 2.13). The substrate is usually a metal or plastic foil. For the electrode production, the respective current collector foils for the anode and cathode side are used. To compensate for the waviness and the curling of the foils and thus to allow for a homogeneous layer application, the foils can be fixed by a vacuum plate. The print head is fed by a reservoir containing the dispersion to be processed. Due to the intentionally set overlap, the drops fuse into a continuous layer structure. Subsequently, the fabricated layer is solidified by a light source, whereby the mechanism of this depends on the dispersion type. Widely used types for technical applications include dispersions containing photosensitive monomers, such as acrylic monomers, or aqueous dispersions. The polymer-based dispersions are cured by polymerization, which is typically initiated by ultraviolet light (MENDES-FELIPE et al. 2019). Water-based dispersions are dried by evaporating the excess water, which is commonly achieved by infrared radiation (MAGDASSI 2010). Subsequently, the print head is elevated in the z-direction by the thickness of one layer. These process steps are repeated until the entire part structures are formed.

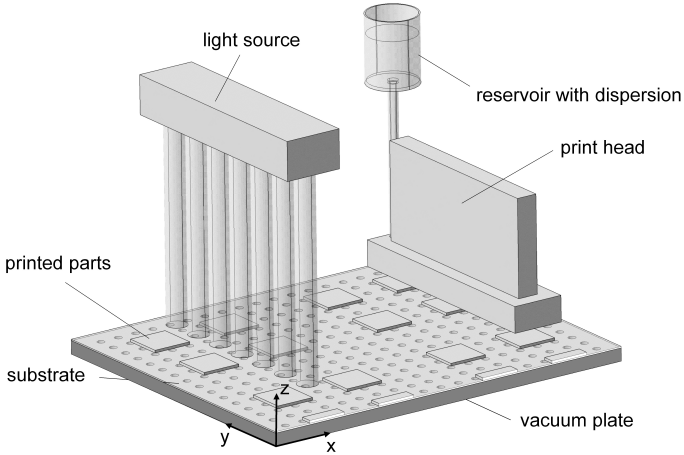


**Figure 2.13:** Principle of the piezoelectric inkjet printing process

### 2.4.2 Principle of the print head

Commonly, a print head consists of a multitude of nozzle channels that are capable of ejecting drops. For simplicity, the principle is explained for one single nozzle channel activated by a piezoelectric actuator. The main constituents are described by TEKIN et al. (2008) (see Figure 2.14).

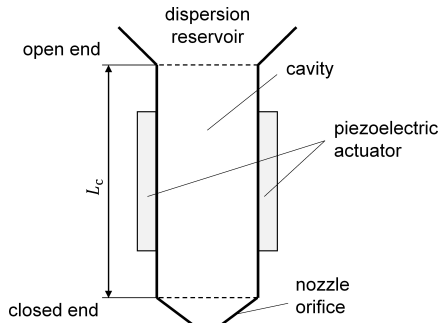


**Figure 2.14:** Schematic illustration of the main constituents of a print head nozzle channel (modified from TEKIN et al. (2008))

The nozzle channel is a fine cavity of the length  $L_c$  with a nozzle orifice at one end, also referred to as the closed end. Through the larger so-called open end, the cavity is supplied with the dispersion. The cavity is enclosed by a piezoelectric actuator. This device is capable of efficiently and accurately transferring electrical input energy into motion through electromechanical coupling (GAO et

al. 2020). Applying an electrical voltage to these piezoelectric materials forces them to expand or compress.

ALAMÁN et al. (2016) outlined the mechanisms occurring in the nozzle channel for the simplest case of a trapezoidal voltage excitation of the piezoelectric actuator (see Figure 2.15).

The voltage increase causes the piezoelectric actuator to deform outwards, resulting in a negative pressure wave in the dispersion. This pressure wave splits into two waves with half of the initial amplitude, propagating in the opposite directions towards the closed and the open end of the cavity. According to the acoustic wave theory, different conditions apply for the cavity boundaries. The nozzle end is assumed as closed, as the nozzle orifice is small compared to the cross-sectional area of the cavity. The open end is considered as open, since the diameter of the reservoir is significantly larger than that of the cavity. Accordingly, the pressure wave that is reflected from the closed end retains its phase. Simultaneously, the wave reflected from the open end is subject to a phase shift. When these pressure wave impulses meet in the middle of the cavity length, the waves superimpose. As the voltage across the piezoelectric actuator decreases, it deforms radially inward, causing an overpressure in the dispersion. This results in a wave with a positive amplitude, which splits into two waves moving in opposite directions. For the reflection at the respective ends of the cavity, the same boundary conditions apply as for the initial waves. The superimposition of these respective waves results in a positive pressure wave, which moves in the direction of the nozzle orifice. If the kinetic energy of the wave is sufficiently high, the dispersion can overcome the surface tension and is released from the nozzle. This process is also known as dispensing (CLASEN et al. 2012).

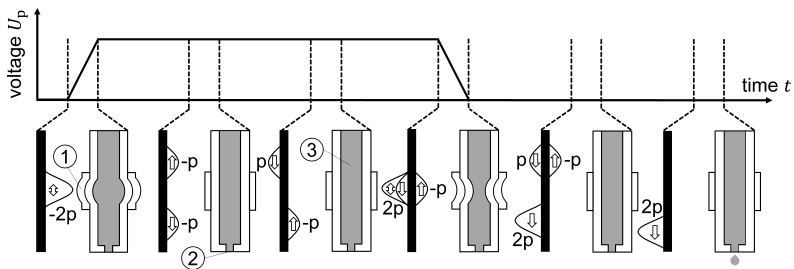


**Figure 2.15:** Schematic depiction of the generation, the propagation, and the reflection of a pressure perturbation  $p$  upon the application of a trapezoidal voltage application  $U_p$  with 1: piezoelectric actuator, 2: nozzle orifice, and 3: cavity (modified from ALAMÁN et al. (2016))

Consequently, the dispensing operation is a complex process during which the piezoelectric actuator, the dispersion, and the nozzle react with one another (JIAO et al. 2021). The process conditions are governed by parameters that can be easily adjusted, and system specifications, which are difficult to alter.

The key adjustable parameters encompass the voltage  $U_p$  and the frequency  $f$ , which reflects the number of piezoelectric excitations within a certain time (WIJSHOFF 2010). The nozzle diameter  $d_{\text{nozzle}}$  represents the predominant print head property, which is inherent to the print head system employed (WIJSHOFF 2010).

### 2.4.3 Potentials and restrictions

The application of the piezoelectric inkjet printing process provides unique potentials, but is also associated with restrictions. The particular aspects are addressed in more detail in the following.

#### Potentials

The predominant opportunities offered by the piezoelectric inkjet printing process are as follows:

- **High degree of design freedom:** The technology is able to create complex part geometries without the necessity for tools, moulds, or dies. Furthermore, there is hardly any direct relationship between the product complexity and the manufacturing costs, as the design does not determine the complexity of the production steps. This is also referred to as „complexity for free“ (GIBSON et al. 2015, p. 7).
- **Superior printing resolution:** The process allows for a precise ejection and deposition of drops through the fine nozzles. This results in an excellent print quality, whereby the achievable resolution depends directly on the nozzle geometry, in particular the diameter of the nozzle orifice (WIJSHOFF 2010). Depending on the dispersions and substrates used, the drop volume can range from pL to  $\mu\text{L}$ , leading to printing resolutions between 100 dpi and 5000 dpi (LANCEROS-MÉNDEZ and COSTA 2018, p. 38). The wet-layer thicknesses that can be achieved are between 50 nm and 10  $\mu\text{m}$  (LANCEROS-MÉNDEZ and COSTA 2018, p. 38).
- **High flexibility and customization:** Since the production is based on a computer-aided design model, the part geometries can be adjusted with low costs and time expenditure (GIBSON et al. 2015, p. 40). This results in a low lead time, which shortens the time-to-market and offers an economical individualized production for each customer (WOHLERS et al. 2021).
- **Excellent multi-material capability:** The fabrication of parts composed of various dispersions can be enabled by using multiple print heads and associated dispersion reservoirs (ABBEL et al. 2014). Furthermore, the particular dispersions can consist of a multitude of different raw materials (GUO et al. 2017).

### Restrictions

Despite the enormous potentials of the piezoelectric inkjet printing process, there are restrictions that impede the leveraging of the technology. The primary drawbacks are as follows:

- **Highly challenging and low-standardized processes for dispersion formulation:** The process places challenging demands on the dispersion to be processed. The dispersion is required to exhibit a high temporal stability to avoid agglomeration and sedimentation. Otherwise, the drop formation and the deposition are influenced negatively and the risk of nozzle clogging and bridging is increased (DERBY and REIS 2003; GUO et al. 2017). The particle size of the powdered raw materials is directly limited by the nozzle orifice diameter, whereby varying thresholds can be found in the literature. DERBY and REIS (2003) stated that the particle diameter should be  $1/20$  compared to the diameter of the nozzle orifice. HUTCHINGS and MARTIN (2012) specified a threshold value of  $1/10$ . GUO et al. (2017) defined a limit value for the particle diameter of  $1/50$  to  $1/20$  of the diameter of the nozzle orifice. In addition, a stable drop formation and drop deposition, and thus the printability, must be achieved by adjusting the dispersion properties to the print head characteristics (CLASEN et al. 2012). This qualification process is even more challenging for non-Newtonian fluids, as hardly any standards exist to fully describe the fluid dynamic behavior and thus to prepare suitable formulations (CLASEN et al. 2012).
- **Currently higher costs:** Due to the comparatively high novelty of the process in diverse industries and the related low market penetration, the application of the technology is associated with higher costs than other technologies that allow for the same or a similar value-adding. Scalability opportunities have not yet been fully exploited to be competitive in demanding industries (ABBEL et al. 2014). Furthermore, the technology necessitates the use of materials which meet the stringent requirements, such as restrictions regarding the particle size (LANCEROS-MÉNDEZ and COSTA 2018).



## Chapter 3

# State of the art in science and technology

## 3.1 Chapter overview

This chapter provides an analysis of the state of the art related to this work. Section 3.1 summarizes the previous achievements in the inkjet printing of electrode dispersions. Section 3.2 assesses the approaches to modeling the dispersion stability on the basis of the extended DLVO theory and their previous applications. Section 3.3 contains the results of the review of the previous studies in the qualification of non-Newtonian fluids for the inkjet printing process, with a focus on the drop formation and the drop deposition. Particular emphasis is placed on the existing formulaic relationships.

For reasons of comprehensibility, the notations of the formula symbols have been standardized. Accordingly, some of the formula symbols used differ from those employed in the original references.

## 3.2 Inkjet printing of water-based electrode dispersions

### 3.2.1 Composition of the dispersions

Electrode dispersions are solid-liquid systems that contain numerous components (KRAYTSBERG and EIN-ELI 2016; WENZEL et al. 2015) (see Section 2.2.2). The interplay of these constituents decisively affects the processability, usually causing a non-Newtonian behavior of the overall dispersion (LANCEROS-MÉNDEZ and COSTA 2018). This complex behavior is strongly determined by the dispersion composition and the proportional share of the respective components (CUSHING et al. 2021; KRAYTSBERG and EIN-ELI 2016). The previous studies concerned with printable aqueous electrode dispersions were examined in terms of these characteristics and are summarized in the following. An overview of the materials employed is provided in Table 3.1.

ZHAO et al. (2006) prepared anode dispersions with tin oxide ( $\text{SnO}_2$ ), acetylene black, two different hyperdispersants, in particular CH10B and CH12B, and the binder sodium carboxymethyl cellulose (SCMC). A mixture of deionized

water, ethanol, iso-propylalcohol, triethanolamine, and diethylene glycol served as a solvent. In a subsequent study, ZHAO et al. (2009) demonstrated that the components in a similar composition are applicable to anode dispersions based on lithium titanate oxide  $\text{Li}_4\text{Ti}_5\text{O}_{12}$  (LTO) (ZHAO et al. 2009).

DELANNOY et al. (2015) prepared water-based cathode dispersions with LFP, carbon black, and poly-acrylic-co-maleic acid (PAMA), which functioned both as a binder and a dispersant.

GU et al. (2015) synthesized aqueous cathode dispersions containing LFP, carbon black, the binder SCMC, and the surfactant TX-100. Hydrochloric acid (HCl) or sodium hydroxide (NaOH) were added to adjust the pH value of the dispersion. Glycerin was used to achieve the target viscosity for printing.

**Table 3.1:** Overview of the compositions of printable electrode dispersions described in literature; N/A: data not available; the dispersant and binder content is related to the employed amount of particulate materials.

Reference	Active material	Conductive additives	Dispersant	Binder	Solid content
	in m%	in m%	in m%	in m%	in m%
<b>Anodes</b>					
ZHAO et al. (2006)	N/A	N/A	N/A	N/A	N/A
ZHAO et al. (2009)	N/A	N/A	N/A	N/A	N/A
<b>Cathodes</b>					
HUANG et al. (2008)	95.24	4.76	0.95	0.48	N/A
DELANNOY ET AL. (2015)	89.50	10.50		5.26	10.0
GU et al. (2015)	88.90	11.11	N/A	11.11	5.0

### Interim conclusion

Despite the burgeoning interest in recent times, very few studies have been devoted to the inkjet printing of aqueous electrode dispersions up to now. This is elucidated by the small number of active material systems that have already been demonstrated. It becomes apparent that the state of the art is not only deficient in novel promising next-generation material systems, but also in commercialized compounds. The previous studies were primarily concerned with cathode dispersions. In contrast, anode dispersions, especially those based on graphite, have not yet been explored. Apart from the material selection, the publications indicate that the dispersion composition significantly depends on the active material system employed. In particular, it can be recognized that the dispersant and the binder contents strongly vary across the studies.

### 3.2.2 Preparation of the dispersions

The preparation of electrode dispersions through a sequence of mixing techniques represents a key process step within the electrode production chain (WENZEL et al. 2015). It governs the morphology of the electrode and thus the network that forms between the active materials, the conductive additives, and the binders (WENZEL et al. 2015). Aiming at a robust network that ensures a persistent ionic exchange and electric contacting as well as mechanical stability, a superior homogeneity and a targeted incorporation of the respective materials into the dispersion system is pursued (WENZEL et al. 2015).

The particular mixing procedures employed depend on the particular electrode compositions and the specifications of the subsequent processing method (BITSCH et al. 2014; WENZEL et al. 2015). Due to the strict printing requirements, the preparation routes of these electrode dispersions differ considerably from conventional process chains. The studies dealing with the synthesis of aqueous electrode dispersions suitable for inkjet printing are summarized below. An abstracted overview of the respective preparation routes is given in Figure 3.1.

ZHAO et al. (2006) and ZHAO et al. (2009) first dispersed the active material in the solvent, which contained the dispersant, by ball milling. Concurrently, the conductive additives were ball milled with the dispersant and the solvent. The as-prepared mixtures were blended and the binder was added. This was followed by an ultrasonication procedure. Lastly, the dispersion was aged and the sediment was removed.

HUANG et al. (2008) started with the ultrasonic dispersion of the active material and the dispersant in the solvent. The conductive additives and the binder were successively added to the as-prepared dispersion, followed by another ultrasonic treatment and a subsequent aging.

DELANNOY et al. (2015) dispersed all components in the solvent through magnetic stirring. This was followed by a ball milling procedure.

GU et al. (2015) started with the dry mixing of the solid components and then dispersed them in solvent solutions of varying pH value. Subsequently, the dispersions were centrifuged to remove large particles. Lastly, further additives were added to the as-prepared dispersion.

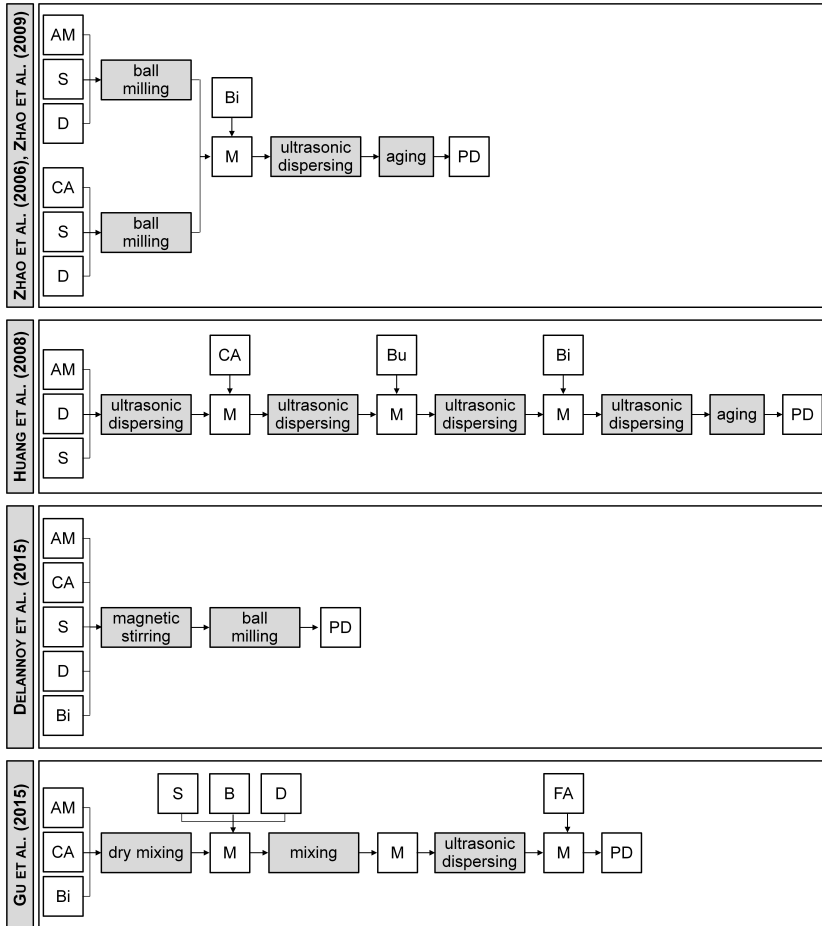


**Figure 3.1:** Summary of the preparation routes of electrode dispersions suitable for inkjet printing in literature with AM: active material, CA: conductive additives, Bi: binder, S: solvent, D: dispersant, BU: buffer, FA: further additive, M: mixture, and PD: printable dispersion

### Interim conclusion

The mixing techniques and their sequence govern the dispersion properties and thus the printability, which in turn affects the morphology and the performance characteristics. However, the number of existing scientific research papers dealing with the synthesis of printable electrode dispersions is low. The preparation route employed is often only a marginal issue and thus only roughly explained. No standardized procedure can be identified across the relevant publications. This indicates that the impact of preparation techniques and their sequence

on the dispersion qualities is often underestimated. In particular, it becomes apparent that the effect of different energy levels induced by different mixing techniques is not thoroughly understood. Furthermore, little attention was directed to the emerging interfaces in the dispersion system, which are primarily determined by the mixing sequence.

### 3.2.3 Reliable processability

The print head places high requirements on the electrode dispersions to be processed (CHANG et al. 2019; TEICHLER et al. 2013). The stability and the printability are considered as vital prerequisites for a reliable processability. To meet the stringent requirements, a systematic dispersion formulation is expected to be of paramount importance (SOUSA et al. 2015; ZHANG et al. 2017).

However, the only thorough approach to qualify a printable electrode dispersion for inkjet printing is given by DELANNOY et al. (2015). They pursued a fully empirical approach. Three dispersions with completely different compositions were preselected, whereby the solid content was kept constant at 10 m%. First, the stability behavior was analyzed through an oscillation test, in which both the amplitude and the frequency were kept constant. The storage modulus  $G'$  and the loss modulus  $G''$  were measured over time to analyze the time-dependent material behavior. With reference to the rule of thumb  $G' > G''$ , one dispersion was predicted to be stable. Subsequently, the pristine dispersion compositions were examined for printability. Controlled shear rate tests were performed to determine the flow behavior. The authors observed that all dispersion compositions show a shear-thinning behavior. Furthermore, they recognized that the degree of shear-thinning depends on the type of polymer contained in the dispersion. The controlled shear rate tests also allowed to determine the viscosity at drop ejection for each dispersion. Therefore, it was assumed that the ejection shear rate is  $\geq 1 \cdot 10^4 \text{ s}^{-1}$ . The viscosity specified by the system was set as an upper limit. The dispersion compositions that were below the limit were classified as printable and the others as non-printable. For validation, the dispersions were subjected to printing. The dispersion being both stable and printable was identified to be processable. The process reliability was not further investigated. GU et al. (2015) performed a few stability studies before processing one dispersion composition with a solid content of 5 m%. The contents of the respective components have been set initially, except for the dispersant. The particle size distribution was analyzed as a function of the dispersant content and the pH value of the solution. The authors observed that the use of a dispersant leads to a considerable reduction in the particle size distribution below the upper limit of 100  $\mu\text{m}$ . Accordingly, the particle size distribution met the limitations imposed by the print head geometry. Furthermore, they reported that the pH value of the solution affects the shape of the particle size distribution.

### Interim conclusion

The requirements arising from a specific print head were insufficiently consolidated. In addition, the interactions between the dispersion compositions and the overall dispersion characteristics are not well understood. Little attention was paid to the non-Newtonian behavior of electrode dispersions and the associated aggravating effects on the printability. Accordingly, very few authors presented a systematic approach to identify suitable dispersion compositions, while leaving some key characteristics out of consideration. A further aspect absent from all publications is the validation of a stable drop formation and drop deposition of the proposed dispersion compositions. Lastly, another area in which additional effort is required, is the a-priori evaluation of the stability and the printability behavior through models and number-based (formulas-based) methods. This demonstrates that the impact of a suitable dispersion formulation on the process reliability is often insufficiently understood and underestimated.

### 3.2.4 Characteristics of the printed electrode layers

Electrode layers are typically characterized electrochemically to determine the battery performance and mechanically to gain insight into their adhesion and cohesion behavior. In this context, the electrochemical characterization provides evidence of the functionality of the electrodes and allows for a benchmarking of the parameters.

The research groups introduced in Section 3.2.1 to Section 3.2.3 conducted electrochemical tests on printed unstructured electrode layers, which were generated from the prepared electrode dispersions. They demonstrated the viability of the printed samples by performing rate capability tests. The pertinent information on the specific capacity is provided in Table 3.2. Furthermore, a low coulombic efficiency was observed for the anode layers during the initial charge-discharge cycle. This was attributed to the significant SEI losses due to the enlarged total surface area of the employed nanosized active material. The *CE* reported for SnO<sub>2</sub> was 28.1% (ZHAO et al. 2006) and for LTO 18.8% (ZHAO et al. 2009).

### Interim conclusion

The characterization of electrode layers allows to prove the viability and the durability of electrode layers. Due to the pioneering character of the previous studies, they were primarily intended to demonstrate the feasibility, rather than to thoroughly benchmark the results. Accordingly, there are major gaps in the state of the art that have not yet been explored. Among other things, this includes the impact of the dispersion composition on the electrochemical and the mechanical characteristics, the latter not having been researched at all.

**Table 3.2:** Overview of the specific capacity values obtained for the printed electrode layers reported in literature

Reference	Active material	Specific capacity
<b>Anodes</b>		
ZHAO et al. (2006)	SnO <sub>2</sub>	812.7 mAh g <sup>-1</sup> at 33 μA cm <sup>-2</sup>
ZHAO et al. (2009)	LTO	128 mAh g <sup>-1</sup> at 0.5C
<b>Cathodes</b>		
HUANG ET AL. (2008)	LCO	120 mAh g <sup>-1</sup> at 180 μA cm <sup>-2</sup>
DELANNOY ET AL. (2015)	LFP	80 mAh g <sup>-1</sup> at 9C, 70 mAh g <sup>-1</sup> at 90C
GU et al. (2015)	LFP	129.9 mAh g <sup>-1</sup> at 0.1C (aluminum foil), 151.3 mAh g <sup>-1</sup> at 0.1C (carbon nanotube paper)

### 3.3 Modeling of the dispersion stability using the DLVO theory

#### 3.3.1 Modeling approaches

The DLVO theory in its original form only takes into account the attraction caused by the van-der-Waals interaction energy  $V_{\text{vdw}}$  and the repulsion effects due to the electrostatic double layer interaction energy  $V_{\text{el}}$  (VERWEY and OVERBEEK 1947). This leads to the expression for the total interaction energy  $V_{\text{T}}$  (ISRAELACHVILI 2011, p. 57):

$$V_{\text{T}} = V_{\text{el}} + V_{\text{vdw}}. \quad (3.1)$$

The extended DLVO theory additionally regards the interaction energies based on the non-DLVO forces, in particular the hydrophobic interaction energy  $V_{\text{hyd}}$ , the depletion interaction energy  $V_{\text{dep}}$ , and the steric interaction energy  $V_{\text{s}}$ . In colloid stability theory, it is commonly assumed that the fractions of both the DLVO theory and the extended DLVO theory are independent (SEEBERGH and BERG 1994). Therefore, a good approximation of the total energy is given by summing up the energy fractions. Accordingly, the total energy  $V_{\text{T,ex}}$  obeys the following equation (ISRAELACHVILI 2011, p. 57):

$$V_{\text{T,ex}} = V_{\text{el}} + V_{\text{vdw}} + V_{\text{hyd}} + V_{\text{dep}} + V_{\text{s}}. \quad (3.2)$$

A schematic overview of the respective interaction energy curves is given in Figure 3.2. The existing models to describe the respective interaction fractions are outlined below. A holistical approach of the entirety of interaction fractions has not been published so far.

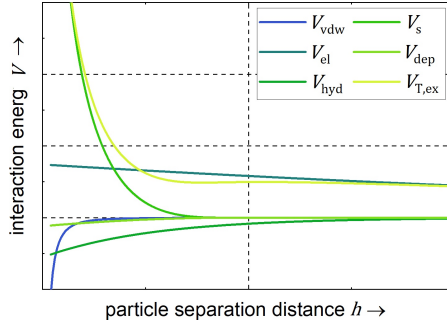


**Figure 3.2:** Schematic depiction of the energy fractions of the extended DLVO theory as a function of the particle distance  $h$ ; the total interaction energy  $V_{T,ex}$  results from the summation of the electrostatic double layer interaction energy  $V_{el}$ , the van-der-Waals interaction energy  $V_{vdw}$ , the hydrophobic interaction energy  $V_{hyd}$ , the steric interaction energy  $V_s$ , and the depletion interaction energy  $V_{dep}$  (principle modified from KUMAR et al. (2019) and ZHANG and ZENG (2021)).

### Electrostatic double layer interaction

The most established model to describe the energy resulting from the electrostatic double layer interaction  $V_{el}$  is given by the Poisson-Boltzmann equation. This model aims to determine the distribution of the electrostatic potential in an ionic medium as a function of the position relative to the charged particle surface.  $V_{el}$  can be formulated as (NGUYEN and SCHULZE 2003, p. 332)

$$V_{el} = \frac{\pi \epsilon \epsilon_0 r_{particle,1} r_{particle,2}}{r_{particle,1} + r_{particle,2}} [4\psi_1 \psi_2 \operatorname{atanh}(e^{-\kappa h}) + (\psi_1^2 + \psi_2^2) \ln(1 - e^{-2\kappa h})], \quad (3.3)$$

where  $r_{particle,1}$  and  $r_{particle,2}$  represent the radii of the particles and  $\psi_1$  and  $\psi_2$  the surface potentials of the particles.  $\epsilon_0$  is the permittivity of the vacuum and  $\epsilon$  the dielectric constant of the medium.  $\kappa$  is designated as the Debye constant. It describes the thickness of the electrostatic double layer and can be calculated as (NGUYEN and SCHULZE 2003, p. 324)

$$\kappa = \left\{ \frac{e^2 \sum_{i=1}^{\infty} n_i z_i^2}{\epsilon \epsilon_0 k_B T} \right\}^{1/2}, \quad (3.4)$$

where  $n_i$  represents the electrolyte concentration of the type  $i$  in the dispersion with the valence  $z_i$ , and  $k_B$  is the Boltzmann constant. For water at a temper-

ature  $T$  of 298.15 K (25 °C), the Debye constant is commonly determined as a function of the ionic strength  $I_s$  (NGUYEN and SCHULZE 2003, p. 324):

$$\kappa = 3.288\sqrt{I_s}. \quad (3.5)$$

The accuracy of the Poisson-Boltzmann equation was found to be sufficient down to particle separations of a few nanometers (PASHLEY et al. 1985). Owing to the assumptions made within the original DLVO theory,  $V_{el}$  relies on constant surface potentials (DERJAGUIN and LANDAU 1941; VERWEY and OVERBEEK 1947). Due to this approximation,  $V_{el}$  is accurate only for low surface potentials (< 25 mV) and for small particle separations (< particle radius). However, it has been demonstrated that this approximation is valid for surface potentials between 0 and 50 mV (NGUYEN and SCHULZE 2003, pp. 323–333).

#### van-der-Waals interaction

The most widely used model to describe the interaction energy from the van-der-Waals forces  $V_{vdw}$  is based on the theories of Hamaker (ISRAELACHVILI 1992). For two spherical particles,  $V_{vdw}$  can be defined as follows (NGUYEN and SCHULZE 2003, p. 300):

$$V_{vdw} = -\frac{A_{132}}{6} \left\{ \frac{2r_{\text{particle},1}r_{\text{particle},2}}{r^2 - (r_{\text{particle},1} + r_{\text{particle},2})^2} + \frac{2r_{\text{particle},1}r_{\text{particle},2}}{r^2 - (r_{\text{particle},1} - r_{\text{particle},2})^2} + \ln \frac{r^2 - (r_{\text{particle},1} + r_{\text{particle},2})^2}{r^2 - (r_{\text{particle},1} - r_{\text{particle},2})^2} \right\}. \quad (3.6)$$

$r$  stands for the inter-center separation distance of the two spheres.  $A_{123}$  represents the Hamaker constant of the dispersion, which can be calculated by combining the constants of the individual particles and the medium (NGUYEN and SCHULZE 2003, p. 300):

$$A_{132} = A_{12} + A_3 - A_{13} - A_{23} = (\sqrt{A_1} - \sqrt{A_3})(\sqrt{A_2} - \sqrt{A_3}). \quad (3.7)$$

Here, the indices 1 and 2 represent the individual particles, whereas the index 3 stands for the continuous phase. Double indices indicate the combination of the Hamaker constants of mixtures (NGUYEN and SCHULZE 2003, p. 300).

However, the interaction is subject to an effect caused by the finite propagation of the electromagnetic waves in the materials, also referred to as electromagnetic retardation (GREGORY 1981). This effect mitigates the van-der-Waals interaction, as reported by SCHENKEL and KITCHENER (1960) as well as GREGORY (1981). To account for this influence, the effective Hamaker constant is introduced (ANANDARAJAH and CHEN 1995; PRIEVE and RUSSEL 1988). In this context, PAILTHORPE and RUSSEL (1982) demonstrated that the application of the effective Hamaker constant yields approximately the same result as the cal-

culation based on the continuum theory postulated by Lifshitz (MAHANTY and NINHAM 1977). Accordingly, NGUYEN and SCHULZE (2003) formulated an approximation of the effective Hamaker constant  $A_{132}$ , in which it is divided into a zero frequency part  $A_{132}^0$  and a non-zero frequency part  $A_{132}^\zeta$ . NGUYEN and SCHULZE (2003, p. 313) postulated that for most minerals the zero-frequency part  $A_{132}^0$  can be approximated as follows:

$$A_{132}^0 = \frac{3k_B T}{4}. \quad (3.8)$$

The non-zero frequency part  $A_{132}^\zeta$  is described by (NGUYEN and SCHULZE 2003, p. 310)

$$A_{132}^\zeta = \frac{3\hbar\omega}{8\sqrt{2}} \frac{(B_1 - B_3)(B_2 - B_3)}{(B_1 + B_3)\sqrt{B_2 + B_3} + (B_2 + B_3)\sqrt{B_1 + B_3}}. \quad (3.9)$$

Here,  $\hbar$  is the Planck's constant divided by  $2\pi$  and  $\omega$  is the characteristic relaxation frequency of the ultraviolet spectrum. For a wide range of materials,  $\omega$  is in the order of  $2 \cdot 10^{16} \text{ rad} \cdot \text{s}^{-1}$  (NGUYEN and SCHULZE 2003, p. 310).  $B_1$ ,  $B_2$ , and  $B_3$  are parameters of the oscillator model, which can be approximated by the square of the refractive indices of the particle 1, the particle 2, or the continuous phase, respectively. In the case of symmetry of the particles, the formulation simplifies to (NGUYEN and SCHULZE 2003, p. 311)

$$A_{132}^\zeta = \frac{3\hbar\omega}{16\sqrt{2}} \frac{(B_1 - B_3)^2}{(B_1 + B_3)^{3/2}}. \quad (3.10)$$

With respect to the electromagnetic retardation effect, the adjusted non-zero frequency term applies as follows (NGUYEN and SCHULZE 2003, pp. 315–316):

$$A_{132}^\zeta = \frac{3\hbar\omega}{8\sqrt{2}} \frac{(B_1 - B_3)(B_2 - B_3)}{(B_1 - B_2)} \left\{ \frac{I_2}{\sqrt{B_2 + B_3}} - \frac{I_1}{\sqrt{B_1 + B_3}} \right\}, \quad (3.11)$$

with

$$I_i = 1/[1 + (h/\lambda_i)^m]^{1/m}, \quad (3.12)$$

and

$$\lambda_i = \frac{c}{\pi^2 \omega} \sqrt{\frac{2}{B_3(B_1 + B_3)}}. \quad (3.13)$$

Here,  $c$  is the speed of light,  $B_1$  a parameter of the oscillator model, and  $m$  a best fit parameter, which results from a data fit of the Hamaker-based approximation to the exact solution postulated by Lifshitz.  $\lambda_i$  represents the characteristic

wavelengths of the interacting materials. For symmetric systems, Equation 3.11 simplifies to (NGUYEN and SCHULZE 2003, p. 316)

$$A_{132}^{\zeta} = \frac{3\hbar\omega}{16\sqrt{2}} \frac{(B_1 + B_3)^2}{(B_1 + B_2)^{3/2}} \{1 + (h/\lambda)^m\}^{-1/m}. \quad (3.14)$$

Taking into account the impact of the electrolyte, the following expression applies for the total Hamaker dispersion constant  $A_{123}$  (NGUYEN and SCHULZE 2003, p. 318):

$$A_{132} = A_{132}^0 (1 + 2\kappa h) e^{(-2\kappa h)} + A_{132}^{\zeta}. \quad (3.15)$$

### Hydrophobic interaction

TABOR et al. (2014) provided a review of existing hydrophobic force laws, which are derived from different measurements. It is apparent that the diverse formulations vary strongly regarding their expression and range. The authors attribute this on a well-founded basis to the fact that the postulated interaction law depends substantially on the underlying methods employed. However, it is noticeable that the majority of models represent a hyperbolic course of the resulting hydrophobic forces. The obtained force values of the various models differ only for small segregation distances in the order of a few nm and then approach the same limit. Comparing the hyperbolic courses of the models for these small ranges, it is evident that the model provided by YANGSHUAI et al. (2017) slightly overestimates the hydrophobic forces compared to the other approaches. Accordingly, this represents a suitable approach when aiming for a conservative assessment of the dispersion stability.

The model of YANGSHUAI et al. (2017) obeys the following equation:

$$V_{\text{hyd}} = -2.51 \cdot 10^{-3} \cdot r_{\text{particle}} \cdot k \cdot \lambda_1 \cdot e^{\left(-\frac{h}{\lambda_1}\right)}. \quad (3.16)$$

$k$  is a hydrophobic modification coefficient with the value of 0.4167 and  $\lambda_1$  the decay length with a value of 5.29 nm (YANGSHUAI et al. 2017). For interactions of different particles,  $r_{\text{particle}}$  is approximated by the harmonic mean of the particle radii (MITCHELL et al. 2005; NGUYEN and SCHULZE 2003).

### Steric interaction

Modeling the steric repulsion is particularly challenging due to the complex phenomena underlying the interaction of the polymer involved and the particles. According to LIKOS et al. (2000), the following differentiation applies for determining  $V_s$ :

$$V_s = \begin{cases} \infty, & \text{if } h < 0. \\ f(h), & \text{if } 0 < h \leq 2L_p. \\ 0, & \text{if } 2L_p < h. \\ \text{direct contact,} & \text{if } h = 0. \end{cases}$$

Here,  $L_p$  represents the thickness of the layer formed by the polymer chains. For  $h = 0$ , the particle surfaces are in direct contact. Accordingly,  $V_s$  is not defined for  $h < 0$ . When  $h$  is larger than  $2L_p$ , the respective polymer shells are no longer in contact and no steric repulsion comes into effect.

An approach to determine  $f(h)$  is provided by NGUYEN and SCHULZE (2003, pp. 377–378), leading to the following expression:

$$f(h) = \frac{64L_p^2 k_B T f_c}{s^3} \left[ \frac{1}{5} \left( \frac{h}{2L_p} \right)^{-1/4} - \frac{1}{77} \left( \frac{h}{2L_p} \right)^{11/4} + \frac{3}{35} \frac{h}{2L_p} - \frac{3}{11} \right], \quad (3.17)$$

with

$$f_c = \frac{2\pi r_{\text{particle},1} r_{\text{particle},2}}{r_{\text{particle},1} + r_{\text{particle},2}}. \quad (3.18)$$

Here,  $s$  represents the mean distance between the chain attachment points at the surface and  $f_c$  the geometric conversion factor of the Derjaguin approximation.

### Depletion

Various formulations exist to describe the depletion. According to LAGALY et al. (1997), an established approach is the one postulated by JONES and VINCENT (1989). This results in the following definition for  $V_{\text{dep}}$ :

$$V_{\text{dep}} = 2 \cdot \pi r_{\text{particle}} \left( \frac{\mu_1 - \mu_1^0}{v_1^0} \right) \left( \Delta + \xi - q + p - \frac{h}{2} \right)^2. \quad (3.19)$$

$\mu_1$  and  $\mu_1^0$  are the chemical potentials of the solvent molecules at bulk volume fraction and  $v_1^0$  is the molar volume of the pure solvent. The term  $(\mu_1 - \mu_1^0)/v_1^0$  represents the osmotic pressure.  $\Delta$  is the range of the depletion effect,  $\xi$  the thickness of the polymer shell,  $q$  the compression of the polymer shell, and  $p$  the extent of the overlap of the polymer shells.

### Interim conclusion

Various modeling approaches exist to mathematically describe the respective interaction fractions of the DLVO theory. It is apparent that individual modeling approaches have emerged as accepted standards in the scientific community. A

framework including the entirety of interaction shares of the extended DLVO theory has, however, not yet been presented. This limits the overall application of the extended DLVO theory and reveals potential for further research.

### 3.3.2 Applications of the DLVO theory

Commonly, the DLVO theory is used to explain stability phenomena in dispersions, rather than to model the interactions. In this context, the DLVO theory has proven to be beneficial for a wide range of dispersions employed in various applications. However, first approaches towards the mathematical description of dispersion stability have been reported. Selected relevant studies are briefly outlined below.

MITCHELL et al. (2005) presented a well-founded model of the extended DLVO theory to describe the coagulation between particles of the copper mineral chalcopyrite and the iron mineral pyrite during flotation. This separation process takes advantage of the varying surface wettability of different particles. Gas bubbles can easily attach to hydrophobic surfaces and impart the buoyancy of the particles, causing them to float. In the framework proposed, they considered the van-der-Waals forces, the electrostatic forces, and the hydrophobic forces. For the respective minerals, the course of the absolute zeta potential over the pH value was determined empirically. This facilitated a calculation of the total interaction energies. The stability factor was used to evaluate the occurrence of coagulation. Flotation tests demonstrated the validity of the model, allowing for an accurate determination of the selective flotation of the intended minerals in the calculated pH value range.

YOON et al. (1997) described the adhesion of gas bubbles to particles during flotation on the basis of the extended DLVO theory. They elaborated a formulaic relationship to calculate the force constant required to determine the hydrophobic forces. Empirical studies were conducted to calibrate the proposed model, and the interaction energies were calculated.

ZHU et al. (2011) developed a three-dimensional model to describe the aggregation behavior between a cathode active material and carbon black in an *N*-Methyl-2-pyrrolidone (NMP) solution containing polyvinylidene fluoride (PVDF) during preparation. They incorporated the van-der-Waals forces and the electrostatic forces to determine the interaction of the particles as a function of the separation distance. Empirical studies demonstrated that the model describes well the aggregation behavior as a function of the particle size, the solid content, and the temperature.

YANGSHUAI et al. (2017) demonstrated a model to describe the stability of aqueous graphite formulations based on the extended DLVO theory. The approach regarded the van-der-Waals forces, the electrostatic forces, and the hydropho-

bic forces. The results were compared with those obtained from employing the DLVO theory in its original form. Empirical studies revealed the validity of the extended approach. They concluded that the hydrophobic interactions significantly influence the stability behavior, as they exceed the impact of the forces regarded in the DLVO theory in its original form.

### **Interim conclusion**

Although the DLVO theory represents a well-known and proven explanatory model, it has rarely been used to model dispersions for practical purposes. Most of the application-oriented publications were concerned with the modeling of flotation. This is due to the fact that the extended DLVO theory allows for a direct incorporation of the hydrophobic forces that govern this separation process. The developed models were found to describe the stability behavior of the previously investigated dispersions quite accurately. However, the versatility and the complexity of the investigated dispersions so far were low. Dispersants and the associated effects on the stability behavior were not regarded. Therefore, also the modeling capabilities have not yet been fully exploited.

## **3.4 Qualification of non-Newtonian fluids for the inkjet printing process**

### **3.4.1 Drop formation**

The kinetic energy resulting from the voltage-driven deflection of the piezoelectric actuator (see Section 2.4.2) causes the formation of a filament at the nozzle orifice, also known as tail (WIJSHOFF 2010). Once the equilibrium is no longer constituted by the gravitational and the surface tension force, the tail begins to thin out (CLASEN et al. 2012; WIJSHOFF 2010). Eventually, the tail pinches off and adopts a drop-shaped morphology of a lower surface area (RAPP 2016), whereby the minimum at balanced forces corresponds to a sphere (HOATH 2016, p. 6). A stable equilibrium of forces is, however, under gravity only present, if the volume of the drop is small in relation to its surface. Larger drops are flattened due to the flow resistance.

Depending on the flow regime, two different drop formation mechanisms can occur: the dripping mode and the jetting regime (LARSSON et al. 2012; ZHANG 1999). In the dripping regime, the drop breaks up with a pinch-off close to the nozzle orifice (CLANET and LASHERAS 1999). The tail length is strongly affected by the viscosity of the fluid (CLANET and LASHERAS 1999; HENDERSON et al. 1997). Due to the inherent large differences in the rheological behavior, a completely different material behavior appears for Newtonian and non-Newtonian fluids. The jetting regime refers to the condition, in which the drop detaches

from an extended tail that is maintained over a certain length after the nozzle orifice (CLASEN et al. 2012). This appears at higher flow rates, when the drop formation process cannot keep pace with the displacement of the flow profile (WIJSHOFF 2010). Hence, the pinch-off and the break-up occur further away from the nozzle orifice (CLANET and LASHERAS 1999; TYLER and WATKIN 1932). Consequently, the transition between the dripping and the jetting regime is primarily governed by the print head parameters. Aiming at a reliable processability, an operation in the jetting mode is pursued, as this leverages a higher precision (CLASEN et al. 2012). This is attributed to the non-discrete ejection (CLASEN et al. 2012). In addition, this deserves attention in terms of productivity increases (WIJSHOFF 2010).

According to WIJSHOFF (2010), a stable drop formation describes the printing condition in which only a single drop is generated. By contrast, the appearance of extra drops, also referred to as satellite drops, indicates instability. The drop formation behavior can be favorably evaluated in the dripping mode.

### Nondimensional numbers

The drop formation of a Newtonian fluid is thoroughly characterized by the dimensionless Ohnesorge number  $Oh$ , which can be expressed by the Weber number  $We$  and the Reynolds number  $Re$  (DERBY 2010):

$$Oh = \frac{\sqrt{We}}{Re} = \frac{\eta}{\sqrt{\sigma_{lg}\rho L}}. \quad (3.20)$$

Here,  $\eta$  represents the dynamic viscosity,  $\rho$  the density, and  $L$  the characteristic length. Mostly,  $L$  as a characteristic length is, in this case, approximated by the nozzle diameter  $d_{\text{nozzle}}$  (DERBY 2010; HOATH 2016; POLSAKIEWICZ and KOLLENBERG 2011) or the nozzle radius  $r_{\text{nozzle}}$  (CLASEN et al. 2012; WIJSHOFF 2010).  $Oh$  allows to predict the stability of the drop formation. Different conclusions were drawn regarding the printing regimes in the literature. The respective ranges for  $Oh$  are summarized in Table 3.3.

Low values of  $Oh$  cause the formation of long filaments that are susceptible to forming satellite drops (DERBY 2010). High values of  $Oh$  lead to viscous dissipation, which prevents the ejection of drops (DERBY 2010).

While the rheological behavior of Newtonian fluids is fully described by the Ohnesorge number  $Oh$ , further numbers are required to determine the behavior of non-Newtonian fluids (HOATH 2016; MARTIN et al. 2008). CLASEN et al. (2012) presented an approach to evaluate the printability of non-Newtonian fluids based on a set of nondimensional numbers. The model was designed for a volumetric flow-controlled dispensing under steady state conditions. A partial validation was performed for the direct ink writing process, which represents a related process of inkjet printing. In addition to the intrinsic material properties, these numbers incorporate printing parameters. Apart from  $Oh$ , the set

consists of five additional numbers. These describe either fluid dynamic properties or attributes related to the nature of the fluids.

The fluid-dynamic numbers include in addition to  $Oh$  the Deborah number  $De_0$  and the Elasto-capillary number  $Ec$ , which are further outlined below.

**Table 3.3:** Summary of the different approaches to the classification of  $Oh$  with the corresponding reference value for  $L$

Reference	Range	Reference value
REIS and DERBY (2000)	0.10 – 1	$d_{\text{nozzle}}$
JANG et al. (2009)	0.07 – 0.25	$r_{\text{nozzle}}$
ZHONG et al. (2018)	0.13 – 0.25	$d_{\text{nozzle}}$
LIU and DERBY (2019)	0.05 – 0.50	$d_{\text{nozzle}}$
AQEEL et al. (2019)	0.06 – 0.25	$d_{\text{nozzle}}$
LEHMANN et al. (2021)	0.17 – 0.25	$d_{\text{nozzle}}$

The **Deborah number**  $De_0$  is defined as the ratio of elastic and inertial forces. Small values of  $De_0$  indicate a little pronounced elasticity. For high values of  $De_0$ , the fluid behaves like a strongly elastic solid. A Newtonian fluid is present, if  $De_0 = 0$  (PHAN-THIEN and MAI-DUY 2013). The Deborah number  $De_0$  can be described as (CLASEN et al. 2012)

$$De_0 = \sqrt{\frac{\lambda^2 \sigma_{lg}}{\rho L^3}}, \quad (3.21)$$

where  $\lambda$  represents the relaxation time.

The **Elasto-capillary number**  $Ec$  characterizes the thinning mechanism of the filament. For small values of  $Ec$ , the thinning mechanism is viscosity-controlled and only slightly dependent on elastic effects. For high values of  $Ec$ , the thinning mechanism is dominated by elastic effects, and persistent filaments are formed. The Elasto-capillary number  $Ec$  can be calculated as follows (CLASEN et al. 2012):

$$Ec = \frac{\lambda \sigma_{lg}}{\eta L}. \quad (3.22)$$

The material-property-based numbers comprise the Capillary number  $Ca$ , the Weber number  $We$ , and the Weissenberg number  $Wi$ , which are introduced in the following.

The **Capillary number**  $Ca$  allows to characterize the forces resulting from the movement of the fluid in relation to the surface tension forces (RAPP 2016). This is relevant when the fluid is being moved in gas after the drop ejection. If  $Ca$  is smaller than one, the drop ejected attempts to adopt the ideal shape of the smallest surface energy (RAPP 2016). For larger values of  $Ca$ , the drop remains deformed (RAPP 2016). The Capillary number  $Ca$  is defined as (CLASEN et al. 2012)

$$Ca = \frac{\eta v_{\text{eject}}}{\sigma_{\text{lg}}}, \quad (3.23)$$

with the velocity of the drop upon ejection  $v_{\text{eject}}$ .

The **Weber number**  $We$  allows to evaluate whether the energy of the dosing is sufficient to eject a drop (ALAMÁN et al. 2016; DERBY 2010). This condition applies if the velocity of the jet and thus  $We$  is high enough to overcome the surface energy (ALAMÁN et al. 2016; DERBY 2010).

The Weber number  $We$  can be determined as follows (CLASEN et al. 2012):

$$We = \frac{\rho v_{\text{eject}}^2 L}{\sigma_{\text{lg}}}. \quad (3.24)$$

The **Weissenberg number**  $Wi$  indicates the extent of the viscoelasticity. High values of  $Wi$  reveal that the fluid exhibits a distinct viscoelasticity and tends to the formation of persistent filaments (HAQUE et al. 2015; MCILROY et al. 2013). The Weissenberg number  $Wi$  obeys the following relationship (CLASEN et al. 2012):

$$Wi = \frac{\lambda v_{\text{eject}}}{L}. \quad (3.25)$$

According to the theory of CLASEN et al. (2012), the dispensing of a non-Newtonian fluid is fully characterized by any set of two fluid-dynamic numbers and one material property-based number. An overview of the entire set of numbers is provided in Table 3.4.

**Table 3.4:** Set of the nondimensional numbers to characterize non-Newtonian fluids according to CLASEN et al. (2012);  $v_{\text{eject}}$ : velocity of the drop upon ejection,  $L$ : characteristic length of the print head nozzle,  $\lambda$ : relaxation time,  $\sigma_{\text{lg}}$ : interfacial energy between the liquid and the gas,  $\eta$ : dynamic viscosity, and  $\rho$ : density

Fluid-dynamic numbers	Material-property-based numbers
Ohnesorge number $Oh = \frac{\eta}{\sqrt{\sigma_{\text{lg}}\rho L}}$	Capillary number $Ca = \frac{\eta v_{\text{eject}}}{\sigma_{\text{lg}}}$
Deborah number $De_0 = \sqrt{\frac{\lambda^2 \sigma_{\text{lg}}}{\rho L^3}}$	Weber number $We = \frac{\rho v_{\text{eject}}^2 L}{\sigma_{\text{lg}}}$
Elasto-capillary number $Ec = \frac{\lambda \sigma_{\text{lg}}}{\eta L}$	Weissenberg number $Wi = \frac{\lambda v_{\text{eject}}}{L}$

CLASEN et al. (2012) used the aforementioned set of numbers to characterize the transition between the dripping and the jetting mode. Furthermore, the authors applied the nondimensional numbers to characterize the tail thinning mechanism. Depending on the dominating forces, the dispensing operation can be either viscosity-, inertia-, or elasticity-controlled. Accordingly, the fluids can be fundamentally classified as follows (CLASEN et al. 2012), whereby the transition areas are not further specified:

#### High-viscosity fluids with $Oh \gg 0.2$

High-viscosity fluids can be further distinguished according to the Elasto-capillary number  $Ec$ :

- $Ec \ll 4.7$ : The fluids are weakly elastic and viscosity-controlled. They are easy to dispense.
- $Ec \gg 4.7$ : The fluids are strongly elastic and thus elasticity-controlled. This behavior promotes persistent tails, which increases the break-up time. Hence, these fluids are difficult to dispense.

#### Low-viscosity or inviscid fluids with $Oh \ll 0.2$

Low-viscosity or inviscid fluids, respectively, can be further categorized according to the Deborah number  $De_0$ :

- $De_0 \ll 1$ : The fluids are low-viscosity Newtonian fluids with a weakly elastic behavior. The thinning mechanism is inertia-controlled. These fluids are easy to dispense.
- $De_0 \gg 1$ : The fluids exhibit inviscid, but elastic behavior. Accordingly, the thinning regime is elasticity-controlled. These fluids are not expected to cause problems in the dispensing operation.

### Interim conclusion

A stable drop formation is required to ensure a high printing resolution and reproducibility. For a precise evaluation, number-based approaches can assist with the a-priori prediction of the drop formation process. This allows to define dispersion-specific operating spaces (process windows), which leads to a significant reduction in the empirical effort. While extensive attempts have been made for Newtonian fluids, little attention has been paid yet to the characterization of non-Newtonian fluids. This is attributable to the complex rheological behavior that even complicates the dispensing through a nozzle. One research group, namely CLASEN et al. (2012), presented a complete description of non-Newtonian fluids and partially validated the model for the dispensing in the direct ink writing process. Accordingly, the transferability to inkjet printing remains to be validated. Moreover, this approach has not been used by other researchers to thoroughly map out operating spaces for a stable drop formation of further dispersion systems.

### 3.4.2 Drop deposition

During the drop deposition, the drop passes through certain phases in which the behavior is dominated by different effects. According to RIOBOO et al. (2002), the following four distinct phases are prevalent (see Figure 3.3):

- **Kinematic phase:** The drop is strongly compressed as a consequence of the high kinematic energies.
- **Spreading phase:** The drop begins to spread, forming a radially expanding film.
- **Relaxation phase:** The film exhibits an oscillating behavior in which it is alternately expanded and contracted.
- **Wetting/Equilibrium phase:** Once the equilibrium state is reached, the film continues to expand.

According to SCHIAFFINO and SONIN (1997), the phases indicate different regimes. While the kinematic and the spreading phases are predominantly impact-driven, the wetting and the equilibrium phase are capillary-driven. The relaxation phase marks an intermediate regime. In the impact-driven regime, the inertial forces dominate (SCHIAFFINO and SONIN 1997; YARIN 2006). Hence, the drop behavior is primarily impacted by the initial drop velocity and the drop diameter (SCHIAFFINO and SONIN 1997; YARIN 2006). By contrast, the capillary-driven regime is predominantly governed by the liquid-solid interactions on the substrate (SCHIAFFINO and SONIN 1997; YARIN 2006).

Aiming at a high printing resolution, DERBY (2010) stated that the deposited structure is required to exhibit shape retention prior to solidification. Considering the categorization of the regimes according to RIOBOO et al. (2002), a stable drop deposition encompasses both a stable drop impact and wetting. This defi-

nition ignores the relaxation phase. However, it is expected to represent a sound approximation, since the drop diameter usually changes only slightly over the entire regime (RIOBOO et al. 2002).

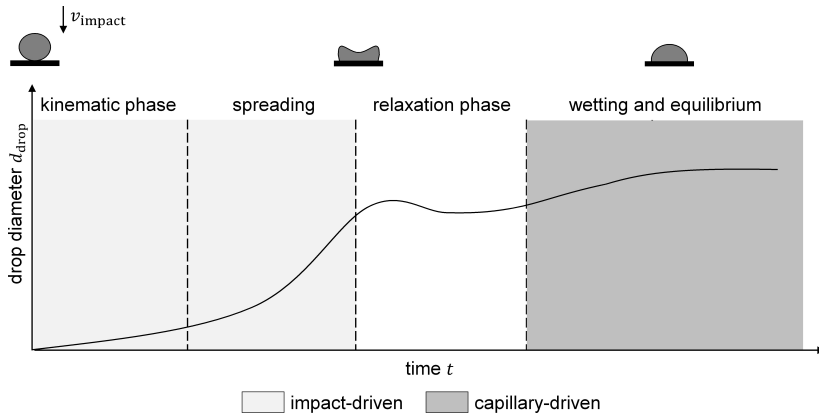


**Figure 3.3:** Schematic illustration of the effects that occur during the deposition of a drop with the impact velocity  $v_{\text{impact}}$  and the induced time-dependent evolution of the drop diameter  $d_{\text{drop}}$  (modified from DERBY and REIS (2003) and RIOBOO et al. (2002))

Similarly to the drop formation, instabilities or unwanted effects can also occur during drop deposition that compromise the printing resolution. According to JOSSERAND and THORODDSEN (2016), the predominant phenomena associated with that are the following:

- **Bouncing:** The drop recoils off the surface with a distinct elasticity (RICHARD et al. 2002).
- **Splashing:** A fine liquid layer of the drop pinches off (JOSSERAND and THORODDSEN 2016). This causes a radial ejection of fine drops along the substrate (JOSSERAND and THORODDSEN 2016). Depending on the substrate and the fluid properties, various types of splashing can occur (WAL et al. 2006).
- **Spreading:** This is a natural phenomenon during drop impact (RIOBOO et al. 2002). It can be detrimental for the application, as it reduces the printing resolution (DERBY 2010). Therefore, the spreading factor must concur with the application requirements (DERBY 2010).

### Drop impact

The drop impact dynamics are governed by the physical fluid properties and the process parameters. Accordingly, these characteristics determine the probability for a specific drop impact scenario. In this context, RIOBOO et al. (2002) evaluated the predominant correlations, which are summarized in Table 3.5.

**Table 3.5:** Summary of the correlations between the parameters and the respective drop impact scenarios according to RHOBOO et al. (2002); (+) indicates that the outcome is more likely with an increasing parameter; (-) indicates that the outcome is less likely with an increasing parameter; N/A: data not available.

Parameter	Stable impact	Bouncing	Splashing
Nozzle diameter $d_{\text{nozzle}}$	-	+	N/A
Drop impact velocity $v_{\text{impact}}$	-	+	N/A
Surface tension $\sigma_{\text{lg}}$	N/A	-	+
Viscosity $\eta$	+	-	N/A

The vast majority of the studies on the drop impact behavior are related to Newtonian fluids (AN and LEE 2012; YARIN 2006). However, research activities on non-Newtonian fluids have also received an increasing attention (AN and LEE 2012). Several studies have been conducted on the impact mechanisms of shear-dependent fluids with different characteristics, such as a shear-thinning (e.g. AN and LEE (2012) and GERMAN and BERTOLA (2009)) and a viscoelastic behavior (e.g. BERGERON et al. (2000) and BERTOLA (2013)) as well as fluids with a yield stress (e.g. GERMAN and BERTOLA (2009) and SAÏDI et al. (2010)). The overall goal was to determine the effects compared to their Newtonian counterparts, which are briefly summarized below.

**Shear-thinning behavior** was identified to promote spreading, causing much larger spreading diameters (AN and LEE 2012; GERMAN and BERTOLA 2009).

**Viscoelastic behavior** was observed to significantly suppress bouncing and splashing (BERGERON et al. 2000; YARIN 2006). In terms of spreading, literature shows contradictory conclusions. While some researchers stated that a tendency was found to be more pronounced (PAULO et al. 2014; TOMÉ et al. 2002), others reported a behavior comparable to Newtonian fluids (BERGERON et al. 2000; SMITH and BERTOLA 2010).

**Fluids with a yield stress** were found to exhibit less distinct spreading (GERMAN and BERTOLA 2009; SAÏDI et al. 2010). This peculiarity was amplified with an increasing yield stress (GERMAN and BERTOLA 2009; SAÏDI et al. 2010).

In reality, fluids often exhibit a combination of different non-Newtonian characteristics. RAHIMI and WEIHS (2011) explored the impact dynamics of a more complex non-Newtonian fluid and observed a mutual interference of the individual effects.

### Wetting

The wetting mechanisms are predominantly determined by the surface roughness and the chemical nature of the substrate, the physical fluid properties, and

the atmospheric conditions (KUMAR and PRABHU 2007; QUÉRÉ 2008).

Similar to the drop impact behavior, most previous studies concerned with wetting were devoted to Newtonian fluids (LU et al. 2016). In recent decades, the behavior of non-Newtonian fluids has also gained growing attention (LU et al. 2016).

NEOGI and YBARRA (2001) observed a similar wetting behavior of non-Newtonian fluids compared to their Newtonian counterparts. However, most other previous explorations corroborate a contradictory behavior. Among these studies are those of CARRÉ and WOEHL (2002) and STAROV et al. (2003), who found that the wetting strongly depends on the shear-rate-dependent behavior of the fluids. In addition, first approaches were shown towards the wetting of more complex non-Newtonian fluids, such as the one explored in the study of LIANG et al. (2010). In these preliminary works, the wetting behavior was examined in conjunction with the prior impact-driven phases, which does not allow for independent conclusions.

### **Interim conclusion**

The drop deposition behavior directly governs the printing resolution and the reproducibility. Only a few studies have been conducted on the drop deposition dynamics of standard non-Newtonian fluids with a definite rheological profile. Even less attention has been paid to non-Newtonian fluids with a more complex behavior and the mutual interference of the respective effects. Since the drop deposition appears to significantly rely on the individual dispersion characteristics, the drop impact and the wetting were preferably investigated empirically.

## Chapter 4

# Problem statement and approach

## 4.1 Chapter overview

This dissertation represents a publication-based doctoral thesis. The content was published in five papers. This chapter addresses the scientific need for action and represents the pursued approach. Based on the state of the art in science and technology (see Chapter 3), a problem statement and associated sub-objectives (SO) are defined (see Section 4.2). Subsequently, the approach with the related work packages (WP) is outlined (see Section 4.3). Lastly, the publications are assigned to the WP, and the individual contributions of the author are presented (see Section 4.4).

## 4.2 Problem statement and sub-objectives

The chapter on the state of the art in science and technology reveals that there are only a few studies that were concerned with the processing of aqueous electrode dispersions in inkjet printing. In particular, little attention has been directed to anode dispersions. This is reflected in the poor knowledge underlying the interactions between the dispersion composition and its preparation as well as the processability. In this context, it is evident that the product and the process requirements were not thoroughly consolidated, nor have methods been standardized to systematically characterize the dispersions and the electrodes prepared thereof.

Approaching the field from a broader perspective elucidates that the qualification of non-Newtonian fluids for inkjet printing in general has not been extensively researched and thus the transferability to electrode dispersions has not been proven. Few studies have been presented that address the stability and the printability behavior, and even fewer that provide an approach for an a-priori evaluation of the respective dispersion characteristics. The only established approach to mathematically describe the stability behavior and thus to an a-priori determination of the boundary conditions was found to be given by the DLVO theory. Despite its evidence, it has seldom been applied to practical and complex

dispersion systems. In terms of the printability, CLASEN et al. (2012) presented a number-based method for an a-priori examination of the drop formation of dispersions. However, this approach has only been validated for the dispensing of selected dispersions in the related process of direct ink writing. The transferability to inkjet printing has not been demonstrated so far. The drop deposition behavior has rarely been investigated for more complex dispersions.

This dissertation aims to address this deficiency by providing a methodology to qualify aqueous anode dispersions for the processing in inkjet printing. The elaborated methodology will be demonstrated using the state-of-the-art anode system of graphite, but is intended to be transferable to other material systems as well. This goal is approached by the following SO:

**SO 1:** The product- and process-specific requirements applying to the electrode dispersions have to be analyzed and consolidated. Target ranges have to be defined for the key component characteristics.

**SO 2:** The key mechanisms impacting the stabilization of the investigated dispersion system are to be explored. A suitable dispersant has to be identified that effectively counteracts the strong attractive forces between the particles.

**SO 3:** In order to gain a deeper comprehension of the physical effects underlying the stabilization of the studied dispersion system, a modeling of the interactions acting between the dispersion components is pursued. This is intended to capture the boundary conditions that represent the prerequisite for an a-priori determination of the stability.

**SO 4:** A methodical approach to evaluate the printability a priori has to be qualified. In this context, the printable range for the active material content has to be systematically determined.

**SO 5:** Considering the role of binders in the dispersion system, the impact on the product and process conditions has to be explored. Suitable parameter ranges with regard to the reference dispersion formulation have to be identified.

### 4.3 Approach

The approach of this work is divided into five WP, each relating to a SO. The approach with each particular WP is depicted in Figure 4.1. The content of the individual WP is briefly summarized below.

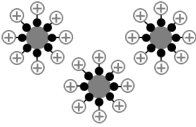
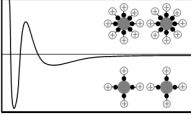
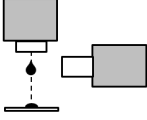
**WP 1:** An in-depth requirements analysis was carried out, in which the product and the process requirements were linked to the dispersion components. This allowed to derive suitable parameter ranges for the respective component characteristics.

**WP 2:** The interdependencies between the occurring instability phenomena and the measurable dispersion characteristics were empirically analyzed to facilitate the systematic identification of a suitable dispersant and its associated favored dispersion qualities.

**WP 3:** The extended DLVO theory was used to elaborate a mathematical model that describes the stability of the investigated dispersion system. The influences arising from the stabilizing dispersant were incorporated in the model. The numerically obtained data was compared with the empirically gained findings.

**WP 4:** Relying on the framework presented by CLASEN et al. (2012), a number-based approach to assess the printability a priori was qualified. Printable dispersion compositions were systematically determined by extensive empirical and analytical studies with varying active material content. The printability was validated and the capability of the numbers was evaluated.

**WP 5:** The impact of the binders on the product and process characteristics was empirically examined. This allowed the parameter ranges to be narrowed down depending on the binder derivative employed.

WP 1	 <p>product requirements      process requirements</p> <p><b>Work package 1</b> Analysis of the product- and process-specific requirements</p>	Requirements
WP 2	 <p><b>Work package 2</b> Stabilization of the investigated dispersion system using a suitable dispersant</p>	Stability
WP 3	 <p><b>Work package 3</b> Modeling of the dispersion stability on the basis of the DLVO theory</p>	
WP 4	 <p><b>Work package 4</b> Number-based approach for an a-priori evaluation of the printability</p>	Printability
WP 5	 <p><b>Work package 5</b> Analysis of the role of binders concerning the product and process characteristics</p>	

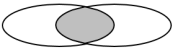
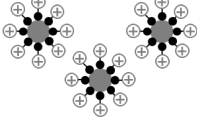
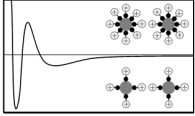
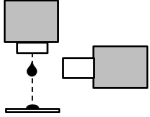
**Figure 4.1:** Approach with the five work packages

Each of the five WPs was covered in one publication. A brief summary and the findings as well as main conclusions of the respective publications are given in Chapter 6 to Chapter 10.

#### 4.4 Scientific contributions of the author

The individual publications that represent the scientific basis for this work were elaborated in collaboration with other researchers. In relation to the objectives of this work, five publications are of relevance, for which the lead authorship was designated to the author of this work. The contributions of all authors to the publications relevant to this work are summarized in Figure 4.2, highlighting the individual contribution of the leading author. The contributions of the respective authors represent the sum of the individual shares for the conceptu-

alization, the execution of the theoretical and empirical work, the data analysis, and the elaboration of the publications.

WP 1	<p>product requirements      process requirements</p> 	<p><b>Publication I</b></p> <table border="1" data-bbox="557 245 925 284"> <tr> <td>C. G. Kolb 82.5 %</td> <td>R</td> </tr> </table> <p><sup>R</sup>M. Lehmann 5 %      J. Kriegler 2.5 %  J.-L. Lindemann 2.5 %      A. Bachmann 2.5 %  M. F. Zaeh 5 %</p>	C. G. Kolb 82.5 %	R
C. G. Kolb 82.5 %	R			
WP 2		<p><b>Publication II</b></p> <table border="1" data-bbox="557 411 925 450"> <tr> <td>C. G. Kolb 85 %</td> <td>R</td> </tr> </table> <p><sup>R</sup>M. Lehmann 5 %      J.-L. Lindemann 2.5 %  A. Bachmann 2.5 %      M. F. Zaeh 5 %</p>	C. G. Kolb 85 %	R
C. G. Kolb 85 %	R			
WP 3		<p><b>Publication III</b></p> <table border="1" data-bbox="557 571 925 609"> <tr> <td>C. G. Kolb 70 %</td> <td>R</td> </tr> </table> <p><sup>R</sup>M. Lehmann 5 %      D. Kulmer 20 %  M. F. Zaeh 5 %</p>	C. G. Kolb 70 %	R
C. G. Kolb 70 %	R			
WP 4		<p><b>Publication IV</b></p> <table border="1" data-bbox="557 735 925 774"> <tr> <td>C. G. Kolb 70 %</td> <td>R</td> </tr> </table> <p><sup>R</sup>M. Lehmann 5 %      C.-M. Teixeira 17.5 %  S. Maleksaeedi 2.5 %      M. F. Zaeh 5 %</p>	C. G. Kolb 70 %	R
C. G. Kolb 70 %	R			
WP 5		<p><b>Publication V</b></p> <table border="1" data-bbox="557 900 925 938"> <tr> <td>C. G. Kolb 67.5 %</td> <td>R</td> </tr> </table> <p><sup>R</sup>A. Sommer 7.5 %      M. Lehmann 5 %  C.-M. Teixeira 10 %      H. Panzer 2.5 %  S. Maleksaeedi 2.5 %      M. F. Zaeh 5 %</p>	C. G. Kolb 67.5 %	R
C. G. Kolb 67.5 %	R			

**Figure 4.2:** Contribution of the individual authors to the publications that form the basis for this work; R represents the remaining authors.



## Chapter 5

# Materials and methods

## 5.1 Chapter overview

This chapter provides an overview of the materials and methods employed in this work. Due to the great variety of the studies executed, they are described only in the depth of detail that is consistent across all publications. The detailed description of the particular material compositions and the procedures are outlined in the respective publications.

First, the dispersions are outlined in terms of their constituents, mixing devices for the synthesis, and characterization methods (see Section 5.2). In this context, the test setups used for the monitoring of the drop formation and the drop deposition are elucidated. Subsequently, the electrodes and cells are further addressed in terms of the materials employed, the fabrication routes, and the characterization methods (see Section 5.3).

Further details can be found in the publications described in Chapter 6 through Chapter 10.

## 5.2 Dispersions

### 5.2.1 Materials

The methodology elaborated in this work was demonstrated for aqueous graphite-based anode dispersions. The raw material employed was a natural graphite nanopowder provided by the supplier Nanografi Nano Technology (Ankara, Turkey). The key properties are provided in Table 5.1.

**Table 5.1:** Properties of the natural graphite nanopowder employed in this work according to TECHNOLOGY (2021)

Particle size in nm	Purity in %	BET in m <sup>2</sup> /g	Density in g/cm <sup>3</sup>	Morphology -
30	> 99.99	195	2.00	Flaky

The constituents used to prepare the anode dispersions besides the active material graphite are summarized in Table 5.2.

**Table 5.2:** Overview of the further constituents used in the investigated dispersions

Constituent	Material	Provider
Solvent	Deionized water	-
Dispersant	Polyvinylpyrrolidone (PVP)	PVP-17 (BASF SE, Germany) PVP-30 (Merck KGaA, Germany)
Binders	Carboxymethyl cellulose (CMC)	Nippon Paper Industries Co., Ltd., Japan; Merck KGaA, Germany
	Styrene-butadiene rubber (SBR)	Zeon Corp. K.K., Japan
Buffers	Sodium hydroxide (NaOH)	-
	Acetic acid (CH <sub>3</sub> COOH)	-
Electrolyte	Sodium chloride (NaCl)	-

Different preparation routes were applied for the various stability and printability studies addressed in this work. For this purpose, various mixing devices were used to synthesize the anode dispersions, which encompass the following:

- **A magnetic stirrer** provides low shear rates, which allow for a wetting of the particles and an initial deagglomeration (WENZEL et al. 2015).
- **An ultrasonic homogenizer** (FS-300N, Vevor, China) was employed to further deagglomerate and homogenize the mixture (see Section 2.3.1).
- **A roller mixer** (RM2, Edmund Bühler GmbH, Germany) was used to store the mixture until processing and thus to keep it homogenized.

### 5.2.2 Characterization

Miscellaneous measurements were carried out to characterize the anode dispersions studied in this work. This allowed to thoroughly evaluate the stability and the printability behavior. Among the decisive dispersion characteristics are numerous rheological parameters:

- **The shear-rate dependent viscosity** was examined by a controlled shear rate test. For this, the shear rate was varied between  $1 \cdot 10^{-2}$  and the limit of the measuring device of  $1 \cdot 10^4 \text{ s}^{-1}$ . This allowed to assess the flow behavior during shearing.
- **The viscosity at constant shear rate** was analyzed by a single-shear rate test. For this purpose, a constant shear rate of  $80 \text{ s}^{-1}$  was set, which appears to be in a range with minimal deviation.
- **The LVE range** was derived from an amplitude sweep (see Section 2.3.1), whereby the deformation was varied between  $1 \cdot 10^{-2}$  and  $1 \cdot 10^{-1}\%$ .

- **The storage modulus, the loss modulus, and the relaxation time** were determined through a frequency sweep (see Section 2.3.1) in the range from 1 to 100 Hz.

The rheological parameters were measured with a rotational rheometer (Kinexus lab+, Netzsch GmbH & Co. KG, Germany), which was equipped with a passive solvent trap. A 40 mm plate-plate geometry with a sample gap of 0.1 mm was employed. Each measurement was performed at ambient temperature after an equilibration time of 5 min. In addition to the rheological behavior, further key characteristics were determined, which are summarized in Table 5.3.

**Table 5.3:** Overview of further key dispersion characteristics explored in this work

Dispersion characteristic	Measuring instrument	Type and provider
Surface tension	Stalagmometer	-
Density	Density meter	DMA 5001 (Anton Paar GmbH, Austria)
Zeta potential	Zetasizer	Nano ZSP (Malvern Panalytical Ltd., UK)
Particle size distribution	Static laser diffraction analyzer	SALD-2201 (Shimadzu K.K., Japan)
pH value	pH meter	PH-100 ATC (Votcraft, Switzerland)
Gray value	Gray value analysis	-
Contact angle	Drop shape analyzer	DSA25E (Krüss Scientific GmbH, Germany)

### 5.2.3 Test setups for the drop monitoring

The drop formation and the drop deposition were assessed using various drop monitoring techniques, which are further outlined below.

#### Drop formation

The drop formation was observed in a binder jetting system (VTS128, Voxeljet AG, Germany) that is also suitable to perform inkjet printing. The printing system was extended by LEHMANN et al. (2021) to allow for an in-situ monitoring. A schematic depiction of the entire test setup is provided in Figure 5.1 a.

The drops were generated using a piezoelectric print head (Spectra SL-128 AA, Fujifilm K.K., Japan) with a nozzle diameter of 50  $\mu\text{m}$ . The drop formation was captured by a high-speed camera (iSpeed, Olympus K.K., Japan) with a Sigma objective lens with 105 mm. A high-power LED (M405LP1, Thorlabs Inc., USA) opposite to the high-speed camera served as a light source. The LED was equipped with a collimator (SM2P50-A, Thorlabs Inc., USA) and controlled by an LED driver (LEDD1B T-Cube, Thorlabs Inc. USA).

## Drop deposition

The in-situ drop impact in inkjet printing was imitated by a custom test setup (see Figure 5.1 b). This allows to observe the drop impact behavior on various substrates from different heights. For the studies on anode dispersions carried out in this work, a copper current collector foil attached to a glass plate served as a substrate.

The drops were generated manually (as opposed to automatically) using a syringe with a precise nozzle tip. The drop impact behavior was observed with the high-speed camera used to monitor the drop formation.

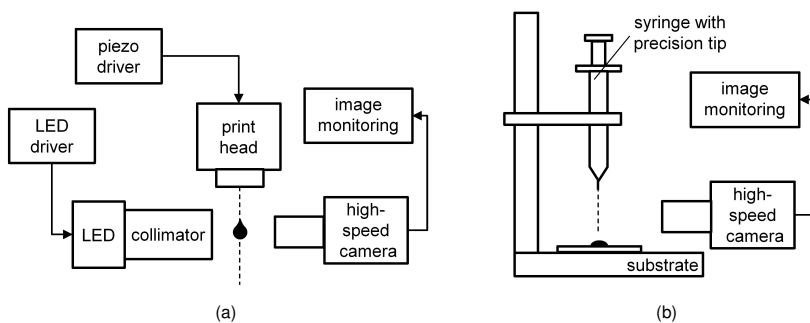


**Figure 5.1:** Schematic depiction of the (a) in-situ process monitoring setup to capture the drop formation (modified from LEHMANN et al. (2021)) and (b) the custom test setup to observe the drop impact behavior

## 5.3 Electrodes and cells

### 5.3.1 Materials

The materials used to assemble the half cells are summarized in Table 5.4.

**Table 5.4:** Summary of the constituents used in the half cells

Constituent	Material	Provider
Separator	Glass fiber separator	Type 691 (VWR LLC, USA)
Electrolyte	1 M LiPF <sub>6</sub> in a 3:7 mass ratio of ethylene carbonate (EC) and ethyl methyl carbonate (EMC) with 2 m% vinylene carbonate (VC)	LP572 (BASF SE, Germany)
Counter electrode	Lithium foil	PI-KEM Ltd., United Kingdom

### 5.3.2 Electrode fabrication and cell assembly

The electrode dispersions were coated onto copper current collector foils (Cu-PHC, Schlenk SE, Germany) using a tape casting coater (MSK-AFA-III, MTI Inc., USA), which was equipped with a doctor blade. The coatings were dried at 60 °C in a convection oven (Mehrzweck-Heissluftofen, Bartscher GmbH, Germany). The as-prepared electrode coatings were used to assemble half 2023-type coin cells (CR2032, Hohsen Corp., Japan). For this purpose, electrodes with a diameter of 15 mm were cut out of coatings with a hand punch (00565, Nogami Co., Ltd., Japan). In order to remove residual moisture, the electrodes and the separator were dried overnight in a vacuum oven (B-585, Büchi AG, Switzerland) at 120 °C. Upon drying, the coin cells were assembled in a dry room, which exhibits a dew point of -50 °C. Each half cell consisted of a sealing ring, a metal spacer (thickness: 0.5 mm), the lithium foil (diameter: 14 mm, thickness: 250 μm), two glass fiber separators (diameter: 16 mm, thickness: 150 μm), the graphite electrode, another spacer (thickness: 1 mm), and a contact spring, which were successively stacked centered in the cell housing. Each coin cell was infiltrated with 110 μL of the employed electrolyte.

Standard reference graphite anodes were fabricated to serve as a benchmark for the conventional electrode manufacturing. They contained 94 m% graphite (SMGA5, Hitachi K.K., Japan), 3.0 m% SBR (SBR, Zeon Corp. K.K., Japan), 2.0 m% CMC (CMC, Zeon Corp. K.K., Japan), and 1.0 m% conductive carbon (C65, Imerys S.A., France). An industrial roll-to-roll coating machine (BC50, Coatema GmbH, Germany) equipped with an infrared dryer was used to coat the electrode dispersion onto a copper foil (Schlenk Metallfolien GmbH & Co. KG, Germany). A doctor blade with a gap width of 96 μm was employed and the coating speed was adjusted to 1 m min<sup>-1</sup>. The dried coatings were compacted using a calender (EA 102, Coatema GmbH, Germany) with a maximum line load of 1000 N mm<sup>-2</sup> and a roller diameter of 400 mm. A constant roller speed of 1.0 m s<sup>-1</sup> was set to achieve a final porosity of approximately 30%. The active material loading was determined to be 9.20 mg cm<sup>-2</sup>.

### 5.3.3 Characterization

Various studies were conducted to characterize the electrodes fabricated in this work. The investigated electrode properties are summarized in Table 5.5 along with the required measuring equipment.

In addition to the studies on the electrode level, the formation behavior was studied on the cell level. In order to do that, the half cells were investigated using a battery cell test system (CTS, BaSyTec GmbH, Germany). They underwent a total of three charge and discharge cycles at a constant C-rate of 0.1C, at an ambient temperature of 25 °C, and within a voltage of 0.01 and 1.5 V. After each full charge or discharge, the formation program was paused for 20 min.

**Table 5.5:** Summary of the decisive electrode characteristics studied in this work

<b>Electrode characteristic</b>	<b>Measuring instrument</b>	<b>Type and provider</b>
Morphology	Scanning electron microscope	JSM-IT200 InTouchScope (Jeol Ltd., Japan)
Adhesion cohesion behavior	Universal tensile test machine	ProLine Z050 (ZwickRoell GmbH & Co. KG, Germany)

---

## Chapter 6

# Publication I: Analysis of the product- and process-specific requirements according to KOLB ET AL. (2022a)

## 6.1 Summary

This publication presents a top-down analysis of the key product- and process-specific requirements for the processing of electrode dispersions in inkjet printing. The overall aim was to identify suitable parameter ranges for the respective dispersion components.

Based on an in-depth examination of the product, the core dispersion components and their characteristics were derived and consolidated. This led to the definition of the key product requirements (battery performance characteristics), which for this application are given by the energy density, the power density, and the cycle stability (see Figure 6.1). Subsequently, the process and its conditions were analyzed. They were found to be primarily governed by the stability and the printability of the dispersions, allowing to further derive subordinate requirements.

Following this approach, the cause-effect relationships between the component characteristics and both the product- and process-specific requirements were systematically analyzed. Particular attention was paid to be particle-related effects on the process conditions.

On this basis, the correlations between the predominant component characteristics (influencing variables) and the product as well as the process requirements (target characteristics) were analyzed. A grading system was introduced to allow for a methodical evaluation.

Lastly, target ranges were derived, which were intended to balance the partly conflicting objectives between the product and the process side. Here the process requirements were specified as restrictive for the feasibility. Aiming at superior performance characteristics, the product requirements were approximated on the premise of fulfilled process requirements.

		product requirements			process requirements		target range	
		energy density	power density	cycle stability	stability	printability		
influencing variables	target characteristics							
	active materials	particle diameter $d_{\text{particle}}$	-	-	+	-	-	medium (100 to 300 nm) or lower (<100 nm) nanometer range
shape factor $\phi$		-	-	-	-	-	spherical	
particle span $\Delta x$		monodisperse	-	-	-	-	-	monodisperse distribution with a small span (narrow distribution)
		polydisperse	+	-	-	-	+	polydisperse distribution with a large span (wide distribution)
volume fraction $\phi$		+	+	+	+	-	maximized, provided that the viscosity does not exceed the limit values for printing	
conductive additives	particle size $d_{\text{particle}}$	x	-	-	-	-	medium (100 to 300 nm) or lower (<100 nm) nanometer range	
	shape factor $\phi$	x	x	x	+	-	spherical	
	particle span $\Delta x$	monodisperse	x	x	x	-	-	monodisperse distribution with a low span (narrow distribution)
		volume fraction $\phi$	-	+	x	-	-	minimized, provided that a sufficient power density is achieved
solvents (S), binders (Bi), and dispersants (D)	volume fraction (S) $\phi$	x	x	x	-	+	solvent content to be set in two stages <ul style="list-style-type: none"> <li>solvent content large enough to ensure that the components can be dispersed or solved sufficiently well</li> <li>solvent content gradually increased until the viscosity and the nondimensional numbers meet the requirements</li> </ul>	
	volume fraction (Bi) $\phi$	-	-	-	+	-	minimized, provided that a sufficient cohesion and adhesion are achieved	
	volume fraction (D) $\phi$	-	+	+	+	+	minimized, provided that the dispersing of the particles is sufficient for printing	

**Figure 6.1:** Depiction of the correlations between the predominant influencing variables and the target characteristics as well as the derivation of the target range for active materials, the conductive additives, the solvents (S), the binders (Bi), and the dispersants (D); a positive correlation (+) indicates that the target characteristics increase with increasing influencing variables. A negative correlation (-) indicates that the target characteristics decrease with increasing influencing variables.

## 6.2 Summary of the key findings and contributions of the lead author

The key findings (KF) of the publication of KOLB ET AL. (2022a) can be consolidated as follows:

**KF 1:** The product and the process conditions appear to be significantly impacted by the particle size and the morphology of the employed active material.

**KF 2:** The results corroborate that a wide range of commercially available active materials can be processed in inkjet printing if the overall dispersion properties are adapted to the process requirements.

**KF 3:** Binders and dispersants indicate to play a decisive role in the qualification of dispersions, as they strongly affect the product and the process characteristics.

The contributions of the lead author to Publication I are listed in Table 6.1.

**Table 6.1:** Percentage of the lead author's contributions to the conceptualization, the elaboration of the results, and the documentation of Publication I as well as the average

	Conceptualization	Elaboration of the results	Documentation	Average
C. G. Kolb	82.5%	80%	85%	82.5%



## Chapter 7

# Publication II: Stabilization of the dispersions according to KOLB ET AL. (2021)

## 7.1 Summary

According to the printing requirements outlined in Chapter 6, this publication aimed to systematically identify a suitable dispersant for the stabilization of graphite particles in an aqueous solution.

Due to the varying standards for exploring the effectiveness of dispersants, the cause-and-effect relationships between the indicators of instability and the measurable variables were consolidated. Hence, the correlations relevant to thoroughly characterize a dispersant were derived.

Initially, a preparation route was qualified for aqueous graphite dispersions that facilitates the break up of agglomerates. Following this synthesis route, graphite dispersions with varying dispersant content and pH value were prepared and their stability was extensively examined. Two different dispersants, in particular PVP and TX-100, were employed.

First, the influence of the dispersant content on the viscosity was investigated to determine the minimum required dispersant content at the onset of the quasi-constant progression (see Figure 7.1 a). Subsequently, the zeta potential (see Subsection 2.3.2) was measured for the identified dispersion compositions at different pH values. Following prevalent rules of thumb for the zeta potential, the pH-dependent stability was quantitatively evaluated. Here, the reader is kindly referred to the guidelines proposed by GREENWOOD (2003), ROUXEL et al. (2011), and WHITE et al. (2007). In this context, the dependence of the pH value on both the dispersant and the graphite content was further examined. Taking into account the pH value range of the maximum stability in the zeta potential analysis, the impact of the pH value on the initially determined viscosity behavior was studied. Lastly, the particle size distribution of the graphite dispersions with the minimum required dispersant content at the optimum pH value range was determined (see Figure 7.1 b).

The overall results allowed to assess the effectiveness of the dispersants with respect to the product and the process requirements outlined in Chapter 6.

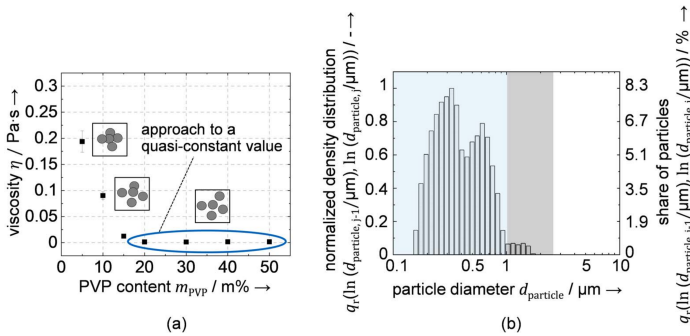


**Figure 7.1:** Identification of a suitable dispersant for the graphite dispersions with (a) the progression of the viscosity  $\eta$  over the PVP content  $m_{\text{PVP}}$  indicating a successive breakup until a quasi-constant viscosity value is reached at maximum deagglomeration and (b) the density distribution  $q_r(\ln(d_{\text{particle},j-1}/\mu\text{m}), \ln(d_{\text{particle},j}/\mu\text{m}))$  according to DIN ISO 9276-1 displayed both normalized to the largest number of particles detected and as the share of particles over the particle diameter  $d_{\text{particle}}$  at the minimum required dispersant content; the blue coloring indicates the printable region, whereas the gray coloring marks the transition reported in the literature (see Subsection 2.4.3).

## 7.2 Summary of the key findings and contributions of the lead author

The main KF of the publication of KOLB ET AL. (2021) are as follows:

**KF 1:** Unlike TX-100, PVP has proven to be a suitable dispersant for the stabilization of graphite particles in an aqueous solution. Viscosity measurements showed that the highest stability can be achieved at a minimum PVP content of 20 m% with respect to the amount of graphite employed. However, the particle size distributions revealed that a PVP content of 15 m% already effects a distribution that is below the threshold required for a reliable processing in inkjet printing.

**KF 2:** The pH value of the dispersion strongly affects the interactions between the dispersant and the graphite particles. While a pH value in the neutral range favors the stabilizing mechanism, an acid solution is detrimental.

The contributions of the lead author to Publication II are listed in Table 7.1.

**Table 7.1:** Percentage of the lead author's contributions to the conceptualization, the elaboration of the results, and the documentation of Publication II as well as the average

	Conceptualization	Elaboration of the results	Documentation	Average
C. G. Kolb	85%	85%	85%	85%

## Chapter 8

# Publication III: Modeling of the dispersion stability according to KOLB ET AL. (2022b)

## 8.1 Summary

Based on the findings of Chapter 7, this publication elaborated an analytical model based on the extended DLVO theory to describe the stability of graphite dispersions containing the dispersant PVP.

Initially, the energy fractions pertaining to the classical DLVO theory were adapted to the conditions that apply to graphite dispersions (see Subsection 3.3.1). Subsequently, the effects associated with the incorporation of the dispersant PVP were addressed by the non-DLVO forces. This required an extensive modeling of the steric and hydrophobic forces. Effects from depletion were found to be negligible. A superposition of the respective energy fractions resulted in the holistic model.

To evaluate the capabilities of the model, two PVP derivatives with varying molecular weight, in particular PVP K-17 and PVP K-30, were studied.

The model values were acquired using data from the zeta potential measurements and the material-specific parameters drawn from the literature. In this context, the total interaction energies  $V_{T,ex}$  were determined over the particle distance  $h$  (see Figure 8.1 a). In addition, the stability factor  $W$  was calculated, which can be interpreted as the probability of coagulation when two particles collide. This key number categorizes the dispersions into a stable and a non-stable behavior.

The stability behavior was empirically characterized by a sedimentation analysis (see Figure 8.1 b). This allowed to determine the average gray value over time for the graphite dispersions with varying PVP content. While a constant gray value indicated a stable dispersion without a substantial coagulation, an increase in the gray value signified the occurrence of coagulation.

Lastly, the results from the sedimentation analyses were compared with the calculated total interaction energy levels and the determined values for the stability factor.

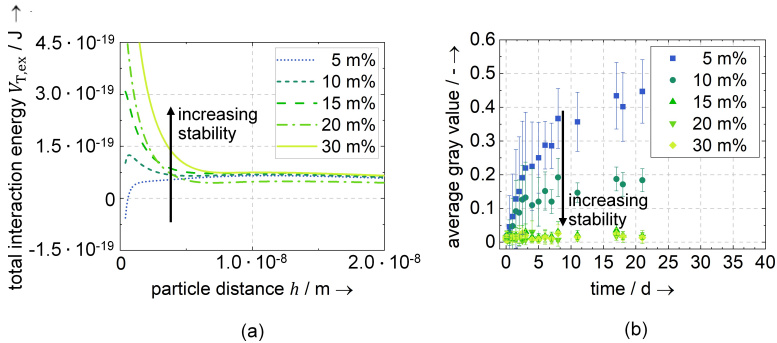


**Figure 8.1:** Exemplary comparison of the data obtained for PVP K-17 with (a) the total interaction energies  $V_{T,ex}$  as a function of the particle distance  $h$  and (b) the average gray values over time; the arrow indicates the direction of increased stability.

## 8.2 Summary of the key findings and contributions of the lead author

The KF resulting from the publication of KOLB ET AL. (2022b) can be summarized as follows:

**KF 1:** The elaborated model relying on the extended DLVO theory has proven to be applicable to graphite dispersions.

**KF 2:** The incorporation of the dispersant PVP and the related effects in the model appear to be feasible.

**KF 3:** The sedimentation analyses elucidate that the trend of the gray value data is reflected in the calculated values of the total interaction energy. Accordingly, the results demonstrate that the model is appropriate to describe the stability behavior of graphite dispersions containing PVP.

**KF 4:** For most dispersions, the behavior observed in the sedimentation analyses coincides very well with the classification given by the stability factor.

The contributions of the lead author to Publication III are listed in Table 8.1.

**Table 8.1:** Percentage of the lead author's contributions to the conceptualization, the elaboration of the results, and the documentation of Publication III as well as the average

	Conceptualization	Elaboration of the results	Documentation	Average
C. G. Kolb	85%	40%	85%	70%

## Chapter 9

# Publication IV: A-priori evaluation of the dispersion printability according to KOLB ET AL. (2023a)

## 9.1 Summary

According to the printing requirements consolidated in Chapter 6, this publication presents a systematic approach for an a-priori evaluation of the printability of graphite dispersions.

Based on the findings of Chapter 7, a preparation route was qualified that encompasses the gradual incorporation of all constituents required to form a working anode dispersion (see Section 2.2.2). Following this synthesis route, graphite dispersions with varying graphite content were prepared and the printability was evaluated through a characterization of the drop formation (see Figure 9.1) and the drop deposition behavior (see Figure 9.2).

The drop formation was observed by an in-situ process monitoring setup, which was designed to capture the entire mechanism from the filament formation to the pinch off and the behavior in free fall (see Subsection 3.4.1). The drop deposition was investigated in ex-situ test setups, which were customized to examine both the drop impact and the wetting behavior (see Section 3.4.2). This allowed to assess the respective stability conditions according to the definitions given in Section 3.4.

Aiming to calculate the nondimensional numbers introduced by CLASEN et al. (2012) (see Section 3.4.1), the dispersion-specific parameters were determined by thorough empirical studies. In this context, extensive effort has been devoted to determine the rheological quantities, such as the relaxation time  $\lambda$  and the viscosity at drop ejection  $\eta_{\text{eject}}$ .

The capability of the numbers to evaluate the printability was analyzed with regard to the experimentally obtained drop monitoring data. First, the dependence of the numbers on the graphite content was discussed. Second, the initial filament thinning mechanism and thus the complexity of the dispensing operation was evaluated (see Section 3.4.1). Accordingly, the dispersions were attributed to a less challenging or a challenging processing condition.

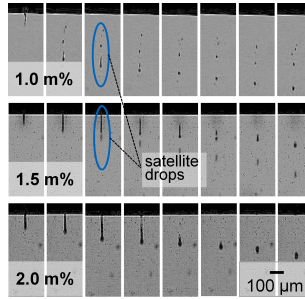


**Figure 9.1:** Imaging of the drop formation behavior; the blue highlights indicate characteristics of instability.

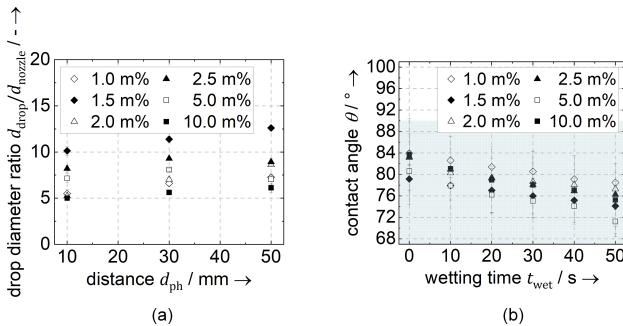


**Figure 9.2:** Depiction of the drop deposition behavior with (a) the drop diameter ratio  $d_{\text{drop}}/d_{\text{nozzle}}$  over the distance  $d_{\text{ph}}$  and (b) the contact angle  $\theta$  over wetting time  $t_{\text{wet}}$ ; the blue coloring signifies the stable wetting regime.

## 9.2 Summary of the key findings and contributions of the lead author

The following KF can be derived from the publication of KOLB ET AL. (2023a):

**KF 1:** The presented approach allows to systematically identify a stable and printable graphite dispersion prior to processing. In addition, the outlined experiments can serve for a standardized characterization.

**KF 2:** The dispersion with 2.0 m% graphite shows a stable drop formation without the occurrence of satellite drops. Dispersions with a higher graphite content caused a strong increase in the elastic behavior, which impeded the drop ejection. The amplification of the elastic behavior was primarily attributed to the binders contained in the dispersion.

**KF 3:** All dispersions exhibit a stable drop deposition. During drop impact, no splashing and bouncing were observed. In terms of spreading, it appears to be beneficial to minimize the distance between the print head and the substrate.

**KF 4:** The nondimensional numbers were identified to allow for a rough a-priori evaluation of the dispensing behavior. However, they seem less sufficient for a sound assessment in terms of the drop formation stability.

**KF 5:** The nondimensional numbers determined for the stable dispersion with 2.0 m% graphite can serve as a reference for future studies.

The contributions of the lead author to Publication IV are listed in Table 9.1.

**Table 9.1:** Percentage of the lead author's contributions to the conceptualization, the elaboration of the results, and the documentation of Publication IV as well as the average

	<b>Conceptualization</b>	<b>Elaboration of the results</b>	<b>Documentation</b>	<b>Average</b>
C. G. Kolb	85%	40%	85%	<b>70%</b>



## Chapter 10

# Publication V: Analysis of the role of binder derivatives on product and process conditions according to KOLB ET AL. (2023b)

## 10.1 Summary

Considering the findings of Chapter 9 on the relevance of the binders, this publication aimed to explore their impact on the product and the process conditions in greater detail.

The dispersion composition identified as printable in Chapter 9 was used as a reference for the studies. The elaborated preparation route was followed to synthesize graphite dispersions with varying binder content. Two CMC derivatives with strongly different molecular weight were employed, which were designated as low-molecular-weight (l-mw) CMC and high-molecular-weight (h-mw) CMC. The influence of the intrinsic polymer properties on the characteristics of the dispersions and the electrodes as well as the cells prepared thereof was investigated. Various comparative studies were conducted at the dispersion, the electrode, and the cell level.

At the dispersion level, the stability and the printability were examined through extensive rheological studies (see Subsection 5.2.2), followed by an evaluation of the drop formation (see Figure 10.1 a) and the drop deposition (see Figure 10.1 b). While the drop formation was assessed using the in-situ monitoring setup (see Subsection 3.4.1), the drop deposition was analyzed in ex-situ mode (see Subsection 5.2.2).

At the electrode level, pull-off tests were performed to determine the total adhesion strength (see Subsection 5.3.3). The cohesion behavior was derived from the particular failure mechanism observed.

At the cell level, the formation behavior was thoroughly investigated by characterizing the voltage profiles, the capacity profiles, and the coulombic efficiencies (see Figure 10.2 a and Subsection 5.3.3). The data obtained was compared with the behavior of conventional reference half cells (see Figure 10.2 b).

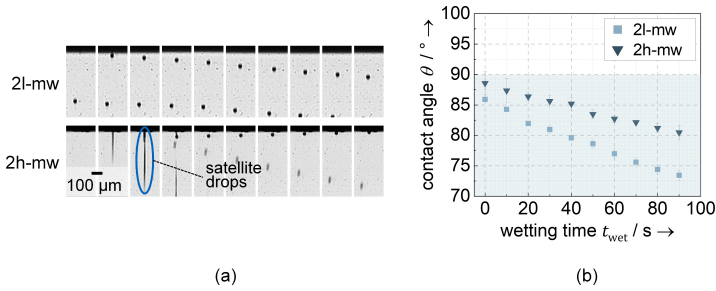


**Figure 10.1:** Exemplary comparison of the 2l-mw and 2h-mw samples with (a) the drop formation behavior and (b) the contact angle  $\theta$  over wetting time  $t_{\text{wet}}$ ; the blue coloring marks the stable wetting regime.

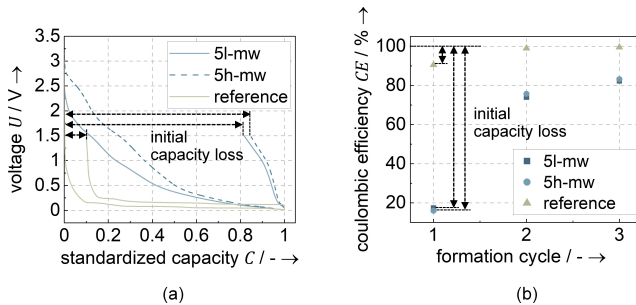


**Figure 10.2:** Exemplary comparison of the formation behavior of the 5l-mw and the 5h-mw samples against the reference cell with (a) the capacity profile of the first cycle and (b) the coulombic efficiencies  $CE$  of the first three cycles; the arrows indicate the initial capacity losses.

## 10.2 Summary of the key findings and contributions of the lead author

The publication of KOLB ET AL. (2023b) allows to draw the following KF:

**KF 1:** In terms of the processability, the application of the l-mw CMC has proven to be advantageous. The dispersion with 2.0 m% l-mw CMC exhibits both a stable drop formation and drop deposition.

**KF 2:** Regarding the mechanical properties, a conflict of objectives is apparent. While the l-mw CMC has a beneficial effect on the cohesion at the expense of the adhesion, the h-mw CMC causes the reverse effect. For the l-mw samples, a jump in the adhesion strength values was observed at a binder content of at least 5 m%. The formation behavior was found to be positively impacted by employing the l-mw CMC, although no distinct dependence on the binder content was observed.

**KF 3:** It has been demonstrated that the l-mw and h-mw samples are electrochemically active, with the l-mw CMC leading to slightly lower initial capacity losses.

**KF 4:** Considering the entirety of the investigated characteristics, it can be concluded that the l-mw CMC affects most of the studied qualities more favorably than the h-mw CMC. Provided that there are no application-specific particular requirements for the mechanical properties, a binder content of 2 m% should be targeted.

The contributions of the lead author to Publication V are listed in Table 10.1.

**Table 10.1:** Percentage of the lead author's contributions to the conceptualization, the elaboration of the results, and the documentation of Publication V as well as the average

	<b>Conceptualization</b>	<b>Elaboration of the results</b>	<b>Documentation</b>	<b>Average</b>
C. G. Kolb	72.5%	52.5%	77.5%	<b>67.5%</b>



## Chapter 11

# Discussion

In the light of the state of the art in science and technology, the scientific contribution of this publication-based dissertation is discussed. Within the scope of this work, the following achievements (A) were attained (see Figure 11.1):

**A 1:** Publication I, for the first time, presents a condensed summary of the key product- and process-specific requirements applying to electrode dispersions in inkjet printing. Compared to the previous state of the art in science and technology (see Section 3.2), the suitable parameter ranges for the respective dispersion components that promote a stable processability are known.

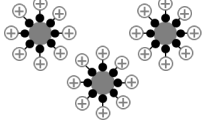
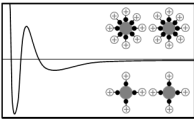
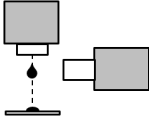
**A 2:** Publication II provides a stable aqueous dispersion that meets the requirements of the inkjet printing process in terms of the particle size distribution. In contrast to the state of the art in science and technology before P II (see Section 3.2), a dispersant is identified that leverages a graphite dispersion suitable for inkjet printing to work as an anode dispersion.

**A 3:** Publication III demonstrates a model based on the extended DLVO theory that is capable of a-priori describing the stability of aqueous graphite dispersions containing the dispersant PVP. Compared to the previous state of the art in science and technology (see Section 3.3), this model thoroughly captures the energy fractions that apply to graphite dispersions. In addition, the electrosteric effects associated with the incorporation of the dispersant are comprehensively considered.

**A 4:** Publication IV, for the first time, presents a stable processing of an aqueous graphite dispersion in the inkjet printing process, which was designed for the use in lithium-ion batteries. In contrast to the state of the art in science and technology prior to P IV (see Section 3.2 and 3.4), the processability was proven by an in-situ characterization of the drop formation and an ex-situ characterization of the drop deposition. A novel number-based approach has been shown that facilitates systematically identifying a stable and printable graphite dispersion prior to processing.

**A 5:** Publication V points out the role of binders in water-based graphite dispersions. Compared to the previous state of the art in science and technology (see Section 3.2), the impact on the product and the process characteristics are re-

vealed. This allows to further narrow down the parameter windows with regard to the binder derivative and the content.

WP 1	 <p><b>Publication I</b></p> <ul style="list-style-type: none"> <li>• Summary of the key product- and process requirements</li> <li>• Parameter ranges for the dispersion components</li> </ul>	Requirements
WP 2	 <p><b>Publication II</b></p> <ul style="list-style-type: none"> <li>• Evidence for a stable dispersion</li> <li>• Dispersant that effectively stabilizes the dispersion system</li> </ul>	Stability
WP 3	 <p><b>Publication III</b></p> <ul style="list-style-type: none"> <li>• Model that describes the stability behavior of the dispersion system</li> <li>• Incorporation of the dispersant</li> </ul>	Stability
WP 4	 <p><b>Publication IV</b></p> <ul style="list-style-type: none"> <li>• Proof of a stable processing</li> <li>• Number-based method for an a-priori evaluation of the processability</li> </ul>	Printability
WP 5	 <p><b>Publication V</b></p> <ul style="list-style-type: none"> <li>• Impact of binders on the product and the process characteristics</li> <li>• Parameter windows for the binder derivative and the content</li> </ul>	Printability

**Figure 11.1:** Overview of the achievements of this publication-based dissertation

The achievements constitute an overall methodology that assists the qualification of water-based anode dispersions for the processing in inkjet printing. Accordingly, this dissertation allows for a systematic identification of stable and printable dispersion compositions at a minimum empirical effort. The stabilization and the definition of the boundary conditions were facilitated by a mathematical model based on the extended DLVO theory. The validity of the overall methodology was proven by a characterization of the drop formation and the drop deposition. In addition, parameter ranges were proposed for the central dispersion components and their characteristics. This methodology thus provides the prerequisite for the future generation of arbitrary electrode architectures. The application of the elaborated approach was demonstrated for the

---

state-of-the-art anode system of graphite, but the approach offers great potential to be applied to further material systems.

The results of Chapter 6 indicate that, in many aspects, a conflict prevails between the product and the process requirements. The consecutive studies outlined in Chapter 7 to Chapter 10 confirm that the modifications required to formulate a stable and printable electrode dispersion compromise the battery performance characteristics. This is primarily attributed to the much smaller particle size distribution of the active material employed compared to conventional coating techniques. The associated large total surface area promotes capacity losses during the first charge cycles. Due to the strong particle-particle interactions, a dispersant is required to stabilize the particles in the aqueous medium (see Chapter 7 and Chapter 8). The large total surface area of the particles requires a significant amount of dispersant and also of the used binders, which is detrimental to the energy density (see Chapter 10). The binders, however, predominantly strengthen the non-Newtonian behavior of the electrode dispersions, which severely hinders their processability. This is at the expense of the processable active material content, which must be reduced to still allow for reliable processing. These correlations are inherent to printable electrode dispersions. The characteristics that are comparable to the previously investigated cathode active materials have also been observed by other research groups, such as DELANNOY et al. (2015) and GU et al. (2015).

Overall, it becomes apparent that the theoretical merits of printed electrodes have not yet been fully proven. Once appropriate architectures can be reliably fabricated, the battery performance characteristics will need to be re-examined. This is expected to elucidate the application fields in which printed electrodes are superior to their conventional counterparts. In addition, it allows for the comparison with structured electrodes realized by different processes mentioned in the literature (see Subsection 2.2.5).



## Chapter 12

# Summary and outlook

Inkjet printing is a disruptive additive manufacturing technology with the prospect of generating customized lithium-ion batteries by tailored electrode dispersions. The high achievable resolution allows for a unique control of the geometries that promises to improve the performance characteristics. However, electrode dispersions exhibit a complex non-Newtonian behavior, which severely complicates the processability. A systematic dispersion formulation is considered as the key for achieving a reliable process. Despite the relevance of this topic, little effort has been directed towards electrode dispersions, and in particular, anode dispersions.

Aiming to address this deficiency, this doctoral thesis constitutes a methodology to qualify water-based anode dispersions for the inkjet printing process. The approach was demonstrated with the predominant state-of-the-art anode active material graphite. First, the central product- and process-specific requirements that apply to the dispersions to be processed were aggregated (see Chapter 6). Subsequently, a suitable dispersant was empirically determined to stabilize the graphite particles in an aqueous solution (see Chapter 7). In this context, a model was elaborated that allows to describe the dispersion stability (see Chapter 8). This was followed by a number-based approach to qualify a printable dispersion whose capability has been validated (see Chapter 9). Particular attention was paid to the incorporation of the binders and the related effects on the product and the process characteristics (see Chapter 10).

The findings of this dissertation unveil miscellaneous aspects that remain to be addressed in future studies. Two central research areas can be identified, which are discussed below.

First, the transferability of the presented methodology to other material systems needs to be proven. In this context, the identification of a suitable dispersant is considered as a prerequisite for the successful utilization. Accordingly, the direct applicability to anode active materials that can be effectively dispersed by PVP, such as graphene (HTWE and MARIATTI 2021), is likely. For other carbon-based anode active materials or materials of different nature, the suitability of PVP remains to be investigated. Hence, the approach has to be adapted to the respective dispersant system to retain validity.

Apart from anode active materials, it is expected that the methodology can be adopted to cathode dispersions by making minor adjustments due to the inclusion of conductive additives and their associated effects. In this context, KOLB et al. (2021) demonstrated that Triton X-100 favors the dispersibility of carbon black. In addition, some promising dispersant candidates for cathode active materials have already been identified (see Table 12.1).

**Table 12.1:** Summary of previously identified effective dispersants for water-based cathode dispersions

Material	Dispersant	Reference
LFP	Poly(4-styrene sulfonic acid) (PSSA)	LI et al. (2010) and LI et al. (2011)
	Poly(ethyleneimine) (PEI)	LI et al. (2012)
LCO	Ammonium salt of poly(acrylic acid) (PAA-NH <sub>4</sub> )	LI et al. (2006)
NCA	Poly(acrylic acid) (PAA)	HAWLEY et al. (2021)

Second, the applicability of the elaborated methodology to related additive manufacturing technologies, such as of the material extrusion category, remains to be investigated. This could provide new potentials for robust and reliable hybrid manufacturing by combining diverse technologies to exploit their particular merits. Following the study of MCOWEN et al. (2018), this facilitates the simultaneous use of dispersions with different inherent characteristics. Accordingly, two central dispersion types can be distinguished, which are referred to as conformal dispersions or self-supporting dispersions. These dispersions differ greatly in their rheological behavior, so that self-supporting dispersions exhibit a considerably more complex non-Newtonian behavior. This could be due to varying solid contents of the binder systems employed. While conformal dispersions lead to thin layers, self-supporting dispersions are rather used to create structures. This novel approach of multi-material processing appears to be promising to realize three-dimensional electrode architectures with a graded structure along the electrode thickness coordinate to achieve superior lithium-ion and electron mobility. Apart from the materials employed, the hybrid use of different technologies can weaken the process-dependent trade-off between the achievable printing resolution and the build-up rate. This can contribute to a more efficient process utilization and thus offers the potential to increase the yields.

Apart from the process-related aspects, this dissertation reveals a substantial demand in the field of nanopowders and their specific surface properties that need to be tailored to the requirements in battery technology. Once electrode structures of different material systems can be reliably produced in varying resolution and design, the research focus should be directed to the physical inter-

actions between the feasible interlocking geometries and the resulting electrochemical characteristics. Modeling approaches can assist to identify appropriate electrode structures allowing for an application-based optimum power-density-to-energy-density ratio.

The aforementioned aspects are considered as key challenges in turning the concept of industrially relevant customized lithium-ion batteries into reality and thus providing a unique solution to the pressing trade-off between the core characteristics *energy density* and *power density*.



## Bibliography

- ABELL, R., TEUNISSEN, P., RUBINGH, E., LAMMEREN, T. van, CAUCHOIS, R., EVERAARS, M., VALETON, J., GEIJN, S. van de, and GROEN, P., (2014). "Industrial-scale inkjet printed electronics manufacturing—production up-scaling from concept tools to a roll-to-roll pilot line." In: *Translational Materials Research* 1, p. 015002.
- ALAMÁN, J., ALICANTE, R., PEÑA, J. I., and SÁNCHEZ-SOMOLINOS, C., (2016). "Inkjet printing of functional materials for optical and photonic applications." In: *Materials* 9, p. 910.
- ALLART, D., MONTARU, M., and GUALOUS, H., (2018). "Model of Lithium Intercalation into Graphite by Potentiometric Analysis with Equilibrium and Entropy Change Curves of Graphite Electrode." In: *Journal of The Electrochemical Society* 165, p. 380.
- AN, S. J., LI, J., DANIEL, C., MOHANTY, D., NAGPURE, S., and WOOD III, D. L., (2016). "The state of understanding of the lithium-ion-battery graphite solid electrolyte interphase (SEI) and its relationship to formation cycling." In: *Carbon* 105, pp. 52–76.
- AN, S. M. and LEE, S. Y., (2012). "Maximum spreading of a shear-thinning liquid drop impacting on dry solid surfaces." In: *Experimental Thermal and Fluid Science* 38, pp. 140–148.
- ANANDARAJAH, A. and CHEN, J., (1995). "Single correction function for computing retarded van der Waals attraction." In: *Journal of Colloid and Interface Science* 176, pp. 293–300.
- ANDRE, D., KIM, S. J., LAMP, P., LUX, S. F., MAGLIA, F., PASCHOS, O., and STIASZNY, B., (2015). "Future generations of cathode materials: an automotive industry perspective." In: *Journal of Materials Chemistry A* 3, pp. 6709–6732.
- ANDREA, D., (2010). *Battery Management Systems for Large Lithium-Ion Battery Packs*. Norwood: Artech House.
- AQEEL, A. B., MOHASAN, M., LV, P., YANG, Y., and DUAN, H., (2019). "Effects of nozzle and fluid properties on the drop formation dynamics in a drop-on-demand inkjet printing." In: *Applied Mathematics and Mechanics* 40, pp. 1239–1254.

- ASENBAUER, J., EISENMANN, T., KUENZEL, M., KAZZAZI, A., CHEN, Z., and BRESSER, D., (2020). “The success story of graphite as a lithium-ion anode material—fundamentals, remaining challenges, and recent developments, including silicon (oxide) composites.” In: *Sustainable Energy Fuels* 4, pp. 5387–5416.
- BAE, C. J., ERDONMEZ, C. K., HALLORAN, J. W., and CHIANG, Y. M., (2013). “Design of Battery Electrodes with Dual-Scale Porosity to Minimize Tortuosity and Maximize Performance”. In: *Advanced Materials* 25, pp. 1254–1258.
- BARNES, H. A., (2000). *A handbook of elementary rheology*. Wales: University of Wales, Institute of Non-Newtonian Fluid Mechanics.
- BEIDAGHI, M. and WANG, C., (2012). “Micro-Supercapacitors Based on Interdigital Electrodes of Reduced Graphene Oxide and Carbon Nanotube Composites with Ultrahigh Power Handling Performance.” In: *Advanced Functional Materials* 22, pp. 4500–4510.
- BERGERON, V., BONN, D., MARTIN, J. Y., and VOVELLE, L., (2000). “Controlling droplet deposition with polymer additives.” In: *Nature* 405, pp. 772–775.
- BERTOLA, V., (2013). “Dynamic wetting of dilute polymer solutions: the case of impacting droplets.” In: *Advances in Colloid and Interface Science* 193, pp. 1–11.
- BIRKL, C. R., ROBERTS, M. R., MCTURK, E., BRUCE, P. G., and HOWEY, D. A., (2017). “Degradation diagnostics for lithium ion cells.” In: *Journal of Power Sources* 341, pp. 373–386.
- BITSCH, B., BRAUNSCHWEIG, B., and WILLENBACHER, N., (2016). “Interaction between polymeric additives and secondary fluids in capillary suspensions.” In: *Langmuir* 32, pp. 1440–1449.
- BITSCH, B., DITTMANN, J., SCHMITT, M., SCHARFER, P., SCHABEL, W., and WILLENBACHER, N., (2014). “A novel slurry concept for the fabrication of lithium-ion battery electrodes with beneficial properties.” In: *Journal of Power Sources* 265, pp. 81–90.
- BLOMGREN, G. E., (2003). “Liquid electrolytes for lithium and lithium-ion batteries.” In: *Journal of Power Sources* 119, pp. 326–329.
- BOCKRIS, J. M., DEVANATHAN, M. A. V., and MUELLER, K., (1963). “On the structure of charged interfaces.” In: *Electrochemistry: Proceedings of the First Australian Conference on Held in Sydney. February 13–15, Sydney, Australia*, pp. 832–863.
- BRESSER, D., BUCHHOLZ, D., MORETTI, A., VARZI, A., and PASSERINI, S., (2018). “Alternative binders for sustainable electrochemical energy storage—the transition to aqueous electrode processing and bio-derived polymers.” In: *Energy Environmental Science* 11, pp. 3096–3127.
- BRODD, R. J., (2012). *Batteries for Sustainability: Selected Entries from the Encyclopedia of Sustainability Science and Technology*. New York: Springer.

- BROWN, A. B. D. and RENNIE, A. R., (2001). "Images of shear-induced phase separation in a dispersion of hard nanoscale discs." In: *Chemical Engineering Science* 56, pp. 2999–3004.
- BRYNTESEN, S. N., STRØMMAN, A. H., TOLSTOREBROV, I., SHEARING, P. R., LAMB, J. J., and STOKKE BURHEIM, O., (2021). "Opportunities for the state-of-the-art production of LIB electrodes—A review." In: *Energies* 14, p. 1406.
- CAI, X., LUO, Y., LIU, B., and CHENG, H. M., (2018). "Preparation of 2D material dispersions and their applications." In: *Chemical Society Reviews* 47, pp. 6224–6266.
- CARRÉ, A. and WOEHLE, P., (2002). "Hydrodynamic behavior at the triple line of spreading liquids and the divergence problem." In: *Langmuir* 18, pp. 3600–3603.
- CHAE, S., CHOI, S. H., KIM, N., SUNG, J., and CHO, J., (2020). "Integration of graphite and silicon anodes for the commercialization of high-energy lithium-ion batteries." In: *Angewandte Chemie International Edition* 59, pp. 110–135.
- CHANG, P., MEI, H., ZHOU, S., DASSIOS, K. G., and CHENG, L., (2019). "3D printed electrochemical energy storage devices." In: *Journal of Materials Chemistry A* 7, pp. 4230–4258.
- CHEN, K. and XUE, D., (2016). "Materials chemistry toward electrochemical energy storage." In: *Journal of Materials Chemistry A* 4, pp. 7522–7537.
- CHHABRA, R. P. and BASAVARAJ, M. G., (2019). *Coulson and Richardson's Chemical Engineering: Volume 2A: Particulate Systems and Particle Technology*. Oxford: Butterworth-Heinemann.
- CHHABRA, R. P. and RICHARDSON, J. F., (2008). *Non-Newtonian Flow and Applied Rheology: Engineering Applications*. Oxford: Butterworth-Heinemann.
- CHO, J., JEONG, S., and KIM, Y., (2015). "Commercial and research battery technologies for electrical energy storage applications." In: *Progress in Energy and Combustion Science* 48, pp. 84–101.
- CHOI, J., SON, B., RYOU, M. H., KIM, S. H., KO, J. M., and LEE, Y. M., (2013). "Effect of LiCoO<sub>2</sub> cathode density and thickness on electrochemical performance of lithium-ion batteries." In: *Journal of Electrochemical Science and Technology* 4.1, pp. 27–33.
- CLANET, C. and LASHERAS, J. C., (1999). "Transition from dripping to jetting." In: *Journal of Fluid Mechanics* 383, pp. 307–326.
- CLASEN, C., PHILLIPS, P. M., PALANGETIC, L., and VERMANT, A. J., (2012). "Dispensing of rheologically complex fluids: The map of misery". In: *AIChE Journal* 58, pp. 3242–3255.
- COBB, C. L. and HO, C. C., (2016). "Additive Manufacturing: Rethinking Battery Design". In: *The Electrochemical Society Interface* 25, p. 75.
- CONLEY, R., (1996). *Practical Dispersion: A Guide to Understanding and Formulating Slurries*. New York: Wiley.

- COSTA, C. M., GONCALVES, R., and LANCEROS-M ÉNDEZ, S., (2020). "Recent advances and future challenges in printed batteries." In: *Energy Storage Materials* 28, pp. 216–234.
- CUSHING, A., ZHENG, T., HIGA, K., and LIU, G., (2021). "Viscosity analysis of battery electrode slurry." In: *Polymers* 13, p. 4033.
- DEIMEDE, V. and ELMASIDES, C., (2015). "Separators for lithium-ion batteries: a review on the production processes and recent developments." In: *Energy technology* 3, pp. 453–468.
- DELANNOY, P. E., RIOU, B., BROUSSE, T., LE BIDEAU, J., GUYOMARD, D., and LESTRIEZ, B., (2015). "Ink-jet printed porous composite LiFePO<sub>4</sub> electrode from aqueous suspension for microbatteries." In: *Journal of Power Sources* 287, pp. 261–268.
- DERBY, B., (2010). "Inkjet printing of functional and structural materials: fluid property requirements, feature stability, and resolution." In: *Annual Review of Materials Research* 40, pp. 395–414.
- DERBY, B. and REIS, N., (2003). "Inkjet printing of highly particulate suspensions." In: *MRS Bulletin* 28, pp. 815–818.
- DERJAGUIN, B. and LANDAU, L., (1941). "Theory of the stability of strongly charged lyophobic sols and of the adhesion of strongly charged particles in solutions of electrolytes." In: *Acta Physico Chemica* 14, pp. 30–59.
- DICKEY, D. S. and FASANO, J. B., (2004). "How geometry viscosity influence mixing: look at the flow patterns to help select the best mixer impeller." In: *Chemical Engineering* 111, pp. 42–47.
- DOBIAS, B., QIU, X., and RYBINSKI, W., (1999). *Solid-liquid dispersions*. Boca Raton: CRC Press.
- DUVIVIER, D., BLAKE, T. D., and DE CONINCK, J., (2013). "Toward a predictive theory of wetting dynamics." In: *Langmuir* 29, pp. 10132–10140.
- ELWERT, T., HUA, Q. S., and SCHNEIDER, K., (2019). "Recycling of lithium iron phosphate batteries: future prospects and research needs." In: *Materials Science Forum* 959, pp. 49–68.
- GAO, X., YANG, J., WU, J., XIN, X., LI, Z., YUAN, X., SHEN, X., and DONG, S., (2020). "Piezoelectric actuators and motors: materials, designs, and applications." In: *Advanced Materials Technologies* 5, p. 1900716.
- GENOVESE, D. B., (2012). "Shear rheology of hard-sphere, dispersed, and aggregated suspensions, and filler-matrix composites." In: *Advances in Colloid and Interface Science* 171, pp. 1–16.
- GERMAN, G. and BERTOLA, V., (2009). "Impact of shear-thinning and yield-stress drops on solid substrates." In: *Journal of Physics: Condensed Matter* 21, p. 375111.
- GIBSON, I., ROSEN, D., and STUCKER, B., (2015). *Additive Manufacturing Technologies: 3D Printing, Rapid Prototyping, and Direct Digital Manufacturing*. New York: Springer.

- GLAZIER, S. L., LI, J., LOULI, A. J., ALLEN, J. P., and DAHN, J. R., (2017). "An Analysis of Artificial and Natural Graphite in Lithium Ion Pouch Cells Using Ultra-High Precision Coulometry, Isothermal Microcalorimetry, Gas Evolution, Long Term Cycling and Pressure Measurements." In: *Journal of The Electrochemical Society* 164, A3545.
- GONZALEZ-GARCIA, C. M., GONZALEZ-MARTIN, M. L., GOMEZ-SERRANO, V., BRUQUE, J. M., and LABAJOS-BRONCANO, L., (2000). "Determination of the free energy of adsorption on carbon blacks of a nonionic surfactant from aqueous solutions." In: *Langmuir* 16, pp. 3850–3956.
- GREENWOOD, R., (2003). "Review of the measurement of zeta potentials in concentrated aqueous suspensions using electroacoustics." In: *Advances in Colloid and Interface Science* 106, pp. 55–81.
- GREGORY, J., (1981). "Approximate expressions for retarded van der Waals interaction." In: *Journal of Colloid and Interface science* 83, pp. 138–145.
- GU, Y., WU, A., SOHN, H., NICOLETTI, C., IQBAL, Z., and FEDERICI, J. F., (2015). "Fabrication of rechargeable lithium ion batteries using water-based inkjet printed cathodes." In: *Journal of Manufacturing Processes* 20, pp. 198–205.
- GULBINSKA, M. K., (2014). *Lithium-ion Battery Materials and Engineering: Current Topics and Problems from the Manufacturing Perspective*. London: Springer.
- GUO, Y., PATANWALA, H., BOGNET, B., and MA, A., (2017). "Inkjet and inkjet-based 3D printing: connecting fluid properties and printing performance". In: *Rapid Prototyping Journal* 23, pp. 562–576.
- HABEDANK, J. B., ENDRES, J., SCHMITZ, P., ZAEH, M. F., and HUBER, H. P., (2018). "Femtosecond laser structuring of graphite anodes for improved lithium-ion batteries: Ablation characteristics and process design." In: *Journal of Laser Applications* 30, p. 032205.
- HABEDANK, J. B., KRIEGLER, J., and ZAEH, M. F., (2019). "Enhanced fast charging and reduced lithium-plating by laser-structured anodes for lithium-ion batteries." In: *Journal of The Electrochemical Society* 166, A3940.
- HABEDANK, J., (2021). *Laser Structuring of Graphite Anodes for Functionally Enhanced Lithium-Ion Batteries*. München: utzverlag GmbH.
- HAAQUE, R. I., VIÉ, R., GERMAIN, M., VALBIN, L., BENABEN, P., and BODDAERT, X., (2015). "Inkjet printing of high molecular weight PVDF-TrFE for flexible electronics." In: *Flexible and Printed Electronics* 1, p. 015001.
- HASELRIEDER, W., IVANOV, S., CHRISTEN, D. K., BOCKHOLT, H., and KWAEDE, A., (2013). "Impact of the calendaring process on the interfacial structure and the related electrochemical performance of secondary lithium-ion batteries." In: *ECS Transactions* 50, p. 59.
- HAWLEY, W. B. and LI, J., (2019). "Electrode manufacturing for lithium-ion batteries—Analysis of current and next generation processing." In: *Journal of Energy Storage* 25, p. 100862.

- HAWLEY, W. B., MEYER III, H. M., and LI, J., (2021). “Enabling aqueous processing for  $\text{LiNi}_{0.8}\text{Co}_{0.15}\text{Al}_{0.05}\text{O}_2$  (NCA)-based lithium-ion battery cathodes using polyacrylic acid.” In: *Electrochimica Acta* 380, p. 138203.
- HENDERSON, D. M., PRITCHARD, W. G., and SMOLKA, L. B., (1997). “On the pinch-off of a pendant drop of viscous fluid.” In: *Physics of Fluids* 9, pp. 3188–3200.
- HOATH, S. D., (2016). *Fundamentals of inkjet printing: the science of inkjet and droplets*. Hoboken: John Wiley & Sons.
- HTWE, Y. Z. N. and MARIATTI, M., (2021). “Surfactant-assisted water-based graphene conductive inks for flexible electronic applications”. In: *Journal of the Taiwan Institute of Chemical Engineers* 125, pp. 402–412.
- HUANG, J., YANG, J., LI, W., CAI, W., and JIANG, Z., (2008). “Electrochemical properties of  $\text{LiCoO}_2$  thin film electrode prepared by ink-jet printing technique.” In: *Thin Solid Films* 516, pp. 3314–3319.
- HUHTAMAEMI, T., TIAN, X., KORHONEN, J. T., and RAS, R. H., (2018). “Surface-wetting characterization using contact-angle measurements.” In: *Nature Protocols* 13, pp. 1521–1538.
- HUTCHINGS, I. M. and MARTIN, G. D., (2012). *Inkjet technology for digital fabrication*. Hoboken: John Wiley Sons.
- ISRAELACHVILI, J. N., (1992). “Adhesion forces between surfaces in liquids and condensable vapours.” In: *Surface Science Reports* 14, pp. 109–159.
- (2011). *Intermolecular and surface forces*. Waltham: Elsevier.
- JANG, D., KIM, D., and MOON, J., (2009). “Influence of fluid physical properties on ink-jet printability.” In: *Langmuir* 25, pp. 2629–2635.
- JIAO, T., LIAN, Q., ZHAO, T., and WANG, H., (2021). “Influence of ink properties and voltage parameters on piezoelectric inkjet droplet formation.” In: *Applied Physics A* 127, pp. 1–9.
- JONES, A. and VINCENT, B., (1989). “Depletion flocculation in dispersions of sterically-stabilised particles 2. Modifications to theory and further studies.” In: *Colloids and Surfaces* 42, pp. 113–138.
- JOSSERAND, C. and THORODDSEN, S. T., (2016). “Drop impact on a solid surface.” In: *Annual Review of Fluid Mechanics* 48, pp. 365–391.
- JULIEN, C., MAUGER, A., VIJH, A., and ZAGHIB, K., (2016). *Lithium batteries*. Berlin: Springer.
- KIM, K. M., JEON, W. S., CHUNG, I. J., and CHANG, S. H., (1999). “Effect of mixing sequences on the electrode characteristics of lithium-ion rechargeable batteries.” In: *Journal of Power Sources* 83, pp. 108–113.
- KIM, S. W. and CHO, K. Y., (2015). “Current collectors for flexible lithium ion batteries: A review of materials.” In: *Journal of Electrochemical Science and Technology* 6, pp. 1–6.
- KOLB, C. G., LEHMANN, M., LINDEMANN, J.-L., BACHMANN, A., and ZAEH, M. F., (2021). “Improving the Dispersion Behavior of Organic Components in

- Water-Based Electrode Dispersions for Inkjet Printing Processes.” In: *Applied Sciences* 11, p. 2242.
- KRAYTSBERG, A. and EIN-ELI, Y., (2016). “Conveying Advanced Li-ion Battery Materials into Practice The Impact of Electrode Slurry Preparation Skills.” In: *Advanced Energy Materials* 6, p. 1600655.
- KULSHRESHTHA, A. K., SINGH, O. N., and WALL, G. M., (2010). *Pharmaceutical suspensions: From formulation development to manufacturing. From formulation development to manufacturing*. New York: Springer.
- KUMAR, G. and PRABHU, K. N., (2007). “Review of non-reactive and reactive wetting of liquids on surfaces.” In: *Advances in Colloid and Interface Science* 133, pp. 61–89.
- KUMAR, S., RAY, D., ABBAS, S., SAHA, D., ASWAL, V. K., and KOHLBRECHER, J., (2019). “Reentrant phase behavior of nanoparticle solutions probed by small-angle scattering.” In: *current Opinion in Colloid Interface Science* 42, pp. 17–32.
- KURZWEIL, P. and DIETLMEIER, O. K., (2018). *Elektrochemische Speicher*. Wiesbaden: Springer.
- KWADE, A., HASELRIEDER, W., LEITHOFF, R., MODLINGER, A., DIETRICH, F., and DROEDER, K., (2018). “Current status and challenges for automotive battery production technologies.” In: *Nature Energy* 3, pp. 290–300.
- LAGALY, G., SCHULZ, O., and ZIMEHL, R., (1997). *Dispersionen und Emulsionen: Eine Einführung in die Kolloidik feinverteilter Stoffe einschließlich Tonminerale*. Heidelberg: Springer.
- LANCEROS-MÉNDEZ, S. and COSTA, C. M., (2018). *Printed Batteries: Materials, Technologies and Applications*. Hoboken: John Wiley Sons.
- LARSON, R. G., (1998). *The structure and rheology of complex fluids*. Oxford: Oxford University Press.
- LARSSON, M., HILL, A., and DUFFY, J., (2012). “Suspension stability; why particle size, zeta potential and rheology are important.” In: *Annual Transactions of the Nordic Rheology Society* 20, p. 6.
- LAUTH, J. G. and KOWALCZYK, J., (2016). *Einführung in die Physik und Chemie der Grenzflächen und Kolloide*. Heidelberg: Springer.
- LEE, J. H., PAIK, U., HACKLEY, V. A., and CHOI, Y. M., (2006). “Effect of poly (acrylic acid) on adhesion strength and electrochemical performance of natural graphite negative electrode for lithium-ion batteries.” In: *Journal of Power Sources* 161, pp. 612–616.
- LEHMANN, M., KOLB, C. G., KLINGER, F., and ZAEH, M. F., (2021). “Preparation, characterization, and monitoring of an aqueous graphite ink for use in binder jetting.” In: *Materials Design*, p. 109871.
- LERCHE, D., (2002). “Dispersion stability and particle characterization by sedimentation kinetics in a centrifugal field.” In: *Journal of Dispersion Science and Technology* 23, pp. 699–709.

- LI, C. C., PENG, X. W., LEE, J. T., and WANG, F. M., (2010). "Using Poly(4-Styrene Sulfonic Acid) to Improve the Dispersion Homogeneity of Aqueous-Processed  $\text{LiFePO}_4$  Cathodes". In: *Journal of the Electrochemical Society* 157, A517.
- LI, C.-C., WANG, Y.-H., and YANG, T.-Y., (2011). "Effects of surface-coated carbon on the chemical selectivity for water-soluble dispersants of  $\text{LiFePO}_4$ ". In: *Journal of The Electrochemical Society* 158, A828.
- LI, C., LEE, J., and PENG, X., (2006). "Improvements of dispersion homogeneity and cell performance of aqueous-processed  $\text{LiCoO}_2$  cathodes by using dispersant of PAA –  $\text{NH}_4$ ." In: *Journal of the Electrochemical Society* 153, A809.
- LI, J., ARMSTRONG, B. L., KIGGANS, J., DANIEL, C., and WOOD, D. L., (2012). "Lithium ion cell performance enhancement using aqueous  $\text{LiFePO}_4$   $\text{LiFePO}_4$  cathode dispersions and polyethyleneimine dispersant." In: *Journal of the Electrochemical Society* 160, A201.
- LI, M., LU, J., CHEN, Z., and AMINE, K., (2018). "30 years of lithium-ion batteries." In: *Advanced Materials* 30, p. 1800561.
- LIANG, Z. P., WANG, X. D., DUAN, Y. Y., MIN, Q., WANG, C., and LEE, D. J., (2010). "Dynamic wetting of non-Newtonian fluids: multicomponent molecular-kinetic approach." In: *Langmuir* 26, pp. 14594–14599.
- LIKOS, C. N., VAYNBERG, K. A., LOEWEN, H., and WAGNER, N. J., (2000). "Colloidal stabilization by adsorbed gelatin." In: *Langmuir* 16, pp. 4100–4108.
- LINGAPPAN, N., KONG, L., and PECHT, M., (2021). "The significance of aqueous binders in lithium-ion batteries." In: *Renewable and Sustainable Energy Reviews* 147, p. 111227.
- LIU, G., ZHENG, H., SONG, X., and BATTAGLIA, V. S., (2011). "Particles and polymer binder interaction: a controlling factor in lithium-ion electrode performance." In: *Journal of The Electrochemical Society* 159, A214.
- LIU, W., LIU, H., LIU, W., and CUI, Z., (2021). "Life cycle assessment of power batteries used in electric bicycles in China." In: *Renewable and Sustainable Energy Reviews* 139, p. 110596.
- LIU, Y. and DERBY, B., (2019). "Experimental study of the parameters for stable drop-on-demand inkjet performance." In: *Physics of Fluids* 31, p. 032004.
- LU, G., WANG, X. D., and DUAN, Y. Y., (2016). "A critical review of dynamic wetting by complex fluids: from Newtonian fluids to non-Newtonian fluids and nanofluids." In: *Advances in Colloid and Interface Science* 236, pp. 43–62.
- MAGAMPA, P. P., MANYALA, N., and FOCKE, W. W., (2013). "Properties of graphite composites based on natural and synthetic graphite powders and a phenolic novolac binder." In: *Journal of Nuclear Materials* 436, pp. 76–83.
- MAGDASSI, S., (2010). *The Chemistry Of Inkjet Inks*. Singapore: World Scientific Publishing.

- MAHANTY, J. H. and NINHAM, B. W., (1977). *Colloid science: dispersion forces*. London: Academic Press.
- MARTIN, G. D., HOATH, S. D., and HUTCHINGS, I. M., (2008). "Inkjet printing—the physics of manipulating liquid jets and drops." In: *Journal of Physics* 105, p. 012001.
- MASSÉ, R. C., LIU, C., LI, Y., MAI, L., and CAO, G., (2017). "Energy storage through intercalation reactions: electrodes for rechargeable batteries." In: *National Science Review* 4, pp. 26–53.
- MCCLEMENTS, D., (2015). *Food Emulsions: Principles, Practices, and Techniques*. Boca Raton: CRC Press.
- MCILROY, C., HARLEN, O. G., and MORRISON, N. F., (2013). "Modelling the jetting of dilute polymer solutions in drop-on-demand inkjet printing." In: *Journal of Non-Newtonian Fluid Mechanics* 201, pp. 17–28.
- MCOWEN, D. W., XU, S., GONG, Y., WEN, Y., GODBEY, G. L., GRITTON, J. E., HAMANN, T. R., DAI, J., HITZ, G. T., HU, L., and WACHSMAN, E. D., (2018). "3D-Printing Electrolytes for Solid-State Batteries." In: *Advanced Materials* 30, p. 1707132.
- MEISSNER, E. and RICHTER, G., (2005). "The challenge to the automotive battery industry: the battery has to become an increasingly integrated component within the vehicle electric power system." In: *Journal of Power Sources* 144, pp. 438–460.
- MENDES-FELIPE, C., OLIVEIRA, J., ETXEBARRIA, I., VILAS-VILELA, J. L., and LANCEROS-MENDEZ, S., (2019). "State-of-the-art and future challenges of UV curable polymer-based smart materials for printing technologies." In: *Advanced Materials Technologies* 4, p. 1800618.
- MEWIS, J., (1996). "Flow behavior of concentrated suspensions: predictions and measurements." In: *International Journal of Mineral Processing* 44, pp. 17–27.
- MEZGER, T. G., (2020). *The Rheology Handbook: For Users of Rotational and Oscillatory Rheometers*. Hannover: Vincentz Network.
- MITCHELL, T. K., NGUYEN, A. V., and EVANS, G. M., (2005). "Heterocoagulation of chalcopyrite and pyrite minerals in flotation separation." In: *Advances in Colloid and Interface Science* 114, pp. 227–237.
- MOERTERS, P. and PERES, Y., (1912). *Brownian motion*. Cambridge: Cambridge University Press.
- MUNDSZINGER, M., FARSI, S., RAPP, M., GOLLA-SCHINDLER, U., KAISER, U., and WACHTLER, M., (2017). "Morphology and texture of spheroidized natural and synthetic graphites." In: *Carbon* 111, pp. 764–773.
- NEOGI, P. and YBARRA, R. M., (2001). "The absence of a rheological effect on the spreading of small drops." In: *The Journal of Chemical Physics* 115, pp. 7811–7813.

- NGUYEN, A. and SCHULZE, H. J., (2003). *Colloidal Science of Flotation*. Oxfordshire: Taylor Francis Inc.
- NICHOLS, G., BYARD, S., BLOXHAM, M. J., BOTTERILL, J., DAWSON, N. J., DENNIS, A., DIART, V., NORTH, N. C., and SHERWOOD, J. D., (2002). "A review of the terms agglomerate and aggregate with a recommendation for nomenclature used in powder and particle characterization." In: *Journal of Pharmaceutical Sciences* 91, pp. 2103–2109.
- NING, G., HARAN, B., and POPOV, B. N., (2003). "Capacity fade study of lithium-ion batteries cycled at high discharge rates." In: *Journal of Power Sources* 117, pp. 160–169.
- OLIVETTI, E. A., CEDER, G., GAUSTAD, G. G., and FU, X., (2017). "Lithium-Ion Battery Supply Chain Considerations: Analysis of Potential Bottlenecks in Critical Metals." In: *Joule* 1, pp. 229–243.
- PAILTHORPE, B. A. and RUSSEL, W. B., (1982). "The retarded van der Waals interaction between spheres." In: *Journal of Colloid and Interface Science* 89, pp. 563–566.
- PASHLEY, R. M., MCGUIGGAN, P. M., NINHAM, B. W., and EVANS, D. F., (1985). "Attractive forces between uncharged hydrophobic surfaces: direct measurements in aqueous solution." In: *Science* 229, pp. 1088–1089.
- PAULO, G. S. D., OISHI, C. M., TOM É, M. F., ALVES, M. A., and PINHO, F. T., (2014). "Numerical solution of the FENE-CR model in complex flows." In: *Journal of Non-Newtonian Fluid Mechanics* 204, pp. 50–61.
- PFLEGING, W., (2018). "A review of laser electrode processing for development and manufacturing of lithium-ion batteries." In: *Nanophotonics* 7, pp. 549–573.
- PHAN-THIEN, N. and MAI-DUY, N., (2013). *Understanding Viscoelasticity: An Introduction to Rheology*. Berlin: Springer.
- POLSAKIEWICZ, D. A. and KOLLENBERG, W., (2011). "Highly loaded alumina inks for use in a piezoelectric print head." In: *Materialwissenschaft und Werkstofftechnik* 42, pp. 812–819.
- PORCHER, W., LESTRIEZ, B., JOUANNEAU, S., and GUYOMARD, D., (2010). "Optimizing the surfactant for the aqueous processing of LiFePO<sub>4</sub> composite electrodes." In: *Journal of Power Sources* 195, pp. 2835–2843.
- PBABHU, K. N., FERNANDES, P., and KUMAR, G., (2009). "Effect of substrate surface roughness on wetting behaviour of vegetable oils." In: *Materials Design* 30, pp. 297–305.
- PRIEVE, D. C. and RUSSEL, W. B., (1988). "Simplified predictions of Hamaker constants from Lifshitz theory." In: *Journal of Colloid and Interface Science* 125, pp. 1–13.
- QUÉRÉ, D., (2008). "Wetting and roughness." In: *Annual Review of Materials Research* 38, pp. 71–99.

- RAHIMI, S. and WEIHS, D., (2011). “Gelled fuel simulant droplet impact onto a solid surface.” In: *Propellants, Explosives, Pyrotechnics* 36, pp. 273–281.
- RAMAYWAMY, S., (2001). “Issues in the statistical mechanics of steady sedimentation.” In: *Advances in Physics* 50, pp. 297–341.
- RAPP, B. E., (2016). *Microfluidics: Modeling, Mechanics and Mathematics*. Amsterdam: Elsevier.
- REALE, E. R. and SMITH, K. C., (2018). “Capacitive performance and tortuosity of activated carbon electrodes with macroscopic pores.” In: *Journal of the Electrochemical Society* 165, A1685.
- REINHART, G., ZEILINGER, T., KURFER, J., WESTERMEIER, M., THIEMANN, C., GLONEGGER, M., WUNDERER, M., TAMMER, C., SCHWEIER, M., and HEINZ, M., (2013). “Research and demonstration center for the production of large-area lithium-ion cells.” In: *Future Trends in Production Engineering: Proceedings of the First Conference of the German Academic Society for Production Engineering. June 8–9, 2011, Berlin, Germany*, pp. 3–12.
- REIS, N. and DERBY, B., (2000). “Ink Jet Deposition of Ceramic Suspensions: Modeling and Experiments of Droplet Formation.” In: *MRS Online Proceedings Library. Solid Freeform Additive Fabrication—2000. April 23–26, San Francisco, USA* 625.
- RICHARD, D., CLANET, C., and QUÉRÉ, D., (2002). “Contact time of a bouncing drop.” In: *Nature* 417, p. 811.
- RIOBOO, R., MARENGO, M., and TROPEA, C., (2002). “Time evolution of liquid drop impact onto solid, dry surfaces.” In: *Experiments in Fluids* 33, pp. 112–124.
- ROUXEL, D., HADJI, R., VINCENT, R., and FORT, Y., (2011). “Effect of ultrasonication and dispersion stability on the cluster size of alumina nanoscale particles in aqueous solutions.” In: *Ultrasonics sonochemistry* 18, pp. 382–388.
- RUBIO-HERNÁNDEZ, F. J., SÁNCHEZ-TORO, J. H., and PÁEZ-FLOR, N. M., (2020). “Testing shear thinning/thixotropy and shear thickening/antithixotropy relationships in a fumed silica suspension.” In: *Journal of Rheology* 64, pp. 785–797.
- RUSSEL, W. B., SAVILLE, D. A., and SCHOWALTER, W. R., (1991). *Colloidal dispersions*. Cambridge: Cambridge university press.
- RÜTTEN, M., (2018). *Verallgemeinerte newtonsche Fluide: Thermische und viskose Strömungseigenschaften*. Wiesbaden: Springer.
- SAÏDI, A., MARTIN, C., and MAGNIN, A., (2010). “Influence of yield stress on the fluid droplet impact control.” In: *Journal of Non-Newtonian Fluid Mechanics* 165, pp. 596–606.
- SARRE, G., BLANCHARD, P., and BROUSSELY, M., (2004). “Aging of lithium-ion batteries.” In: *Journal of Power Sources* 127, pp. 65–71.

- SAUTER, U., (2014). *Property Right DE102012215921A1 (Mar. 13, 2014)*. Robert Bosch GmbH, 70469, Stuttgart, DE Pr.: H01M4/70, 2012. Battery e.g. lithium ion battery has porous layered electrode which is provided with several recesses at opposite side of electrode metal sheet.
- SCHENKEL, J. H. and KITCHENER, J. A., (1960). "A test of the Derjaguin-Verwey-Overbeek theory with a colloidal suspension." In: *Transactions of the Faraday Society* 56, pp. 161–173.
- SCHIAFFINO, S. and SONIN, A. A., (1997). "Molten droplet deposition and solidification at low Weber numbers." In: *Physics of fluids* 9, pp. 3172–3187.
- SCHMUCH, R., WAGNER, R., HOERPEL, G., PLACKE, T., and WINTER, M., (2018). "Performance and cost of materials for lithium-based rechargeable automotive batteries." In: *Nature Energy* 3, pp. 267–278.
- SCROSATI, B. and GARCHE, J., (2010). "Lithium batteries: Status, prospects and future." In: *Journal of Power Sources* 195, pp. 2419–2430.
- SEEBERGH, J. E. and BERG, J. C., (1994). "Depletion flocculation of aqueous, electrosterically-stabilized latex dispersions." In: *Langmuir* 10, pp. 454–463.
- SHIN, D., PARK, H., and PAIK, U., (2017). "Cross-linked poly (acrylic acid)-carboxymethyl cellulose and styrene-butadiene rubber as an efficient binder system and its physicochemical effects on a high energy density graphite anode for Li-ion batteries." In: *Electrochemistry Communications* 77, pp. 103–106.
- SIKARWAR, B. S., KHANDEKAR, S., AGRAWAL, S., KUMAR, S., and MURALIDHAR, K., (2012). "Dropwise condensation studies on multiple scales." In: *Heat Transfer Engineering* 33, pp. 301–341.
- SINGH, M., KAISER, J., and HAHN, H., (2015). "Thick electrodes for high energy lithium ion batteries." In: *Journal of the Electrochemical Society* 162, A1196.
- SLOMKOWSKI, S., ALEMÁN, J. V., GILBERT, R. G., HESS, M., HORIE, K., JONES, R. G., KUBISA, P., MEISEL, I., MORMANN, W., PENCZEK, S., and STEPTO, R. F. T., (2011). "Terminology of polymers and polymerization processes in dispersed systems (IUPAC Recommendations 2011)". In: *Pure and Applied Chemistry* 83, pp. 2229–2259.
- SMITH, M. I. and BERTOLA, V., (2010). "Effect of polymer additives on the wetting of impacting droplets." In: *Physical Review Letters* 104, p. 154502.
- SOUSA, R. E., COSTA, C. M., and LANCEROS-MÉNDEZ, S., (2015). "Advances and future challenges in printed batteries." In: *ChemSusChem* 8, pp. 3539–3555.
- STAROV, V. M., TYATYUSHKIN, A. N., VELARDE, M. G., and ZHDANOV, S. A., (2003). "Spreading of non-Newtonian liquids over solid substrates." In: *Journal of Colloid and Interface Science* 257, pp. 284–290.

- TABOR, R. F., GRIESER, F., DAGASTINE, R. R., and CHAN, D. Y., (2014). "The hydrophobic force: measurements and methods." In: *Physical Chemistry Chemical Physics* 16, pp. 18065–18075.
- TADROS, T. F., (2011). *Rheology of Dispersions: Principles and Applications*. Weinheim: Wiley.
- TAYLOR, L., SKUSE, D., BLACKBURN, S., and GREENWOOD, R., (2020). "Stirred media mills in the mining industry: Material grindability, energy-size relationships, and operating conditions." In: *Powder Technology* 360, pp. 1–16.
- TECHNOLOGY, N. N., (2021). *High Purity Natural Graphite: Nanopowder/ Nanoparticles for Li-Ion Battery*. Ankara: Nanografi Nano Technology.
- TEICHLER, A., PERELAER, J., and SCHUBERT, U. S., (2013). "Inkjet printing of organic electronics—comparison of deposition techniques and state-of-the-art developments." In: *Journal of Materials Chemistry C* 1, pp. 1910–1925.
- TEKIN, E., SMITH, P. J., and SCHUBERT, U. S., (2008). "Inkjet printing as a deposition and patterning tool for polymers and inorganic particles." In: *Soft Matter* 4, pp. 703–713.
- TOMÉ, M. F., MANGIAVACCHI, N., CUMINATO, J. A., CASTELO, A., and MCKEE, S., (2002). "A finite difference technique for simulating unsteady viscoelastic free surface flows." In: *Journal of Non-Newtonian Fluid Mechanics* 106, pp. 61–106.
- TYLER, E. and WATKIN, F., (1932). "XCIII. Experiments with capillary jets." In: *The London, Edinburgh, and Dublin Philosophical Magazine and Journal of Science* 14, pp. 849–881.
- UEKI, Y., UEDA, K., and SHIBAHARA, M., (2018). "Thermal conductivity of suspension fluids of fine carbon particles: Influence of sedimentation and aggregation diameter." In: *International Journal of Heat and Mass Transfer* 127, pp. 138–144.
- VERWEY, E. J. W. and OVERBEEK, J. T. G., (1947). "Theory of the stability of lyophobic colloids." In: *The Journal of Physical Chemistry* 51, pp. 631–636.
- VIANCO, P. T. and FREAR, D. R., (1993). "Issues in the replacement of lead-bearing solders." In: *Journal of The Minerals, Metals Materials Society* 45, pp. 14–19.
- WAL, R. L. V., BERGER, G. M., and MOZES, S. D., (2006). "The splash/non-splash boundary upon a dry surface and thin fluid film." In: *Experiments in Fluids* 40, pp. 53–59.
- WEI, M., ZHANG, F., WANG, W., ALEXANDRIDIS, P., ZHOU, C., and WU, G., (2017). "3D direct writing fabrication of electrodes for electrochemical storage devices." In: *Journal of Power Sources* 354, pp. 134–147.
- WENZEL, V., NIRSCHL, H., and NÖTZEL, D., (2015). "Challenges in Lithium-Ion-Battery Slurry Preparation and Potential of Modifying Electrode Structures by Different Mixing Processes." In: *Energy Technology* 3, pp. 692–698.

- WHITE, B., BANERJEE, S., O'BRIEN, S., TURRO, N. J., and HERMAN, I. P., (2007). "Zeta-Potential Measurements of Surfactant-Wrapped Individual Single-Walled Carbon Nanotubes." In: *The Journal of Physical Chemistry C* 111, pp. 13684–13690.
- WHITTINGHAM, M. S., (2004). "Lithium batteries and cathode materials." In: *Chemical reviews* 104, pp. 4271–4302.
- WIJSHOFF, H., (2010). "The dynamics of the piezo inkjet printhead operation." In: *Physics Reports* 491, pp. 77–177.
- WOHLERS, T., CAMPBELL, I., DIEGEL, O., HUFF, R., and KOWEN, J., (2021). *Wohlers Report 2019: 3D Printing and Additive Manufacturing State of the Industry*. Washington: Wohlers Association.
- WOOD III, D. L., LI, J., and DANIEL, C., (2015). "Prospects for reducing the processing cost of lithium ion batteries." In: *Journal of Power Sources* 275, pp. 234–242.
- WU, F., MAIER, J., and YU, Y., (2020). "Guidelines and trends for next-generation rechargeable lithium and lithium-ion batteries." In: *Chemical Society Reviews* 49, pp. 1569–1614.
- YAN, T., SCHROETER, K., HERBST, F., BINDER, W. H., and THURN-ALBRECHT, T., (2017). "What controls the structure and the linear and nonlinear rheological properties of dense, dynamic supramolecular polymer networks?." In: *Macromolecules* 50, pp. 2973–2985.
- YANG, Y., OKONKWO, E. G., HUANG, G., XU, S., SUN, W., and HE, Y., (2021). "On the sustainability of lithium ion battery industry—A review and perspective." In: *Energy Storage Materials* 36, pp. 186–212.
- YANG, Y., YUAN, W., ZHANG, X., YUAN, Y., WANG, C., YE, Y., HUANG, Y., QIU, Z., and TANG, Y., (2020). "Overview on the applications of three-dimensional printing for rechargeable lithium-ion batteries." In: *Applied Energy* 257, p. 114002.
- YANGSHUAI, Q., YONGFU, Y., LINGYAN, Z., WEIJUN, P., and YUPENG, Q., (2017). "Dispersion and agglomeration mechanism of flaky graphite particles in aqueous solution." In: *Journal of Dispersion Science and Technology* 38, pp. 796–800.
- YARIN, A. L., (2006). "Drop impact dynamics: splashing, spreading, receding, bouncing." In: *Annual Review of Fluid Mechanics* 38, pp. 159–192.
- YOON, R. H., FLINN, D. H., and I., R. Y., (1997). "Hydrophobic Interactions between Dissimilar Surfaces." In: *Journal of Colloid and Interface Science* 185, pp. 363–370.
- YOUNG, T., (1805). "An essay on the cohesion of fluids." In: *Philosophical Transactions of the Royal Society of London* 95, pp. 65–87.
- ZACKRISSON, M., AVELLÁN, L., and ORLENUIS, J., (2010). "Life cycle assessment of lithium-ion batteries for plug-in hybrid electric vehicles—Critical issues." In: *Journal of Cleaner Production* 18, pp. 1519–1529.

- ZHANG, F., WEI, M., VISWANATHAN, V. V., SWART, B., SHAO, Y., WU, G., and ZHOU, C., (2017). "3D printing technologies for electrochemical energy storage." In: *Nano Energy* 40, pp. 418–431.
- ZHANG, J. and ZENG, H., (2021). "Intermolecular and Surface Interactions in Engineering Processes." In: *Engineering* 7, pp. 63–83.
- ZHANG, Q., YU, Z., DU, P., and SU, C., (2010). "Carbon nanomaterials used as conductive additives in lithium ion batteries." In: *Recent Patents on Nanotechnology* 4, pp. 100–110.
- ZHANG, X., (1999). "Dynamics of growth and breakup of viscous pendant drops into air." In: *Journal of Colloid and Interface Science* 212, pp. 107–122.
- ZHAO, Y., LIU, G., LIU, L., and JIANG, Z., (2009). "High-performance thin-film  $\text{Li}_4\text{Ti}_5\text{O}_{12}$  electrodes fabricated by using ink-jet printing technique and their electrochemical properties." In: *Journal of Solid State Electrochemistry* 13, pp. 705–711.
- ZHAO, Y., ZHOU, Q., LIU, L., XU, J., YAN, M., and JIANG, Z., (2006). "A novel and facile route of ink-jet printing to thin film  $\text{SnO}_2$  anode for rechargeable lithium ion batteries." In: *Electrochimica Acta* 51, pp. 2639–2645.
- ZHENG, H., LI, J., SONG, X., LIU, G., and BATTAGLIA, V. S., (2012). "A comprehensive understanding of electrode thickness effects on the electrochemical performances of Li-ion battery cathodes." In: *Electrochimica Acta* 71, pp. 258–265.
- ZHONG, Y., FANG, H., MA, Q., and DONG, X., (2018). "Analysis of droplet stability after ejection from an inkjet nozzle." In: *Journal of Fluid Mechanics* 845, pp. 378–391.
- ZHU, C., LIU, T., QIAN, F., CHEN, W., CHANDRASEKARAN, S., YAO, B., SONG, Y., DUOSS, E. B., KUNTZ, J. D., SPADACCINI, C. M., WORSLEY, M. A., and LI, Y., (2017). "3D printed functional nanomaterials for electrochemical energy storage." In: *Nano Today* 15, pp. 107–120.
- ZHU, H., ZHANG, C., TANG, Y., WANG, J., REN, B., and YIN, Y., (2007). "Preparation and thermal conductivity of suspensions of graphite nanoparticles." In: *Carbon* 45, pp. 226–228.
- ZHU, M., PARK, J., and SASTRY, A. M., (2011). "Particle Interaction and Aggregation in Cathode Material of Li-Ion Batteries: A Numerical Study". In: *Journal of The Electrochemical Society* 158, A1155.
- ZHU, X., WANG, H., ALLU, S., GAO, Y., CAKMAK, E., HOPKINS, E. J., VEITH, G. M., and WANG, Z., (2020). "Investigation on capacity loss mechanisms of lithium-ion pouch cells under mechanical indentation conditions." In: *Journal of Power Sources* 465, p. 228314.



## Appendix A

# List of the supervised research projects

Within the scope of this doctoral thesis, several student research projects were supervised by the author. Some of the jointly achieved results have been incorporated into this work and into the publications listed in Chapter 6 to Chapter 10. The author would like to express her sincere gratitude for the inspiring discussions and the tremendous support during the collaboration.

Student	Student research project
Lindemann, J.-L.	German (original): Dispergierung von organischen Elektrodenkomponenten in wässrigen Elektrodispersionen English: Dispersion of organic electrode components in aqueous electrode dispersions Submission: October 2020
Kulmer, D.	English: Analytical modeling of dispersion stability for printable electrode dispersions Submission: July 2021
Lindemann, J.-L.	German (original): Qualifizierung einer wasserbasierten Elektrodispersion für die Verarbeitung in piezogesteuerten Druckköpfen English: Qualification of a water-based electrode dispersion for processing in piezo-controlled print heads Submission: August 2021
Revitch, P.	German (original): Untersuchung der Tropfenablage von wasserbasierten Graphitdispersionen im Inkjet-Printing-Prozess Submission: May 2022
Teixeira, C.-M.	English: Investigation of the processability of water-based graphite dispersions in inkjet printing using high-speed imaging Submission: October 2021
Teixeira, C.-M.	English: Investigation of the role of binders for printable anode dispersions Submission: April 2023



## Appendix B

# Publications of the author

### Core publications incorporated into this doctoral thesis

- Publication I: **Kolb, C. G.**; Lehmann, M.; Kriegler, J.; Lindermann, J.-L.; Bachmann, A.; Zaeh, M. F.: Qualifying water-based electrode dispersions for the inkjet printing process: a requirements analysis. *Rapid Prototyping Journal* 28 (2022) 11, pp. 33–50.
- Publication II: **Kolb, C. G.**; Lehmann, M.; Lindemann, J.-L.; Bachmann, A.; Zaeh, M. F.: Improving the Dispersion behavior of Organic Components in Water-Based Electrode Dispersions for Inkjet Printing Processes. *Applied Sciences* 11 (2021) 5, pp. 2242.
- Publication III: **Kolb, C. G.**; Lehmann, M.; Kulmer, D.; Zaeh, M. F.: Modeling of the stability of water-based graphite dispersions using polyvinylpyrrolidone on the basis of the DLVO theory. *Heliyon* 8 (2022) 12, pp. 1–8.
- Publication IV: **Kolb, C. G.**; Lehmann, M.; Teixeira, C.-M.; Maleksaeedi, S.; Zaeh, M. F.: A priori evaluation of the printability of water-based anode dispersions in inkjet printing. *Production Engineering* (2023), pp. 1–14.
- Publication V: **Kolb, C. G.**; Lehmann, M.; Teixeira, C.-M.; Sommer, A.; Panzer, H.; Zaeh, M. F.: The role of binders for water-based anode dispersions in inkjet printing. *Batteries* 9 (2023) 11, p. 557.

### Other publications

- **Kolb, C. G.**; Bayerlein, F.; Zaeh, M. F.: Active Thermography as a Process Monitoring Technology for Laser Beam Melting: An ex-situ and in-situ Feasibility Study. *Proceedings of the 15th Rapid.Tech Conference Erfurt* (2018), ISBN: 978-3-446-45811-6.
- **Kolb, C. G.**; Mareddy, H. R.; Guenter, F. J.; Zaeh, M. F.: Inkjet Printing of Geometrically Optimized Electrodes for Lithium-Ion Cells: A Concept for a Hybrid Process Chain. *30th Annual Solid Freeform Fabrication Symposium*. August 12–14, Austin, Texas (USA).

- Lehmann, M.; **Kolb, C. G.**; Klinger, F.; Zaeh, M. F.: Preparation, characterization, and monitoring of an aqueous graphite ink for use in binder jetting. *Materials & Design* 207 (2021), p. 109871.
- Wimmer, A.<sup>1</sup>; **Kolb, C. G.**<sup>1</sup>; Assi, M.; Favre, J.; Bachmann, A.; Fraczkiewicz, A.; Zaeh, M. F. Investigations of adapted metal-based alloys on the process of laser beam melting. *Journal of Laser Applications* 32 (2020), p. 022029.
- **Kolb, C. G.**; Zier, K.; Grager, J. C.; Bachmann, A.; Neuwirth, T.; Schmid, S.; Haag, M.; Axtner, M.; Bayerlein, F.; Grosse, C. U.; Zaeh, M. F.: An investigation on the suitability of modern nondestructive testing methods for the inspection of specimens manufactured by laser powder bed fusion. *SN Applied Sciences* 3 (2021), pp. 1–16.
- Zapata, A.; Bernauer, C.; Stadter, C.; **Kolb, C.G.**; Zaeh, M. F.: Investigation on the cause-effect relationships between the process parameters and the resulting geometric properties for wire-based coaxial laser metal deposition. *Metals* 12 (2022) 3, p. 455.
- Lehmann, M.; Panzer, H.; **Kolb, C. G.**; Zaeh, M. F.: Influence of the Pore Radius on the Penetration Depth of Inks in Binder Jetting—A Modification of the Washburn Equation. *Journal of Manufacturing and Materials Processing* 6 (2022) 5, p. 101.
- Lehmann, M.; **Kolb, C. G.**; Gschloessl, J.; Zaeh, M. F.: Using particle-loaded inks to selectively change the material properties in binder jetted WC-Co structures. *Journal of Materials Science* (2023), pp. 1–16.
- Lehmann, M.; **Kolb, C. G.**; Mai, T. P.; Zaeh, M. F.: Prediction of the penetration depth of particle-loaded inks in binder jetting. *Progress in Additive Manufacturing* 10 (2025) 1, pp. 451–463.

---

<sup>1</sup>The authors contributed equally to the publication.